Iran University of Science and Technology
School of Civil Engineering

Three-Dimensional Modeling of Reservoir Eutrophication Based on the EFDC+ Model

A Thesis Submitted in Partial Fulfillment of the Requirements for the Degree of Master of Science in Civil Engineering – Environmental Engineering

By:
Muhamad Amin Kazemzadeh

Supervisors:
Dr. Motahareh Saadatpour
Dr. Ebrahim Jabbari

May 2026

Abstract:

Water quality management in reservoirs, due to thermal stratification, dissolved oxygen depletion in deep layers, and the potential intensification of eutrophication, requires an integrated understanding of hydrodynamic and biogeochemical processes and their interactions. In this study, the three-dimensional EFDC+ hydrodynamic and water quality model was applied to simulate and evaluate the effects of different selective-withdrawal patterns on the thermal structure and water quality of the eutrophic Seymareh Reservoir.

For this purpose, hydrological, meteorological, water temperature, salinity, and water quality data were collected, and the model was configured and implemented for the existing conditions of the reservoir. Model calibration was conducted on a monthly time scale for the period from June 2016 to February 2017, based on the daily water surface elevation and the vertical profiles of temperature and water quality parameters at different depths. During calibration, the average RMSE values for temperature, dissolved oxygen, and chlorophyll-a were 1.17 °C, 0.79 mg/L, and 0.19 μg Chl-a/L, respectively, while the average NSE values for these parameters were 0.59, 0.79, and 0.97, respectively.

Following calibration of the eutrophication model, three operational scenarios were simulated over a ten-year period and compared using key eutrophication indicators. The scenarios included complete withdrawal from an elevation of 665 m above sea level, withdrawal of 70% of the outflow from an elevation of 665 m and 30% from an elevation of 640 m, and equal withdrawal from the two elevations. Under the 70–30 withdrawal scenario, the average dissolved oxygen concentration in reservoir at a depth of 80 m increased from 5.36 to 5.92 mg/L, and the average surface chlorophyll-a concentration, near the dam structure, decreased from 2.96 to 1.61 μg/L in comparison to scenario a.

The results showed that withdrawing part of the outflow from the lower elevation can result in reduction of thermal stratification intensity, improve oxygen conditions in deep waters, and limit surface algal growth. However, relative increases in nutrient concentrations in certain layers of the reservoir and in the outflow indicated that the selective withdrawal strategy should be selected based on a trade off among in-reservoir and outflow dissolved oxygen, chlorophyll-a, and nutrient concentrations. Overall, withdrawal of 70% of the outflow from the 665-m elevation and 30% from the 640-m elevation was identified as a more balanced option for water quality management in the Seymareh Dam Reservoir.

The findings demonstrate the capability of EFDC+ to reproduce the hydrodynamic and water quality conditions of a large, deep, three-dimensional reservoir affected by eutrophication and to evaluate its response to selective-withdrawal operating policies.

Keywords: Water quality modeling, EFDC+, Seymareh Reservoir, Selective withdrawal, Chlorophyll-a.

Table of Contents

1 Introduction....1
1.1 Introduction....1
1.2 Problem Statement....2
1.3 Importance and Necessity of the Research....3
1.4 Research Objectives....5
1.5 Scope and Extent of the Research....5
1.6 Thesis Structure....6
2 Technical Background and Literature Review....7
2.1 Introduction....7
2.2 Theoretical Foundations of Physical and Biogeochemical Processes in Reservoirs....7
2.2.1 Physical Processes....7
2.3 Water Quality Management Strategies and the Role of Modeling in Their Evaluation....14
2.3.1 Modeling as a Decision-Support Tool....14
2.3.2 External Load Management and Integrated Evaluation Using Modeling....15
2.3.3 Internal Load Management, In-Situ Measures, and Reservoir Operation....16
2.3.4 Applications of EFDC+ in the Simulation and Management of Water Bodies....18
2.4 Studies Conducted on Seymareh Dam....23
2.5 Summary and Identification of the Research Gap....24
2.5.1 Summary....24
2.5.2 Research Gap....25
3 Research Methodology....27
3.1 Introduction....27
3.2 Introduction to the EFDC+ Model....27
3.2.1 Hydrodynamic Foundations of the Model....28
3.2.2 Constituent Transport Model....38
3.2.3 Dye Module....39
3.2.4 Temperature and Heat Transport Module....40
3.2.5 Sediment Transport Module....46
3.2.6 Chemical Fate and Transport Module....48

3.2.7 Eutrophication and Water Quality Module 50
3.2.8 Supplementary Capabilities of EFDC+ 59
3.3 Model Development and Preparation 60
3.3.1 Description of the Study Area 61
3.3.2 Characteristics of the Dam, Reservoir, and Operational Structures 61
3.3.3 Operational Data and Hydrodynamic Boundary Conditions 62
3.3.4 Operational Scenarios and Implementation of Outlets in the Model 63
3.3.5 Extraction and Processing of Outflow Water Quality Data 65
3.3.6 Water Quality, Salinity, and Temperature Data for the Reservoir Inflow 66
3.3.7 Initial Conditions of the Model 69
3.3.8 Bed Topography, Computational Domain, and Model Grid 69
3.3.9 Meteorological Data and External Forcing 73
3.4 Model Calibration Process 74
3.4.1 Calibration Method and Target Variables 74
3.4.2 Key Calibration Parameters and Their Scientific Ranges 75
3.4.3 Model Performance Evaluation Criteria 76
4 Results and Discussion 78
4.1 Introduction 78
4.2 Calibration and Analysis of the Hydrodynamic and Temperature Model 78
4.2.1 Water-Surface Elevation and Reservoir Volume Balance 78
4.2.2 Analysis of Vertical Profiles and Thermal Stratification 80
4.2.3 Statistical Evaluation of EFDC+ Accuracy in Temperature Simulation (Error Analysis) 82
4.3 Calibration and Analysis of Water Quality Parameters 83
4.3.1 Calibration and Analysis of Dissolved Oxygen 83
4.3.2 Calibration and Analysis of Organic Load (BOD5) 87
4.3.3 Calibration and Analysis of Nitrogen Compounds 90
4.3.4 Calibration and Analysis of Phosphorus Compounds 97
4.3.5 Calibration and Analysis of Algae (Chlorophyll-a) 101
4.4 Flow-Distribution Scenarios in the Long-Term Simulations 105

4.4.1 Effects of the Scenarios on Reservoir Thermal Structure and Stratification 106
4.4.2 Effects of the Scenarios on Dissolved Oxygen in the Water Column 108
4.4.3 Effects of the Scenarios on Nutrients in the Water Column 110
4.4.4 Effects of the Scenarios on Chlorophyll-a and Organic-Load Components 112
4.4.5 Effects of the Scenarios on Outflow Water Quality 114
4.4.6 Longitudinal Variations in Surface Water Quality under the Baseline Scenario ..116
4.4.7 Comparative Summary of the Operational Scenarios 118
5 Conclusions and Recommendations 120
5.1 Conclusions 120
5.2 Recommendations 123
References 124

List of Figures

Figure 2-1. Three-layer thermal stratification structure in the reservoir water column.....9
Figure 3-1. Conceptual overview of the hydrodynamic module. 29
Figure 3-2. Vertical-layering options in EFDC+: (a) SIG, (b) SGZ-Specified Bottom, and (c) SGZ-Uniform Layering. 31
Figure 3-3. Conceptual overview of the temperature module. 41
Figure 3-4. Geographic locations of the sampling stations in Seymareh Reservoir [56] 67
Figure 3-5. Topographic map of Seymareh Reservoir and the longitudinal profile extracted along the main reservoir axis from the upstream end to the dam site. 71
Figure 3-6. Reference two-dimensional computational grid of Seymareh Reservoir and the bed elevations assigned to the model cells.....72
Figure 3-7. Two-dimensional computational grid used for Seymareh Reservoir and the bed elevations assigned to the model cells.....73
Figure 4-1. Observed and EFDC+-simulated water-surface elevations in Seymareh Reservoir during the calibration period.....79
Figure 4-2. Vertical temperature profiles from July to February during the calibration period of the EFDC+ model for Seymareh Reservoir. 82
Figure 4-3. Comparison of the vertical dissolved oxygen profiles simulated by EFDC+ from June to February with the field observations. 86
Figure 4-4. Comparison of the vertical BOD5 profiles simulated by EFDC+ from June to February with the field observations during the calibration period. 89
Figure 4-5. Comparison of the vertical ammonium-nitrogen profiles simulated by EFDC+ from June to February with field observations during the calibration period. 93
Figure 4-6. Comparison of the vertical nitrate-nitrogen profiles simulated by EFDC+ from June to February with field observations during the calibration period. 96
Figure 4-7. Comparison of the vertical total-phosphate profiles simulated by EFDC+ from June to February with field observations during the calibration period.....100
Figure 4-8. Comparison of the vertical chlorophyll-a profiles simulated by EFDC+ from June to February with field observations during the calibration period.....104
Figure 4-9. Thermal structure of Seymareh Reservoir based on the EFDC+ results under the selective-withdrawal scenarios. 106

Figure 4-10. Surface dissolved oxygen concentrations in Seymareh Reservoir under the three selective-withdrawal scenarios, based on the ten-year mean EFDC+ results. 108
Figure 4-11. Deep-water dissolved oxygen concentrations in Seymareh Reservoir under the three selective-withdrawal scenarios, based on the ten-year mean EFDC+ results. 109
Figure 4-12. Deep-water total phosphorus concentrations in Seymareh Reservoir under the three selective-withdrawal scenarios, based on the ten-year mean EFDC+ results. 111
Figure 4-13. Surface nitrate concentrations in Seymareh Reservoir under the three selective-withdrawal scenarios, based on the ten-year mean EFDC+ results. 112
Figure 4-14. Surface chlorophyll-a concentrations in Seymareh Reservoir under the three selective-withdrawal scenarios, based on the ten-year mean EFDC+ results. 113
Figure 4-15. Outflow dissolved oxygen concentrations under the three selective-withdrawal scenarios, based on the ten-year mean EFDC+ results. 114
Figure 4-16. Outflow total phosphorus concentrations under the three selective-withdrawal scenarios, based on the ten-year mean EFDC+ results. 115
Figure 4-17. Outflow nitrate concentrations under the three selective-withdrawal scenarios, based on the ten-year mean EFDC+ results. 116
Figure 4-18. Comparison of chlorophyll-a concentrations at three locations in Seymareh Reservoir based on the EFDC+ results. 117

List of Tables

Table 3-1. Principal water quality state variables in EFDC+ 51
Table 3-2. Key Model Calibration Parameters, Selected Values, and Recommended Scientific Ranges 75
Table 4-1. Statistical error indices for the EFDC+-simulated water-surface elevation in Seymareh Reservoir during the calibration period.....79
Table 4-2. Statistical evaluation of EFDC+ accuracy in simulating water temperature.....82
Table 4-3. Statistical evaluation of EFDC+ accuracy in simulating dissolved oxygen.....86
Table 4-4. Statistical evaluation of EFDC+ accuracy in simulating BOD5.....90
Table 4-5. Statistical evaluation of EFDC+ accuracy in simulating ammonium nitrogen. 96
Table 4-6. Statistical evaluation of EFDC+ accuracy in simulating nitrate nitrogen. 97
Table 4-7. Statistical evaluation of EFDC+ accuracy in simulating total phosphate. 100
Table 4-8. Statistical evaluation of EFDC+ accuracy in simulating chlorophyll-a. 105

List of Symbols and Abbreviations

Symbol / Abbreviation	Definition	Unit
Hydrodynamic Coordinates and Variables		
g	Gravitational acceleration	m s^{-2}
x	Longitudinal horizontal coordinate	m
y	Transverse horizontal coordinate	m
z	Sigma vertical coordinate	–
t	Time	s
Δt	Time step	s
h	Water depth relative to the reference datum	m
ζ	Free-surface elevation	m
H	Total water-column depth	m
u	Longitudinal velocity component	m s^{-1}
v	Transverse velocity component	m s^{-1}
w	Vertical velocity component	m s^{-1}
f	Coriolis parameter	s^{-1}
p	Dynamic pressure (kinematic form)	m^2 s^{-2}
P_{atm}	Atmospheric pressure (kinematic form)	m^2 s^{-2}
ρ	Water density	kg m^{-3}
ρ_0	Reference water density	kg m^{-3}
S	Water salinity	ppt
T	Water temperature	°C
C	Transported-constituent concentration	mg L^{-1}
A_H	Horizontal diffusivity coefficient	m^2 s^{-1}
A_v	Vertical eddy viscosity	m^2 s^{-1}
A_b	Vertical diffusivity coefficient	m^2 s^{-1}
Source Terms, Grid, Flow, and Hydraulic Structures		
S_u	Momentum source/sink term	m^2 s^{-2}
S_h	Source/sink term in the continuity equation	m^3 s^{-1}
C_s	Smagorinsky coefficient	–

Symbol / Abbreviation	Definition	Unit
Δx	Grid-cell size in the longitudinal direction	m
Δy	Grid-cell size in the transverse direction	m
Q	Discharge	$m^3\ s^{-1}$
$Q_{in,t}$	Daily inflow discharge at time t	$m^3\ s^{-1}$
$Q_{out,t}$	Daily outflow discharge at time t	$m^3\ s^{-1}$
V_t	Reservoir volume at time t	m^3
V_{t-1}	Reservoir volume at the previous time step	m^3
C_d	Gate discharge coefficient	–
b	Effective gate width	m
A	Flow cross-sectional area	m^2
H_{HW}	Upstream head at the hydraulic structure	m
w_{sc}	Settling velocity of the transported constituent	$m\ s^{-1}$
S_c	Transported-constituent source/sink term	$mg\ L^{-1}\ s^{-1}$
Reaction Kinetics		
K	Decay coefficient or reaction-rate constant	d^{-1}
θ	Temperature correction coefficient for reaction rates	–
T_{ref}	Reference temperature for the reaction	°C
Air–Water Heat Exchange		
H_L	Longwave radiation flux	$W\ m^{-2}$
H_E	Latent heat flux	$W\ m^{-2}$
H_C	Sensible heat flux	$W\ m^{-2}$
H_n	Net heat flux	$W\ m^{-2}$
ε	Water-surface emissivity	–
σ	Stefan–Boltzmann constant	$W\ m^{-2}\ K^{-4}$
T_s	Water-surface temperature	°C
T_a	Air temperature	°C
T_e	Equilibrium temperature	°C
T_d	Dew-point temperature	°C
e_a	Actual vapor pressure of air	Pa
e_s	Saturation vapor pressure	Pa
P_a	Atmospheric pressure	Pa
B_c	Cloud-cover coefficient	–

Symbol / Abbreviation	Definition	Unit
c_e	Latent heat transfer coefficient	–
c_h	Sensible heat transfer coefficient	–
ρ_a	Air density	kg m^{-3}
L_E	Latent heat of vaporization	J kg^{-1}
W_s	Wind speed	m s^{-1}
$c_{p,a}$	Specific heat capacity of air	J kg^{-1} °C^{-1}
K_{aw}	Air–water heat exchange coefficient	W m^{-2} °C^{-1}
Solar Radiation and Light Attenuation		
I_0	Incoming solar radiation	W m^{-2}
I_{sw}	Shortwave radiation flux	W m^{-2}
S_f	Shading coefficient	–
K_{ess}	Total light-extinction coefficient	m^{-1}
$K_{e,b}$	Background light-extinction coefficient of water	m^{-1}
$K_{e,TSS}$	Light-extinction coefficient due to total suspended solids	m^{-1} per g m^{-3}
$K_{e,POC}$	Light-extinction coefficient due to particulate organic carbon	m^{-1} per g m^{-3}
$K_{e,DOC}$	Light-extinction coefficient due to dissolved organic carbon	m^{-1} per g m^{-3}
$K_{e,chl}$	Light-extinction coefficient due to chlorophyll-a	–
Water Quality Constituents and Oxygen-Demand Terms		
TSS	Total suspended solids	mg L^{-1}
POC	Particulate organic carbon	mg L^{-1}
DOC	Dissolved organic carbon	mg L^{-1}
Chl	Chlorophyll-a concentration	mg m^{-3}
DO	Dissolved oxygen	mg L^{-1}
SOD	Sediment oxygen demand	g O_2 m^{-2} d^{-1}
CSOD	Carbonaceous sediment oxygen demand	g O_2 m^{-2} d^{-1}
NSOD	Nitrogenous sediment oxygen demand	g O_2 m^{-2} d^{-1}

1 Introduction

1.1 Introduction

Water, as one of the most vital natural resources, plays a key role in ecosystem sustainability, meeting human needs, and supporting sustainable development. Reservoirs, as critical infrastructures for meeting diverse societal demands, including drinking water supply, agriculture, industry, hydropower generation, and flood control, are of great importance [1]. However, population growth and economic development have placed considerable pressure on these resources and have created complex challenges related to both water quantity and quality, threatening human health and the environment.

In many developing countries, including Iran, water scarcity and pollution of water resources have intensified simultaneously over recent decades. Iran's mean annual precipitation is 228 mm, which is less than one-third of the global average of 813 mm, and about 66% of this precipitation evaporates before reaching rivers, thereby exacerbating water scarcity. At the same time, rivers and reservoirs have become heavily polluted due to the discharge of industrial, urban, and rural wastewater, agricultural effluents containing organic matter and waste materials, and even acid rain, which both degrade water quality and damage aquatic ecosystems [1]. These conditions indicate the convergence of stresses on the quantity and quality of water resources. Reduced water volume limits the natural dilution capacity for pollutants and increases their concentrations, while pollution renders existing resources unusable and further intensifies water scarcity. This vicious cycle highlights the need for an integrated and comprehensive approach to water resources management.

Numerical modeling of water quality has emerged as an effective tool for understanding, predicting, and managing water quality issues, and has found numerous applications in research studies over more than the past four decades. Earlier process-based models were mainly simple and one-dimensional and were limited to predicting biochemical oxygen demand and dissolved oxygen. With advances in computational technologies and a deeper understanding of environmental processes, models have moved toward multidimensional, dynamic, and multi-factor simulations capable of representing complex interactions within aquatic ecosystems [2]. Three-dimensional numerical hydrodynamic and water quality models, by representing processes of transport and circulation of mass and energy, external environmental forcings, biochemical reactions, and interactions among water quality parameters in eutrophication processes, provide a more realistic and accurate representation of the real world and enable the assessment of natural and anthropogenic scenarios across temporal and spatial scales. Such detailed modeling enables optimal design, assessment of past, present, and future performance, comparison of different

management options, and evidence-based decision-making, thereby elevating the role of models from merely predictive tools to essential decision-support systems.

Water quality management in reservoirs through approaches such as: (a) controlling pollution sources at the watershed scale, (b) in-situ measures with physical, chemical, and biological characteristics, and (c) reservoir operation policies, has attracted the attention of researchers, decision-makers, planners, and managers for more than the past five decades. Understanding each strategy for improving reservoir water quality, along with the governing equations and processes involved, is highly important in selecting and planning actions to achieve management objectives. Moreover, modeling based on tools capable of representing reservoir water quality conditions under complex and interrelated physical, chemical, and biological processes, together with broad multidimensional, irregular, and complex geometric, hydrological, hydraulic, structural, and pollution-related characteristics, and also capable of simulating the implementation of management approaches, plays a valuable role in supporting decision-making and planning.

Reservoir operation policies, as non-structural, environmentally friendly, and economical measures, affect internal mass and energy circulation processes and influence the transport and dispersion of water quality constituents at longitudinal, lateral, and vertical scales, thereby manifesting in the reservoir's water quality response. The application of numerical hydrodynamic and water quality modeling tools with this level of capability and efficiency in the operation and water quality management of large, long, and wide reservoirs in Iran can open new horizons for researchers and planners in the field of aquatic environmental resources. The EFDC+ (Environmental Fluid Dynamics Code) numerical hydrodynamic and water quality model is a multipurpose model capable of simulating flows, constituent transport, and biochemical and biological processes while accounting for complex geometric features and hydraulic operation structures of reservoirs. Due to its high accuracy and adaptability to different conditions, it is a suitable option for water quality management studies [3]. This numerical model has been successfully applied in more than 100 international studies, including the representation of hydrodynamic and water quality conditions in reservoirs, assessment of the effects of pollution sources on reservoir water quality, and other related applications, and has served as an effective tool for supporting management decisions. Understanding the capabilities and performance of such models can provide access to new and up-to-date tools for both research and practical applications in the country.

1.2 Problem Statement

Reservoirs, as key infrastructure projects, play a vital role in economic, social, and environmental development. These structures are constructed for hydropower generation, storage and supply of agricultural water, flood control, and drinking water supply. However, their large dimensions, high storage capacity, and multipurpose functions have made the management of these resources

complex. Characteristics such as great depth, complex geometry, and long residence time lead to specific water quality and biological processes, making sustainable management essential.

One of the most important water quality issues is thermal stratification. This phenomenon occurs particularly during warm seasons, from late spring to early autumn, and creates separate layers within the water column due to density differences caused by temperature variations. Such conditions restrict vertical mixing and deplete the deep layers of oxygen, leading to consequences such as the release of phosphorus and heavy metals, production of toxic gases such as H_2S, and threats to aquatic ecosystems [4]. Nutrient inputs from the watershed also increase the risk of eutrophication and algal blooms.

Two-dimensional models such as CE-QUAL-W2, due to the assumption of uniform hydrodynamic and water quality conditions in the lateral direction, are not capable of fully representing flows and pollutant transport in wide reservoirs such as Seymareh, which has an average width of 1.5 km at normal water level. Therefore, a research gap exists in this regard. EFDC+, as an advanced three-dimensional tool, can accurately simulate flows, constituent transport, and chemical and biological reactions, and can address this gap. This model also covers complex chemical and biological processes and has produced noteworthy results in international studies [3].

Riverine water resources and reservoirs play an important role in supplying drinking, agricultural, and industrial water. However, population growth, urbanization, and changes in consumption patterns have placed substantial pressure on them. Direct discharge of urban, industrial, and agricultural wastewater has caused widespread pollution and degradation of water quality. Pollutants include industrial and urban wastewater, agricultural effluents, rainfall-induced surface runoff, acid rain, and metal-bearing sediments. The combined effects of these pollutants lead to water quality deterioration, degradation of ecosystems, increased risk of diseases, and reduced efficiency and service life of hydraulic structures.

Therefore, sustainable water quality management in reservoirs requires modern approaches and accurate three-dimensional modeling to represent existing conditions and evaluate multiple natural and anthropogenic scenarios. The use of three-dimensional hydrodynamic and water quality models such as EFDC+ makes it possible to predict, assess, and sustainably manage these water bodies and provides a basis for scientific and evidence-based decision-making.

1.3 Importance and Necessity of the Research

Water quality management in reservoirs, especially in arid and semi-arid regions such as Iran, is one of the major challenges faced by developing societies. Seymareh Reservoir, located in Ilam Province, as a vital resource for agriculture and energy production, faces several water quality issues, highlighting the need for advanced research for its modeling and management. The use of the three-dimensional EFDC+ model enables accurate simulation of flows, pollutant transport, and

chemical and biological processes, and provides a practical tool for scientific and managerial decision-making.

This research is important from several perspectives:

1. Preserving the health of the reservoir aquatic ecosystem: The capability to model oxygen depletion in deep layers, which can lead to widespread mortality of aquatic organisms and the release of harmful compounds such as iron, manganese, and sulfide, makes it possible to predict and control these critical conditions [4].

2. Management of eutrophication and algal blooms: This research investigates the causes of excessive algal growth resulting from excessive nutrient inputs, such as nitrogen and phosphorus, and provides a tool for evaluating control strategies. Eutrophication in reservoirs, particularly in areas receiving inflows containing agricultural and urban wastewater, leads to water quality degradation, production of toxic algae, and increased algal biomass [5]. By simulating hydrodynamic, physical, biological, and chemical processes, the EFDC+ model enables prediction and management of this phenomenon in Seymareh Reservoir, drawing upon successful experiences from its application in similar reservoirs.

3. Providing a decision-support tool for managers: The calibrated model allows dam managers and relevant organizations to simulate and evaluate the effects of different management scenarios, such as changes in dam operation or implementation of pollution reduction measures, before costly real-world implementation. Previous studies have emphasized that hydrodynamic models such as EFDC+, as decision-support tools, can reduce management costs and increase efficiency. This is essential for Seymareh Reservoir, which is affected by human activities.

4. Scientific advancement and addressing the existing research gap: By applying an advanced three-dimensional model, EFDC+, this research overcomes the limitations of previous studies that used two-dimensional models to represent reservoir conditions and provides a more accurate understanding of complex hydrodynamic and water quality processes in Seymareh Reservoir. Three-dimensional models such as EFDC+, due to their capability to simulate thermal stratification, biochemical processes, and algal bloom dynamics, perform better in studies of deep reservoirs with extensive lateral geometry [6]. By focusing on Seymareh Reservoir, which has been the subject of limited research, this study contributes to enriching the scientific literature.

5. Prediction of future impacts: The developed model can be used to predict the effects of external factors, such as climate change or changes in pollutant loading from the watershed, on reservoir water quality in the future. Climate change, through increasing temperature and altering precipitation patterns, can affect thermal stratification, runoff, and phosphorus

loading, leading to greater eutrophication [7]. The application of EFDC+ in forward-looking scenarios enables long-term planning for Seymareh Reservoir.

6. Improving the economic operation of the dam: By managing water quality and preventing undesirable conditions, such as water containing hydrogen sulfide, pH variations, and other adverse conditions, damage to dam facilities, including turbines, can be prevented and maintenance and treatment costs can be reduced. Studies show that water quality phenomena such as H_2S production under oxygen-depleted conditions can lead to equipment corrosion and impose high economic costs [4]. The capability of EFDC+ to simulate such events and predict their occurrence can help optimize the economic operation of Seymareh Dam.

Overall, this research not only addresses local issues in Seymareh Reservoir, but also provides a model for water resources management in other reservoirs in Iran and contributes to environmental and economic sustainability by emphasizing advanced modeling approaches.

1.4 Research Objectives

- Three-dimensional hydrodynamic and water quality modeling of the reservoir, as a reservoir affected by eutrophication and algal blooms, using the EFDC+ model over the long term.
- Investigation of the effect of reservoir operation policy, within the framework of selective withdrawal, on reservoir water quality.
- Evaluation of the performance and capabilities of the EFDC+ model in representing the water quality conditions of Seymareh Reservoir.

1.5 Scope and Extent of the Research

The scope and extent of this research, in order to focus on the key dimensions of the problem and ensure achievement of the defined objectives, are specified as follows:

- Geographical scope: This research focuses on Seymareh Reservoir. The Seymareh River is formed by the confluence of the Qarah Su and Gamasiab rivers and, after receiving flows from tributaries along its course, supplies the inflow to the reservoir; approximately 40% of the reservoir inflow is attributed to these tributaries [8].
- Temporal scope: The time period used for model calibration, based on available data, was defined from June 2016 to February 2017. Reservoir performance over the long-term period from March 2014 to March 2024 was evaluated using the EFDC+ model.
- Parameter scope: This study focuses on the simulation of key physical and biogeochemical parameters that are directly related to thermal stratification and eutrophication. These parameters include temperature, dissolved oxygen, nitrogen compounds including ammonium (NH4) and nitrate (NO3), phosphate (PO4), BOD5, and chlorophyll-a as an indicator of algal biomass. The present study does not address other pollutants such as heavy metals.

- Modeling tool: The main tool used in this research is the three-dimensional EFDC+ model. The focus of the study is on the capabilities of this software.
- Research limitations: This study faced several limitations that should be considered when interpreting the results. One of the main challenges was the lack of comprehensive water quality data for Seymareh Reservoir. Despite extensive searches, access to a complete long-term dataset for all target parameters was not possible, which may affect the model calibration processes.

1.6 Thesis Structure

This thesis has been prepared in five chapters in order to achieve the research objectives in a logical and coherent manner.

Chapter 1 presents the general framework of the research, the problem statement, the importance and necessity of the study, and the definition of the main objectives and research questions. In this chapter, the overall framework of the study and the roadmap for the subsequent chapters are outlined.

Chapter 2 is devoted to a comprehensive review of theoretical foundations and previous studies. In this chapter, the physical and biogeochemical processes governing reservoirs are described, and similar modeling studies conducted in Iran and worldwide are reviewed.

Chapter 3 describes the research methodology in detail. This chapter includes a complete introduction to the study area, Seymareh Dam, an explanation of the theoretical basis and capabilities of the EFDC+ model, as well as the technical details of model development, preparation of input data, and the model calibration process.

Chapter 4 presents the results and discusses them. In this chapter, the results of the model calibration stage are compared with observational data, and the model performance in representing real-world conditions is evaluated to an acceptable extent. Then, by analyzing the model outputs, the long-term hydrodynamic dynamics and water quality of the reservoir are examined. Subsequently, the effect of selective withdrawal on reservoir water quality and the quality of the outflow is investigated.

Finally, Chapter 5 is devoted to summarizing the main findings of the research, drawing conclusions, and providing recommendations for future studies, as well as practical suggestions for improved water quality management of Seymareh Reservoir.

2 Technical Background and Literature Review

2.1 Introduction

Every scientific study requires the establishment of a solid theoretical foundation and a clear understanding of previous achievements in the relevant field. Before addressing complex issues such as water quality modeling in Seymareh Reservoir, it is essential to identify the fundamental processes governing these systems and to determine the position of the present research within the existing body of knowledge. The objective of this chapter is to establish the conceptual and theoretical framework for the present study. In this chapter, after analyzing previous studies, the current state of knowledge in this field is evaluated and research gaps are identified. The chapter begins by reviewing the theoretical foundations of physical and biogeochemical processes and describes the mechanisms controlling reservoir ecosystem dynamics, including thermal stratification and nutrient cycles. Then, water quality management strategies and the role of modeling in their evaluation are discussed, and the advanced EFDC+ model is introduced as the selected tool for this research. Finally, the chapter concludes by summarizing the findings and identifying the research gap, thereby clarifying the need to develop a comprehensive three-dimensional model for Seymareh Reservoir.

2.2 Theoretical Foundations of Physical and Biogeochemical Processes in Reservoirs

A comprehensive understanding of water quality dynamics in complex aquatic systems such as reservoirs requires a deep knowledge of physical, chemical, and biological processes and their complex interactions. Unlike rivers, where flow is continuously moving, reservoirs have unique characteristics due to their long residence time and low flow velocity, which make them complex biogeochemical reactors [9, 10]. Physical processes, such as thermal stratification and hydrodynamic patterns, provide the main framework and setting for the occurrence of biogeochemical reactions. By creating distinct zones within the water column, these processes control the rate and type of chemical and biological reactions and determine the spatial and temporal distribution of key water quality variables, such as dissolved oxygen, nutrients, and phytoplankton communities [11]. Therefore, any attempt to model reservoir water quality must begin with a precise understanding of these fundamentals, because the accuracy of biogeochemical process simulation strongly depends on the accurate representation of physical processes. This section is devoted to explaining the scientific foundations of these key processes.

2.2.1 Physical Processes

Physical processes determine the hydrodynamic and thermal structure of the reservoir and directly affect the dynamics of biogeochemical processes. These processes include the absorption and distribution of thermal energy, as well as water movement and mixing patterns, which define the physical structure of the water column and influence all ecological and chemical aspects of the reservoir.

2.2.1.1 Thermal Stratification

Thermal stratification is one of the most fundamental physical phenomena in lakes and deep reservoirs in temperate regions. It refers to the tendency of the water column to form distinct and stable layers with different temperatures and densities during warm seasons [9, 10]. This natural phenomenon has profound consequences for reservoir water quality and ecology.

• Formation mechanism: The density of freshwater reaches its maximum at approximately 4 °C. With increasing solar radiation in spring, surface layers warm more rapidly than deeper layers. Warmer water, with lower density, remains above colder and heavier layers, and the resulting density difference creates a buoyancy force that resists wind-induced mixing and forms a stable layered structure. The relatively calm flow conditions in reservoirs further enhance the tendency toward stratification [9].

• Three-layer structure: During the period of stable stratification, the water column is generally divided into three main layers (Figure 2-1):

1. Epilimnion: the warmest and least dense layer, in direct contact with the atmosphere; it is characterized by relatively uniform temperature and high dissolved oxygen due to photosynthetic activity and atmospheric exchange.
2. Hypolimnion: a cold, dense, and dark layer that extends to the bed. This layer is isolated from light and air and is prone to severe oxygen depletion.
3. Metalimnion: this transitional layer lies between the epilimnion and the hypolimnion, and its main characteristic is a rapid decrease in temperature with increasing depth. Within this layer, there is a plane with the maximum temperature gradient, known as the thermocline. The thermocline acts as a physical barrier and strongly limits vertical mixing and the exchange of water, nutrients, and dissolved gases, such as oxygen, between surface and deep layers. This separation is the main cause of many water quality problems in the deep layers of reservoirs [9].

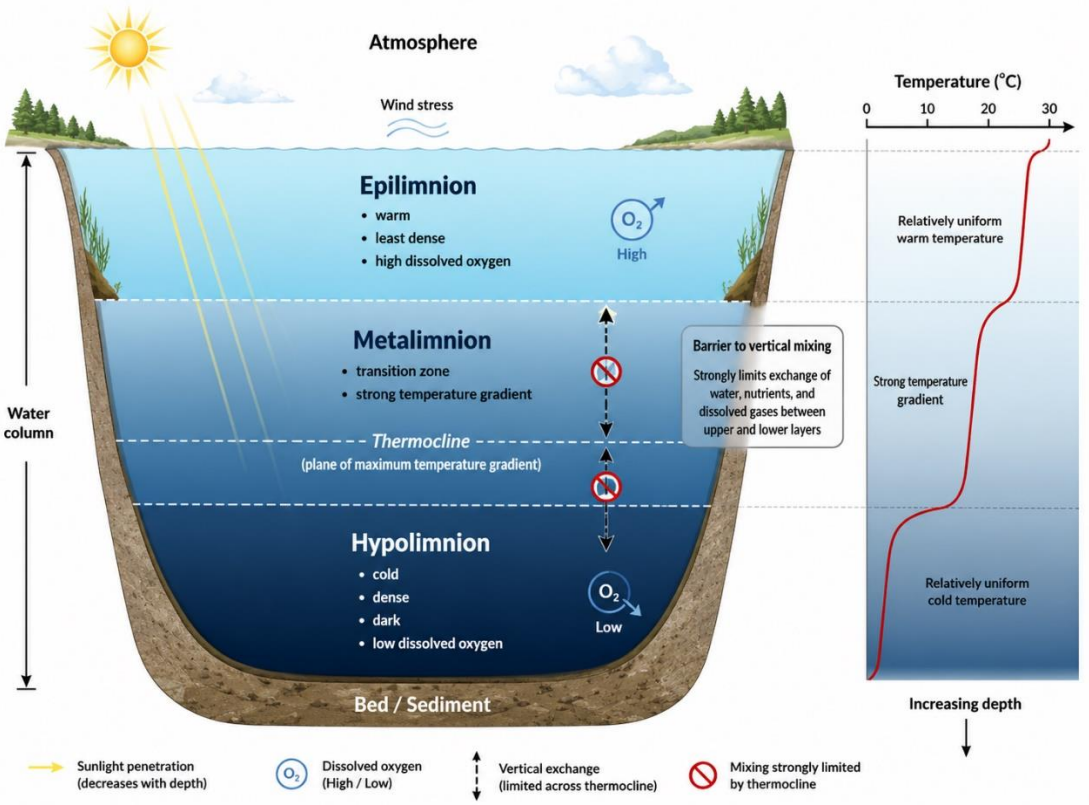

Figure 2-1. Three-layer thermal stratification structure in the reservoir water column

This three-layer structure is not a fixed and permanent feature, but rather a dynamic condition that evolves throughout the year in response to seasonal climatic variations. The formation, stability, and eventual breakdown of this stratification follow a predictable annual pattern, and understanding this pattern is essential for analyzing the overall dynamics of the reservoir.

Seasonal stratification cycle: In reservoirs located in temperate regions that mix twice a year (dimictic lakes), stratification follows a predictable seasonal cycle:

1. Onset of stratification (spring): After the melting of winter ice, increasing air temperature and solar radiation warm the surface water to above 4 °C, making it lighter than the deeper water. As a result, the stratification process begins.
2. Summer stability: During summer, the temperature and density differences between the surface layer and the bottom layer reach their maximum, and the stratified structure attains its most stable state, becoming highly resistant to wind energy.
3. Autumn turnover: As the air cools in autumn, the surface water in the upper layer becomes cooler, denser, and sinks downward. This process gradually weakens and breaks down the thermocline until the entire water column reaches a nearly uniform temperature. Under these conditions, wind is able to mix the entire reservoir from the surface to the bed. This event, known as “turnover” or “autumn turnover,” is vital for the reservoir

ecosystem because it transports oxygen to the deep layers and brings nutrients accumulated in the hypolimnion to the surface.

Thermal stratification is not merely a physical phenomenon; rather, it acts as a major controlling factor that governs nearly all biogeochemical processes in a deep reservoir. By creating two separate reactors—an aerobic upper layer and a potentially anaerobic lower layer—this phenomenon is directly responsible for the development of oxygen depletion at depth and the accumulation of nutrients [12]. Therefore, any water quality model must first be capable of accurately simulating the timing of onset, the intensity, and the breakdown of stratification, because errors in this physical component will propagate into all dependent biogeochemical predictions. Studies conducted on Iranian reservoirs, such as Karun and Latyan, have also confirmed that this process is the dominant physical driver in these reservoirs [13, 14]. In addition, studies indicate that climate change, through rising air temperature, prolongs the stratification period and makes the thermocline shallower, thereby intensifying the negative consequences of stratification, such as oxygen depletion in deep layers [14].

2.2.1.2 Reservoir Hydrodynamics

Unlike rivers, where flow is mainly governed by gravitational force, water movement in reservoirs is driven by a more complex set of forces. Understanding these motion patterns is essential for predicting how heat, nutrients, pollutants, and microorganisms are distributed and transported within the reservoir. The principal driving forces in reservoir hydrodynamics include inflow and outflow currents, wind stress, and buoyancy forces caused by surface heating and cooling.

- Inflow and outflow currents: Inflows from rivers and outflows through dam structures generate important circulation patterns within the reservoir. In particular, differences in density between the incoming water and the ambient reservoir water lead to a phenomenon known as density-driven currents. These density differences may arise from variations in temperature, suspended solids (turbidity), or dissolved solids [15]. Depending on its relative density, the inflow may follow one of three main paths:

    1. Underflow: This occurs when the incoming water, such as cold and sediment-laden floodwater, is denser than the surface water of the reservoir. In this case, the inflow plunges beneath the surface water at a point known as the plunge point and then travels along the bed toward the dam.
    2. Interflow: If the density of the incoming water lies between the densities of the surface and bottom layers of the reservoir, the flow separates from the bed after plunging and spreads horizontally at the depth where its density matches that of the ambient reservoir water. This type of flow usually occurs within the intermediate layer.
    3. Overflow: If the incoming water is lighter than the surface water of the reservoir, such as warm water in summer, it remains buoyant and moves along the surface.

These currents are not merely a hydrodynamic phenomenon; they also act as the principal carriers for injecting external loads of nutrients, sediments, and pollutants into specific layers of the

reservoir [16]. For example, an interflow can directly transport nutrients into a zone with sufficient light but limited mixing, thereby causing a subsurface algal bloom. Similarly, an underflow can deliver nutrient-rich sediments directly into the hypolimnion, where they may later serve as a source of internal loading [9].

- Wind stress: By applying shear stress to the water surface, wind transfers energy to the reservoir. This energy generates surface currents, waves, and turbulence and is the principal driver of mixing in the surface layer. Persistent wind blowing in one direction can tilt the thermocline. After the wind ceases, the thermocline begins to oscillate in order to regain equilibrium. These large-scale oscillations, known as internal waves, can cause significant displacement of water and materials within different parts of the reservoir.
- Convective currents: Surface water cooling, especially at night and during autumn, increases the density of surface water. This heavier water moves downward and mixes with the underlying waters. This process, known as autumn turnover, is one of the major mechanisms of vertical mixing in the surface layer and the gradual weakening of thermal stratification during autumn [17].

2.2.1.3 Dissolved Oxygen Dynamics

Dissolved oxygen (DO) is one of the most important indicators of aquatic ecosystem health because it is essential for the respiration of most aquatic organisms. The dissolved oxygen concentration in a reservoir results from the dynamic balance between oxygen-producing and oxygen-consuming processes.

• Sources of oxygen: There are two primary sources of oxygen input to reservoir water:

1. Surface reaeration: This refers to the direct transfer of oxygen from the atmosphere to the surface layer of the water. The rate of this transfer depends on turbulence at the water surface, which is primarily generated by wind. During periods of complete mixing, surface reaeration is the principal source of oxygen supply to the reservoir.
2. Photosynthesis: Oxygen is produced by phytoplankton and aquatic plants as a by-product of photosynthesis. This process occurs only during daylight hours and within the euphotic zone, which is generally limited to the surface layer, and constitutes an important source of oxygen [15].

• Oxygen-consuming processes: Several biological and chemical processes continuously consume dissolved oxygen:

1. Respiration: All aerobic organisms, including phytoplankton, zooplankton, fish, and bacteria, consume oxygen continuously for their metabolic activities.
2. Decomposition of organic matter: Aerobic bacteria consume large amounts of oxygen while decomposing dead organic matter, such as algae that settle from the surface layer. This oxygen demand can be divided into two main components: water-column oxygen demand, associated with the decomposition of suspended organic matter, and sediment oxygen demand, which occurs at the sediment–water interface during the decomposition

of deposited organic matter. Among these processes, sediment oxygen demand is one of the most important causes of oxygen depletion in the hypolimnion.
3. Nitrification: The microbial oxidation of ammonium to nitrate is a strictly aerobic process that consumes a substantial amount of oxygen and plays an important role in oxygen depletion within the hypolimnion [15].

Development of hypoxia and anoxia: The interaction between thermal stratification and oxygen-consuming processes is the primary cause of water quality deterioration in deep reservoir layers. The thermocline isolates the hypolimnion from surface oxygen sources. At the same time, the continuous settling of dead organic matter from the surface layer into the hypolimnion provides the substrate required for microbial decomposition. This imbalance between the limited oxygen supply and high oxygen demand results in a gradual decline in dissolved oxygen concentrations in the hypolimnion. The condition initially develops into hypoxia, defined as a DO concentration below 2 mg/L, and may ultimately progress to anoxia, defined as the complete absence of dissolved oxygen [12].

2.2.1.4 Eutrophication and Phytoplankton Dynamics

Eutrophication is the process through which a water body becomes enriched with nutrients, particularly nitrogen and phosphorus compounds. This enrichment increases primary production, including the growth of algae and aquatic plants, and ultimately results in water quality deterioration and disruption of ecosystem balance. Nutrient sources are divided into two main categories:

1. External loading: Nutrients entering the reservoir from the watershed through agricultural runoff and municipal and industrial wastewater discharges.
2. Internal loading: The recycling and release of nutrients previously accumulated in reservoir bed sediments. This process, particularly for phosphorus, is intensified under anoxic conditions in the hypolimnion and may delay water quality recovery for many years, even after external nutrient loads have been reduced.

One of the most evident signs of eutrophication is the occurrence of algal blooms, which refers to the rapid growth and accumulation of phytoplankton. This phenomenon has several adverse consequences, including a substantial reduction in water transparency that limits the growth of rooted aquatic plants, the production of unpleasant taste- and odor-causing compounds by certain species that increase drinking-water treatment costs, and considerable oxygen consumption during the decomposition of algal biomass, which further intensifies hypoxia. In addition, certain cyanobacterial species, also known as blue-green algae, can produce hazardous toxins known as cyanotoxins, which are harmful to both aquatic organisms and humans [18].

Phytoplankton communities undergo dynamic changes throughout the year, a pattern known as seasonal succession. In reservoirs located in temperate regions, diatoms, which possess siliceous cell walls, generally dominate during spring, when the water is cold, nutrient-rich, and actively mixing. With the onset of thermal stratification in summer, rising temperatures and declining nutrient concentrations, particularly nitrogen, create favorable conditions for cyanobacterial growth [19, 20]. Many cyanobacteria can outcompete other species because of adaptive

characteristics such as their ability to regulate buoyancy to access light and nutrients and, in some species, their ability to fix atmospheric nitrogen [18].

Eutrophication does not merely involve a quantitative increase in algal biomass; it also represents a qualitative shift toward less desirable species. Because of their large size and filamentous or colonial forms, cyanobacteria are not readily consumed by zooplankton, and some species are also toxic. Consequently, the energy produced by cyanobacteria is not efficiently transferred to higher trophic levels of the food web [19]. Instead, after death, their large biomass settles into the deeper layers, where its decomposition intensifies oxygen consumption and internal nutrient loading, thereby perpetuating a self-reinforcing cycle.

2.2.1.5 Phosphorus Cycle

Phosphorus is considered the limiting nutrient in most freshwater ecosystems; therefore, its management is one of the principal strategies for controlling eutrophication [10]. Unlike nitrogen, the phosphorus cycle does not have a significant gaseous phase, and its primary natural source is the weathering of phosphate-bearing rocks within the watershed.

The most important internal process in the phosphorus cycle is its release from bed sediments under anoxic conditions. Under oxic conditions, phosphate binds to iron oxides and hydroxides and is retained within the sediments. However, when oxygen concentrations decline in the hypolimnion, ferric iron, Fe(III), is reduced to ferrous iron, Fe(II). This reduction disrupts the iron–phosphate bond, resulting in the release of dissolved phosphate from the sediments into the water column.

Consequently, sediments in eutrophic reservoirs can act as a persistent internal source of phosphorus. Even after external nutrient loading has been reduced, the release of phosphorus accumulated in sediments as a result of historical loading may continue for many years and sustain recurring algal blooms. This process is one of the principal reasons for delayed water quality recovery in reservoirs and lakes [10].

2.2.1.6 Nitrogen Cycle

Nitrogen is also an essential element for life and plays a fundamental role in the structure of amino acids and proteins. Although phosphorus is generally the primary limiting nutrient, nitrogen may also limit growth under certain conditions. The nitrogen cycle is more complex than the phosphorus cycle because nitrogen occurs in several chemical forms that are transformed through microbial processes.

The main processes involved in the nitrogen cycle are as follows:

1. Mineralization or ammonification: During this process, organic nitrogen contained in dead cells and waste materials is converted into ammonium (NH_4^+). This process can occur under both aerobic and anaerobic conditions.

2. Nitrification: This is an aerobic process in which ammonium is first converted into nitrite and then into nitrate. Nitrification is one of the major oxygen-consuming processes in the water column and sediments.
3. Denitrification: This process occurs under anoxic conditions, during which nitrate is converted into nitrogen gas (N2) and removed from the aquatic system. Denitrification is the most important natural mechanism for the permanent removal of nitrogen from aquatic ecosystems [21].

The nitrogen cycle is strongly dependent on oxygen conditions. Nitrification occurs in oxygenated zones, particularly in the surface layer and other oxygenated parts of the reservoir, whereas denitrification is limited to anoxic environments, such as sediments and deeper water layers. This spatial separation is an important consideration in reservoir water quality modeling [21].

2.3 Water Quality Management Strategies and the Role of Modeling in Their Evaluation

Water quality management in reservoirs, particularly large and strategically important reservoirs, requires a comprehensive and preventive approach. The principal threats to water quality in these reservoirs include excessive nutrient inputs, algal blooms, and the development of persistent thermal stratification, which may lead to oxygen depletion in deeper layers. In this context, numerical modeling is an effective tool for predicting reservoir responses to natural pressures and human interventions and for evaluating management strategies before their actual implementation [22].

Reservoir water quality management strategies can be classified into three main groups:

1. External load management: focusing on controlling pollutants at the watershed scale.
2. In-situ measures within the reservoir: including physical, chemical, and biological methods for controlling internal loading, reducing algal growth, and improving oxygen conditions.
3. Reservoir operation management: including modification of withdrawal patterns, scheduling of releases, and selective withdrawal from different elevations to influence stratification, residence time, outflow water quality, and nutrient distribution.

2.3.1 Modeling as a Decision-Support Tool

Numerical water quality models such as EFDC+ integrate physical, chemical, and biological processes within a mathematical framework and therefore function as a “virtual laboratory.” These models allow the investigation of different management scenarios whose full-scale implementation is generally costly, difficult, or associated with considerable risk. Consequently, models play an important role in decision-support systems by helping managers compare the consequences of different alternatives before implementation [22].

An example of numerical model application is a study conducted on Buyuk Melen Reservoir in Türkiye [23]. In that study, three management scenarios were evaluated using the CE-QUAL-W2 model:

1. No-action scenario, which resulted in hypertrophic conditions and severe algal blooms.
2. Control of point sources, in which the treatment and diversion of municipal and industrial wastewater considerably improved water quality.
3. Simultaneous control of point and nonpoint sources, which produced the greatest improvement in water quality.

An important consideration in such studies is that the primary value of models, particularly under data-limited conditions, lies more in the relative comparison of scenarios than in the absolute prediction of values. In other words, even when uncertainty exists in the exact model outputs, the model can still identify which management alternative is more effective. This capability makes modeling an efficient tool for scientific decision-making and management planning [23].

2.3.2 External Load Management and Integrated Evaluation Using Modeling

External loads refer to pollutants, particularly nutrients and sediments, that originate from the upstream watershed and enter the reservoir through tributary rivers. Reservoir water quality cannot therefore be assessed independently of watershed conditions, because the reservoir's water quality reflects the hydrological and environmental processes occurring throughout the entire watershed. Consequently, evaluating external-load management measures, such as improving agricultural practices or upgrading wastewater treatment facilities, requires an integrated approach that quantitatively represents the relationship between watershed processes and reservoir responses [24].

One commonly used framework in this field is the coupling of the SWAT watershed model with the EFDC+ reservoir model [24]. Within this framework, SWAT simulates rainfall-runoff processes, erosion, sediment transport, and pollutant-load generation at the watershed scale. This model is particularly suitable for assessing the effects of measures such as conservation agriculture, vegetated buffer strips, fertilizer management, and other management practices intended to reduce incoming loads. SWAT outputs, including discharge and pollutant concentrations, are subsequently introduced into EFDC+ as boundary conditions to simulate the hydrodynamic and water quality responses of the reservoir. EFDC+ is responsible for simulating hydrodynamic, transport, and biogeochemical reaction processes within the reservoir.

The principal advantage of this approach is that it continuously represents the cause-and-effect chain extending from watershed management to reservoir water quality. In other words, it allows assessment of how a watershed-scale change, such as reduced fertilizer application or improved runoff control, affects incoming nutrient loads and ultimately influences parameters such as chlorophyll-a, dissolved oxygen, and the probability of algal blooms within the reservoir. The integrated framework applied in that study transformed recognized qualitative relationships into

quantitative, causal predictions and bridged the gap between watershed-management policies and water-resource protection.

Another important consideration in this type of modeling is uncertainty. In practice, different combinations of watershed-model parameters may generate acceptable results. For this reason, the principal value of integrated modeling often lies in the relative comparison of scenarios rather than solely in the absolute prediction of values. Even if some uncertainty exists in the precise estimation of concentrations, the model can still identify the more effective management alternative and estimate the extent to which it can improve reservoir water quality [24, 25]. Therefore, this approach is a suitable tool for risk-based decision-making and water quality management planning at both watershed and reservoir scales.

2.3.3 Internal Load Management, In-Situ Measures, and Reservoir Operation

Internal load management, or in-situ measures, refers to actions implemented directly within the reservoir to control problems that have already developed within the system, such as oxygen depletion in deeper layers, phosphorus release from sediments, and intensified eutrophication. These strategies are not limited to physical and chemical methods; biological measures and reservoir operation management can also contribute to controlling or mitigating the consequences of eutrophication. The evaluation of these strategies requires three-dimensional models such as EFDC+, because such models can more accurately simulate vertical and horizontal variations in water quality, thermal stratification, flow pathways, outflow water quality, and reservoir responses to changes in withdrawal elevation or timing [18].

a) Physical Measures

Two common methods in this category are artificial aeration and withdrawal from deeper layers. Artificial aeration increases oxygen concentrations in deeper waters and prevents the development of anaerobic conditions, thereby potentially reducing the release of phosphorus and certain metals from sediments. Under some conditions, aeration may also reduce the intensity of thermal stratification by promoting mixing. However, the effectiveness of aeration depends on system location, aeration intensity, and operational timing. Therefore, three-dimensional modeling is necessary for its design and optimization [19].

Another method is deep-water or hypolimnetic withdrawal. In this method, cold, nutrient-rich water is withdrawn and discharged from the deeper parts of the reservoir to prevent these nutrients from returning to the surface layer during turnover. This strategy may be effective in reservoirs where internal loading plays an important role in sustaining eutrophication [20]. Three-dimensional models are also important in this context because they can evaluate the effects of withdrawal location, release rate, and implementation timing on the reservoir’s thermal structure and water quality.

In addition to aeration and hypolimnetic withdrawal, other physical methods have been proposed to control eutrophication and reduce algal blooms in reservoirs. Floating covers can limit algal growth by reducing light and solar-radiation penetration into the water and may also decrease

evaporation in certain cases. Ultrasonic waves have also been suggested as a method for disrupting or weakening certain algal groups, particularly cyanobacteria. Nevertheless, the effectiveness of these methods depends on reservoir scale, dominant algal species, light and thermal conditions, and operational constraints. Other methods, such as mechanical mixing, horizontal flushing, and the installation of curtains perpendicular to the flow direction, may also influence reservoir water quality by modifying residence time, flow pathways, or algal access to light and nutrients.

b) Chemical Measures

One commonly used strategy in this category is phosphorus inactivation. In this method, materials such as alum are applied to immobilize dissolved phosphorus. Alum reacts with phosphorus and converts it into an insoluble form; the resulting compounds then settle and become unavailable to algae. This method can also limit the subsequent release of phosphorus from sediments [26]. However, its effectiveness depends on the applied dose, water chemistry, and reservoir characteristics. Modeling can therefore play an important role in determining the optimal dose and evaluating both short- and long-term effects.

In addition to alum, substances such as iron compounds, copper sulfate, hydrogen peroxide, and chlorine have been used in some applications to control algae or immobilize nutrients. However, chemical methods are generally associated with limitations such as toxicity to other aquatic organisms, changes in pH, short-term effectiveness, accumulation in sediments, or the formation of by-products. Their application must therefore be based on careful environmental assessment and adapted to the specific conditions of each reservoir.

c) Biological Measures

Biological strategies are based on using living organisms or modifying the biological structure of the system to reduce algal biomass and control eutrophication. These methods may involve the use of algal consumers, such as certain phytoplanktivorous fish or zooplankton, to reduce algal abundance. Aquatic plants or macrophytes may also suppress algal growth by competing for light and nutrients.

Despite their potential benefits, biological methods require caution because changes in biological-community structure may create unintended ecological consequences. For example, some consumer species may reduce beneficial phytoplankton species in addition to harmful ones or may spread beyond the intended treatment area if not adequately controlled. These methods should therefore generally be considered as part of an integrated management strategy accompanied by biological monitoring.

d) Reservoir Operation Management

In addition to controlling incoming loads and applying in-situ measures, reservoir operation can also serve as a water quality management tool. Changing the withdrawal elevation, selectively withdrawing water from different layers, adjusting the timing and magnitude of releases, and

using outlet structures at different elevations can affect thermal stratification, residence time, dissolved oxygen, nutrient distribution, algal biomass, and outflow water quality.

This method is particularly important in reservoirs equipped with outlets or intake structures at different elevations, where water can be withdrawn from different layers of the water column. Under such conditions, reservoir operation is not merely a quantitative issue associated with water supply or energy production; it can also be used as a water quality management instrument. Nevertheless, this approach may involve considerations such as changes in downstream water quality, the release of cold or nutrient-rich water, and effects on downstream river ecosystems. Its evaluation therefore requires the simultaneous modeling of hydrodynamics and water quality.

e) Trade-Off Analysis Using Three-Dimensional Modeling

The evaluation of in-situ measures and operational alternatives usually involves trade-offs between benefits and unintended consequences. For example, artificial aeration may increase dissolved oxygen in deeper layers; however, if poorly designed, it may disturb sediments and cause renewed phosphorus release. Similarly, hypolimnetic withdrawal or changes in outlet elevation may help remove part of the nutrient load from the reservoir but may adversely affect the quality of water released downstream. Certain interventions may also alter the thermal stratification structure and create unforeseen consequences for the reservoir ecosystem.

Under such conditions, three-dimensional models such as EFDC+ are suitable tools for analyzing these trade-offs because they can simultaneously simulate the positive and negative effects of a given strategy. This capability enables managers to move beyond asking only, “Is this strategy effective?” and instead determine, “At what intensity, location, and time should this strategy be implemented to maximize benefits and minimize adverse consequences?” For this reason, three-dimensional modeling in internal-load management is not merely an analytical tool but also an instrument for engineering optimization and decision support [19] [18].

2.3.4 Applications of EFDC+ in the Simulation and Management of Water Bodies

The EFDC model and its enhanced version, EFDC+, have been applied in various studies to simulate hydrodynamics, constituent transport, sediment transport, water quality, eutrophication, and management scenarios in water bodies. The importance of this model lies in its ability to represent physical and water quality processes within an integrated spatial and temporal framework. It is therefore a suitable tool for systems such as reservoirs, coastal wetlands, rivers, estuaries, and urban waterways, where interactions among flow, stratification, pollutant transport, sediment, nutrients, and dissolved oxygen are important.

In a study of Guájaro Reservoir in Colombia, EFDC+ was used to simulate hydrodynamics and manage water levels. The reservoir is connected to Canal del Dique through hydraulic structures, and water-level management is important for the sustainable provision of water resources. Model calibration results for dry and wet periods showed that EFDC+ reproduced water-level variations

with satisfactory accuracy. The study therefore demonstrated that the model can support decision-making in reservoir operation management [27].

The model was also applied to evaluate hydrodynamics and water quality in Ciénaga de Mallorquín, a coastal lagoon in Colombia. Owing to its ecological value and role in biodiversity conservation, this lagoon is included among the wetlands of international importance under the Ramsar Convention. Variables such as temperature, dissolved oxygen, nutrients, and eutrophication indicators were examined. The results showed that lagoon water quality was simultaneously affected by inflow, wind, tidal exchange, and pollutant loads and that EFDC+ simulated these spatial and temporal variations with acceptable accuracy [28].

Another important application of the model is the simulation of sediment and suspended-solids transport. Sedimentation in reservoirs not only reduces useful storage capacity but may also affect turbidity, nutrient transport, and the movement of particle-bound pollutants. In one study, the SWAT watershed model was coupled with EFDC to provide an integrated assessment of sediment generation, transport, and deposition from the upstream watershed to the downstream reservoir. Within this framework, SWAT estimated watershed runoff and sediment loads, and its outputs were introduced into EFDC as boundary conditions. This approach demonstrates that reservoir sediment management should be assessed in conjunction with watershed management [24].

EFDC+ was also used to simulate discharge and total suspended solids in the vicinity of Baekje Weir on the Geum River in Korea. The results showed that TSS concentrations increased with rainfall and that the operation of the weir gates could influence the reduction or persistence of suspended-solids concentrations both upstream and downstream. The model was therefore applied to analyze the effects of hydraulic structures on sediment transport and river water quality management [29].

In recent years, EFDC has also been used in combination with data-driven methods and machine learning. In one study, observational data, numerical-model outputs, and hyperspectral imagery were integrated in a deep-learning model to predict cyanobacterial cell concentrations. In this approach, the numerical-model outputs contributed to a better understanding of the physical and spatial conditions of the system, while the deep-learning model extracted complex patterns from multisource data [30]. In another study, reinforcement learning was used to automatically calibrate EFDC water quality parameters and improve chlorophyll-a predictions. These studies indicate that combining EFDC with artificial intelligence can contribute to the development of water quality prediction and early-warning systems [31].

EFDC has also been used for three-dimensional water quality modeling in the Chicago Area Waterway System. This system includes a network of rivers, artificial canals, treated wastewater discharges, combined sewer overflows, pumping stations, and control structures. Because of the complexity of flow and the presence of unsteady and multidirectional conditions, one- and two-dimensional models are insufficient for such a system. The use of the EFDC hydrodynamic core enabled analysis of dissolved oxygen and organic-load distributions within this complex urban system [32].

In an ecologically oriented application, EFDC was used to design a fish passage in the Dahaerteng River diversion project to Dange Reservoir in China. In this study, the velocity field near the structure and along the proposed fish-passage route was simulated so that the passage design could be matched to the biological requirements and swimming ability of the target species, a loach belonging to the genus Triplophysa. The study demonstrated that EFDC hydrodynamic outputs can also be used in the design of structures compatible with aquatic habitats [33].

In Zhangze Reservoir in China, EFDC was used to investigate the effects of wastewater-treatment-plant effluent on reservoir water quality. Different effluent-discharge scenarios and the role of a constructed wetland in supplementary treatment were evaluated. The results indicated that direct effluent discharge had a considerable effect on reservoir water quality. The constructed wetland improved water quality but was not sufficient to reduce total nitrogen and total phosphorus to the desired standards in the short term. These results showed that reservoir water quality responses to pollutant-load reduction are neither immediate nor linear and depend on residence time, hydrodynamic conditions, and internal reservoir processes [34].

Particle-tracking capability is another EFDC application. In the Yangtze River Deepwater Navigation Channel, the three-dimensional EFDC model was used to investigate the transport pathways of fine silt particles originating from dredged sediments. The results showed that particles generally moved along the river axis toward the open sea, although some entered lateral areas and increased the possibility of redeposition within the navigation channel. This application demonstrates that EFDC can be used to identify appropriate disposal locations for dredged sediment and reduce the risk of sediment returning to navigation routes [35].

In the Gallinas River in Mexico, EFDC+ was applied to estimate self-purification capacity and determine pollutant-assimilative capacity. In this type of study, the numerical model can determine the extent to which a water body can dilute pollutants and reduce their effects without water quality exceeding acceptable limits [36]. In Shenzhen Reservoir in China, a three-dimensional EFDC-based hydrodynamic and eutrophication model was developed to evaluate algal-bloom control scenarios. The results showed that eliminating nutrient loads from all inflowing tributaries alone had a limited effect on chlorophyll-a reduction, whereas controlling hydraulic conditions and reducing nutrient loading from the main water-transfer source had a greater effect on eutrophication control [37].

The integration of EFDC with geographic information systems has also been considered in some studies. In the lower Charles River Basin, coupling EFDC with GIS improved input-data preparation, data management, map-based visualization of outputs, and analysis of the spatial distribution of water quality variables. This approach can improve the efficiency of modeling and management decision-making, particularly in projects involving large volumes of spatial and temporal data [38].

EFDC has also been used to analyze salinity intrusion, inundation, the effects of major structures, and pollutant risk. In the Seomjin River in Korea, EFDC showed that flow reduction caused by dam construction and inter-basin water transfer could extend the salinity-intrusion zone upstream [39]. In the Fish River and Weeks Bay in Alabama, nested EFDC modeling was

used to examine the combined effects of storm surge and river flooding, and the results demonstrated nonlinear patterns in the expansion of inundated areas [40]. EFDC simulation in Poyang Lake, China, showed that although higher water levels may increase water storage, the associated reduction in flow velocity may increase the risk of eutrophication [41]. Hydrodynamic outputs from EFDC were also used to evaluate the risk associated with hazardous-material loading in four major lakes in China, and the results showed that the spatial distribution of risk was strongly dependent on flow patterns and water movement [42].

Another practical capability of EFDC is the simulation of wetting and drying processes in shallow environments. In Morro Bay, California, where a large portion of the area becomes exposed during low tide, the model reproduced tidal variations, temperature, salinity, flow velocity, and wetting-and-drying patterns with satisfactory accuracy. This capability is particularly important for modeling wetlands, shallow estuaries, and coastal areas subject to substantial water-level variations [43].

In Erwangzhuang Reservoir in Tianjin, China, EFDC was used to evaluate the spatial and temporal status of eutrophication. This reservoir serves as an urban water-storage source and is affected by algal growth and water quality deterioration because of its relatively limited capacity and low self-purification ability. Rather than relying only on limited monitoring-station data, the study used EFDC outputs to estimate the trophic-state index across the entire reservoir. The results showed that wind and submerged vegetation influenced water exchange and residence time. Favorable wind direction increased water exchange, whereas submerged vegetation reduced near-bed flow velocity. Water residence time exceeded one year, and water quality deteriorated during July and August. The study demonstrated that EFDC can be used not only to simulate water quality but also to classify eutrophication spatially and temporally and identify the limiting factor for algal growth [44].

In Jingpo Lake in northern China, EFDC was used to simulate water quality in a cold-region water body with seasonal ice cover. The study focused on the transport and dispersion of permanganate chemical oxygen demand (CODMn) and ammonia nitrogen (NH3-N) under open-water and ice-covered conditions. The results showed considerable differences in hydrodynamic and water quality processes between the ice-covered and open-water periods because ice cover altered flow and mixing structures, while low temperatures reduced pollutant biodegradation rates. Simulation accuracies for CODMn and NH3-N were reported as 71.90% and 79.79%, respectively. The importance of this study lies in demonstrating that climatic and seasonal conditions, particularly ice cover and temperature changes, can substantially influence reaction rates and pollutant dispersion in water quality modeling [45].

At Jordan Lake in North Carolina, USA, a three-dimensional mechanistic model based on EFDC+ was developed to evaluate water quality responses to nutrient-load reductions. The primary objective was to examine the effects of reducing nitrogen and phosphorus loads from the watershed on chlorophyll-a concentrations and the lake's trophic status. The study used five years of monitoring data, a new computational grid, and a sediment-diagenesis submodel to simulate constituent exchange between the water column and the bed more accurately. The model represented physical, chemical, and biological processes in both the water column and sediments and evaluated nutrient-reduction scenarios, the influence of Haw River inflows, and

the role of constrictions and flow-limiting passages. The study review indicated that, in eutrophic reservoirs, the evaluation of external-load-reduction scenarios must account for bed sediments, residence time, water circulation, and both short- and long-term system responses [46].

In Mamloo Reservoir in Iran, the three-dimensional EFDC model was used to simulate the thermal regime and water quality parameters. Calibration and validation data were collected from six stations over one year, and parameters including temperature, dissolved oxygen, total nitrogen, total phosphorus, and chlorophyll-a were investigated. The results showed that thermal stratification remained stable for several months, limiting oxygen transfer to deeper layers and reducing dissolved oxygen concentrations in the hypolimnion to less than 2 mg/L. The highest chlorophyll-a concentration was observed in the euphotic zone during August, and phosphorus was identified as the limiting factor for algal growth. This study is particularly relevant to the present research because it demonstrates, in an Iranian reservoir, that EFDC can represent the three-dimensional relationships among thermal stratification, deep-water oxygen depletion, phosphorus, and chlorophyll-a [47].

In Danjiangkou Reservoir in China, EFDC was used to evaluate eutrophication risk in one of the strategic reservoirs of the South-to-North Water Diversion Project. A three-dimensional eutrophication model incorporating a sediment-diagenesis submodel was developed, and variables including dissolved oxygen, ammonia nitrogen, total nitrogen, total phosphorus, and chlorophyll-a were used for model calibration and validation. The model was subsequently applied to nine scenarios involving variations in water transfer, increased total nitrogen, and reduced inflow to identify spatial and temporal patterns of algal-bloom risk. The results showed that changes in flow patterns and increased residence time could increase nutrient retention and the risk of algal growth. The emphasis on bed sediments also indicated that evaluating eutrophication based only on incoming loads is insufficient and that internal sediment fluxes must also be included in the model [48].

A comparative study of three lakes in Minnesota, USA, evaluated the performance of the one-dimensional MINLAKE model and the three-dimensional EFDC+ model in simulating temperature, ice cover, and dissolved oxygen. The results showed that EFDC+ performed satisfactorily in simulating temperature and dissolved oxygen during open-water periods, with mean RMSE values of 1.32 °C and 1.48 mg/L, respectively. However, EFDC+ predicted a shorter ice-covered period and thinner ice because it does not directly account for the effect of snow in ice simulations. The study concluded that one-dimensional models are faster and less computationally expensive for long-term simulations and climate scenarios, whereas EFDC+ is more suitable for large reservoirs or systems with multiple inflows and outflows because it represents spatial variability, complex bathymetry, and the exact locations of inflows and outlets [49].

At Asan Lake in South Korea, EFDC+ was used to develop a water-pollution accident prediction system and simulate the release of hazardous chemicals into the water body. The study reconstructed an actual 2024 release of ethylenediamine (ED) and methyl ethyl ketone (MEK) and evaluated scenarios involving changes in discharge amount, season, pollutant type, and operating conditions. To reduce computational costs and enable rapid assessment, the model's dye/tracer module was used instead of the complete chemical-fate module. The results showed

that higher discharge rates caused pollutants to arrive more rapidly, increased peak concentrations, and prolonged persistence. Summer stratification also produced vertical concentration differences and increased pollutant persistence in middle and downstream areas. This study demonstrates the importance of EFDC+ in emergency water quality management because the model can predict pollutant arrival times, peak concentrations, and high-risk areas to support rapid decision-making during contamination events [50].

Overall, the reviewed studies demonstrate that EFDC/EFDC+ is not merely a computational tool for simulating flow, but rather an integrated framework for the simultaneous analysis of hydrodynamic, thermal, sedimentary, chemical, biological, and management processes in water bodies. Applications of the model in reservoirs, wetlands, rivers, estuaries, urban waterways, and lakes have shown that water quality is generally not determined solely by incoming pollutant loads. It also depends on factors such as residence time, thermal stratification, circulation patterns, vertical exchange, internal sediment loading, operational conditions, inflows and outflows, and seasonal variations.

Among the reviewed studies, those concerning Erwangzhuang, Zhangze, Shenzhen, Jordan, Mamloo, and Danjiangkou reservoirs are more directly related to the present research because they address eutrophication, dissolved oxygen, chlorophyll-a, nutrients, bed sediments, wastewater, pollutant-load reduction, and management scenarios. In contrast, studies involving fish-passage design, tracking of dredged particles, salinity intrusion, inundation, and pollution accidents primarily demonstrate the broader range of EFDC/EFDC+ capabilities and provide complementary insight into its practical applications.

Therefore, the use of EFDC+ for Seymareh Reservoir is scientifically consistent with current research trends, because the present study also aims to conduct a three-dimensional analysis of the interactions among thermal stratification, dissolved oxygen, nutrients, BOD5, chlorophyll-a, and reservoir operation scenarios. This indicates that the selected model is suitable for investigating the principal processes controlling water quality in Seymareh Reservoir and can be used as a tool to support management decision-making.

2.4 Studies Conducted on Seymareh Dam

Studies conducted on Seymareh Dam have thus far addressed various aspects, including water quality, limnology, hydrology, and modeling, and have provided a multidimensional understanding of the reservoir’s water quality conditions.

One of the earliest comprehensive assessments was conducted by Mahab Ghodss Consulting Engineering Company in 2014 [51]. These studies, initiated following reports of fish mortality in 2011, focused on field monitoring and analysis of water quality data. The results showed that Seymareh Reservoir is susceptible to strong thermal stratification during the warm seasons, a phenomenon that causes a substantial decline in dissolved oxygen and the development of anoxic conditions in the deeper layers. By examining incoming pollutant loads, the report also classified the trophic status of the reservoir within the mesotrophic-to-eutrophic range.

Subsequently, Moradi Mousavi et al. (2021) [8] used numerical modeling to simulate the reservoir's water quality. In that study, the two-dimensional CE-QUAL-W2 model was applied to simulate the thermal profile and selected water quality parameters. The modeling results demonstrated satisfactory performance in reproducing the reservoir's thermal stratification and confirmed the findings of the Mahab Ghodss report.

In parallel with these studies, Mansour Khalifeh Nilsaz at the Iranian Fisheries Science Research Institute [52] conducted research projects to evaluate reservoir water quality and aquaculture potential. Based on water quality indices and the assessment of parameters such as chlorophyll-a, the results classified the reservoir as mesotrophic. It was also found that although parameters such as BOD5 were within the range associated with clean water, total nitrogen and total phosphorus concentrations were high at the inflow stations, primarily as a result of agricultural and urban runoff from the watershed.

To identify pollutant sources, Ganjayi and Saadatpour (2023) [53] applied the SWAT hydrological model to the Seymareh Dam watershed. Their findings showed that nonpoint pollution sources, particularly agricultural activities and soil erosion, contributed substantially to nutrient loads entering the reservoir.

Overall, previous studies have been valuable in identifying the reservoir's initial and principal problems. However, most have been descriptive in nature or have relied on two-dimensional models and watershed-oriented analyses.

2.5 Summary and Identification of the Research Gap

This chapter reviewed the theoretical foundations governing water quality dynamics in reservoirs, management strategies for controlling and improving water quality, and previous studies conducted in this field. The literature review showed that reservoirs are complex, dynamic, and multiprocess systems in which physical, chemical, and biological processes are closely interconnected and interact with one another. Therefore, understanding the mechanisms governing these interactions and predicting reservoir responses to natural and management-induced changes are essential prerequisites for achieving sustainable water quality management in such systems.

2.5.1 Summary

The review of theoretical foundations and previous studies reveals several fundamental points. First, the water quality behavior of reservoirs is fundamentally influenced by the physical structure of the water column, particularly thermal stratification. By separating surface and deep layers and restricting vertical mixing, this phenomenon creates different conditions in various parts of the water column and consequently controls the distribution of temperature, dissolved oxygen, nutrients, and other water quality variables. Accurate representation of physical processes is therefore a necessary condition for a valid analysis of reservoir biogeochemical behavior.

Second, reservoir water quality results from the simultaneous interaction of a set of interdependent processes. Reduced vertical mixing and declining oxygen concentrations at depth

can affect the fate and transport of nutrients. These changes, in turn, influence algal growth patterns, the distribution of organic loads, and water quality in different layers. Under such conditions, the responses of surface, intermediate, and deep layers are not necessarily similar, and a management intervention may have different effects in different parts of the reservoir. Reservoir water quality analysis therefore cannot be based solely on describing existing conditions; rather, it requires an integrated, process-based approach.

Third, the evolution of numerical models from simpler one- and two-dimensional models toward advanced three-dimensional models reflects increasing recognition of the inherent complexity of these systems. In large and deep reservoirs, longitudinal spatial heterogeneity, vertical variations, density differences, and the differing sensitivity of reservoir zones to the operation of outlet structures all contribute to determining water quality behavior. Accordingly, the application of advanced three-dimensional models such as EFDC+ is not merely a technical choice but a scientific requirement for realistically representing reservoir thermal and water quality behavior, particularly in scenario-based studies.

2.5.2 Research Gap

Despite the strategic importance of Seymareh Dam for water supply, hydropower generation, and flood control, a review of previous studies indicates that existing knowledge of the internal mechanisms governing water quality in this reservoir remains incomplete and fragmented. Most previous research has focused on field monitoring, remote sensing, trophic-status assessment, watershed modeling, or simpler simulation approaches. Although each of these studies has scientific value, methodological limitations have prevented them from providing a comprehensive and integrated representation of the spatial and temporal behavior of water quality within the reservoir.

Although field monitoring provides accurate and reliable information, it is generally limited in its temporal and spatial coverage and cannot continuously reconstruct reservoir behavior at seasonal, annual, and long-term scales. Remote sensing is also generally limited to surface-water characteristics and does not directly permit analysis of deep-water processes, thermal stratification, oxygen depletion at depth, or subsurface variations. Watershed models, although useful for estimating inflows and pollutant loads, do not directly simulate internal reservoir mechanisms, including interactions among thermal structure, oxygen, nutrients, algae, and outflow water quality. Consequently, the internal mechanisms affecting water quality in Seymareh Reservoir, particularly the interactions among thermal stratification, oxygen, nutrients, and outflow water quality, have not yet been fully explained and quantified.

One of the most important gaps in the literature concerning this reservoir is the insufficient consideration of outlet-structure operation as a management factor influencing water quality. The existence of two outlet elevations with different functions in Seymareh Reservoir makes it possible to modify the proportion of water withdrawn from different reservoir layers. Nevertheless, no comprehensive study has yet evaluated how changes in the withdrawal proportions from the different outlets may affect the intensity of thermal stratification, oxygen conditions in the deep layers, vertical nutrient distribution, algal patterns, organic loading, and

ultimately the quality of water released from the dam. This gap is particularly important because outlet operation management may serve as a practical, in-situ tool for improving both reservoir water quality and the quality of released water.

Furthermore, most previous studies have either focused on describing the general condition of the reservoir or covered only a limited period. However, a reliable evaluation of management alternatives requires the analysis of different operational scenarios over a long-term horizon and at multiple spatial scales. In other words, it remains unclear how Seymareh Reservoir responds to selective withdrawal configurations in different reservoir zones, from the dam area to the middle and upstream reaches, and how stable these responses remain over time. This issue represents an important methodological gap in the existing studies.

Accordingly, the principal gaps in research related to Seymareh Reservoir can be summarized in three main areas. First, there is no comprehensive and calibrated three-dimensional model capable of simultaneously simulating thermal and water quality processes within the reservoir. Second, there is no scenario-based framework for evaluating the effects of different withdrawal proportions from the reservoir outlets on both in-reservoir water quality and released-water quality. Third, there is a lack of process-based and mechanistic analyses capable of moving beyond the description of existing conditions and explaining the causes of observed variations through the interactions among stratification, oxygen, nutrients, algae, and organic loading.

The present study aims to address these gaps. By developing, calibrating, and applying the three-dimensional EFDC+ model, the thermal and water quality behavior of Seymareh Reservoir is investigated within a long-term simulation framework. The effects of different flow-distribution scenarios between the reservoir outlets are then evaluated in terms of thermal structure, dissolved oxygen, nutrients, chlorophyll-a, BOD5, and outflow water quality. In this way, the study seeks to move beyond the description of existing conditions and provide an integrated, process-based, and management-oriented analysis that establishes a scientific basis for water quality–oriented operation of Seymareh Reservoir.

3 Research Methodology

3.1 Introduction

Chapter 3 describes the research methodology and the stages involved in developing, implementing, and calibrating the three-dimensional model of Seymareh Reservoir. Given the complexity of physical and biogeochemical processes in deep reservoirs, EFDC+ was selected as the principal simulation tool in this study. The model was chosen because of its capability to simultaneously simulate hydrodynamics, constituent transport, temperature, sediment, and water quality within an integrated framework.

This chapter first introduces the EFDC+ model and the capabilities used in the present study. The principal concepts governing the simulation of hydrodynamics, constituent transport, heat exchange, and water quality are then presented in a concise and practical manner. This section focuses on concepts that directly contribute to the development and analysis of the Seymareh Reservoir model, while avoiding unnecessary and overly detailed equations. This approach was adopted to maintain methodological clarity and prevent the chapter from becoming excessively lengthy.

The subsequent sections describe the model implementation procedures, including computational-grid generation, definition of initial and boundary conditions, preparation of hydrological and meteorological data, and the methods used for model calibration. Accordingly, this chapter establishes the technical framework required for analyzing the results and evaluating management scenarios in the subsequent chapters.

3.2 Introduction to the EFDC+ Model

EFDC+ is a surface-water modeling system capable of simulating one-, two-, and three-dimensional hydrodynamics, as well as the transport of various constituents within the water column. The model was developed from the public-domain, open-source version of EFDC and has been improved in terms of computational speed, stability, and accuracy. EFDC+ and its earlier versions have been applied to a wide range of water bodies, including rivers, lakes, reservoirs, wetlands, and estuaries.

An important feature of EFDC+ for the present study is its integrated structure. Hydrodynamics, constituent transport, and water quality processes are solved within a common computational framework, eliminating the need for separate coupling between a flow model and a water quality model. This characteristic represents an important advantage for simulating reservoirs such as

Seymareh Reservoir, where interactions among thermal stratification, nutrient transport, and water quality variations are of particular importance.

Among the numerous capabilities of EFDC+, several are especially relevant to this research. The first is its ability to simulate three-dimensional hydrodynamics and constituent transport within the water column. The second is the Sigma-Zed (SGZ) vertical-layering approach, which helps reduce pressure-gradient errors when modeling water bodies with steep variations in bed topography, such as reservoirs. The third is the direct coupling of the hydrodynamic module with the temperature, sediment, and water quality modules, enabling the simultaneous analysis of physical and biogeochemical processes.

Although EFDC+ includes numerous modules and capabilities, such as particle tracking, ice dynamics, vessel effects, and NetCDF output, the present study focuses only on the modules directly applied to the simulation of Seymareh Reservoir. Therefore, the following sections describe only the theoretical and computational foundations of hydrodynamics, constituent transport, temperature, sediment, and water quality that are directly relevant to this study. The theoretical foundations and governing relationships presented in this section are primarily based on the EFDC+ Theory Document [55].

3.2.1 Hydrodynamic Foundations of the Model

The EFDC+ hydrodynamic module constitutes the core of the modeling system and simulates water flow based on the fundamental principles of fluid mechanics. This module calculates the flow field, free-surface fluctuations, and the effects of temperature and salinity. Its outputs are subsequently used as the basis for other submodels, including constituent transport and water quality. In other words, the accuracy of water quality simulations in EFDC+ largely depends on the accurate representation of hydrodynamic processes. The EFDC+ Theory Document also identifies the hydrodynamic module as the fundamental component of the model, internally and integrally coupled with the other modules.

3.2.1.1 Governing Equations

The theoretical foundation of hydrodynamics in EFDC+ is based on the conservation laws of mass, momentum, and energy. The model employs the Navier–Stokes equations for an incompressible fluid with variable density; however, these equations are appropriately simplified for application to natural water bodies. Two fundamental assumptions are adopted in this formulation: the hydrostatic assumption in the vertical direction and the Boussinesq approximation for accounting for density variations. The EFDC+ Theory Document also emphasizes that this formulation is appropriate for environmental flows in which the horizontal length scale is substantially greater than the vertical length scale.

To better understand the model structure, it is important to note that EFDC+ solves the more complete momentum equations in the horizontal directions because variations in horizontal velocity are affected by several forces, including water-surface slope, pressure gradients, friction, Coriolis effects, and turbulence. In the vertical direction, however, the hydrostatic assumption

reduces the vertical momentum equation to a simpler relationship between pressure and density. This simplification is computationally important because, without it, three-dimensional simulations of large water bodies would require substantially greater computational resources.

Figure (3-1) also illustrates that, in addition to flow, EFDC+ accounts for several important processes, including surface wind stress, bed shear stress, precipitation, evaporation, waves, and groundwater exchange. This demonstrates that hydrodynamic simulation in EFDC+ is not merely the solution of a simple velocity field but rather the representation of interactions among multiple physical forces affecting the aquatic system.

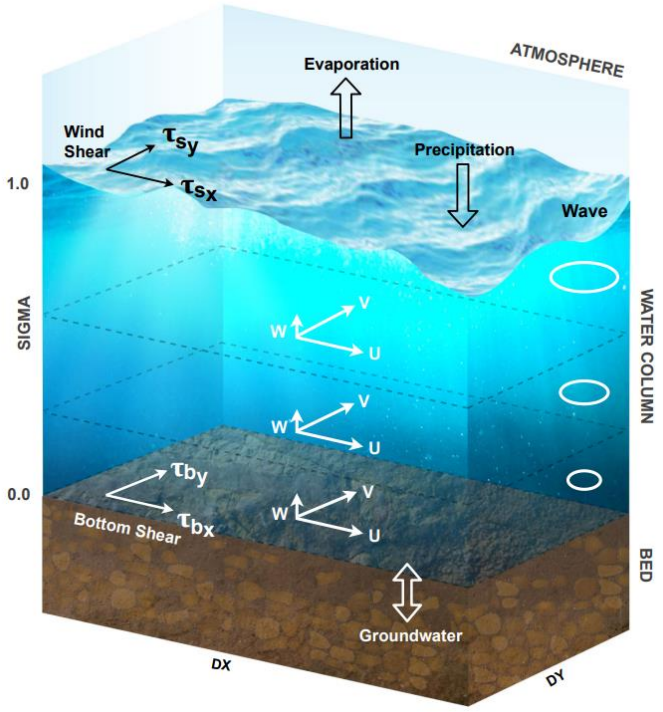

Figure 3-1. Conceptual overview of the hydrodynamic module.

3.2.1.2 Coordinate System and Vertical Layering Method

To accurately simulate water bodies with complex geometries, a model must be capable of conforming to both irregular horizontal boundaries and spatially varying bed topography. For this purpose, EFDC+ employs an orthogonal curvilinear coordinate system in the horizontal directions. The principal advantage of this coordinate system is that the computational grid can more closely conform to the actual geometry of a reservoir, lake, or river, thereby reducing the need for excessive geometric simplification. The EFDC+ Theory Document also specifies that the horizontal coordinates, (x) and (y), are defined using an orthogonal curvilinear system. This means that the grid lines can conform to the actual geometry of the model domain while remaining orthogonal at their intersections.

In the vertical direction, the model applies a sigma-coordinate transformation. The main concept underlying this transformation is that water columns of different physical depths are mapped onto a normalized computational domain. Consequently, the governing equations can be solved on a more regular grid without neglecting the actual bed geometry or variations in the free-surface elevation. The transformation is defined as follows:

$$z = \frac{z^* + h}{\zeta + h} = \frac{z^* + h}{H} \qquad 3\text{-}1$$

where (z) is the sigma coordinate, (z^*) is the physical vertical coordinate relative to the reference datum, (h) is the water depth, (ζ) is the free-surface elevation, and (H) is the total water-column depth.

Conceptually, this relationship indicates that each point within the water column is represented by its relative position in the water column rather than solely by its physical elevation. Accordingly, points located near the surface or near the bed can be consistently represented and compared among all computational cells, even when the physical depths of the cells differ substantially.

One of the important advantages of EFDC+ is its ability to use two principal approaches for vertical layering:

a) Standard Sigma Approach

In this method, the number of vertical layers remains constant throughout the entire model domain. Therefore, all water columns, whether deep or shallow, contain the same number of layers. The main advantages of this approach are its simplicity and continuity across the domain. However, in areas with steep bed slopes, the calculation of horizontal pressure gradients may be subject to numerical errors (Figure 3-2a).

b) Sigma-Zed Approach

To reduce the errors associated with the standard sigma approach over steeply sloping beds, EFDC+ incorporates the hybrid Sigma-Zed approach. In this method, the number of active vertical layers can vary according to the water depth in each cell. Consequently, shallow cells contain fewer active layers. In addition to reducing pressure-gradient errors, this feature decreases the total number of computational cells and thereby reduces model execution time. This capability is particularly useful for reservoirs, which commonly consist of a deep main channel and shallower lateral areas.

The two principal configurations of this approach are as follows:

• SGZ-Specified Bottom: In this configuration, the number of active vertical layers in each horizontal cell is specified directly by the user. Therefore, the vertical arrangement of layers can be adjusted according to the depth and conditions of each cell (Figure 3-2b).

• SGZ-Uniform Layering: In this configuration, the number of active layers may also vary from one cell to another according to water depth. However, its principal characteristic is that the lower boundaries of the vertical layers are maintained at consistent horizontal elevations, thereby producing a more regular and uniform vertical-layer arrangement (Figure 3-2c).

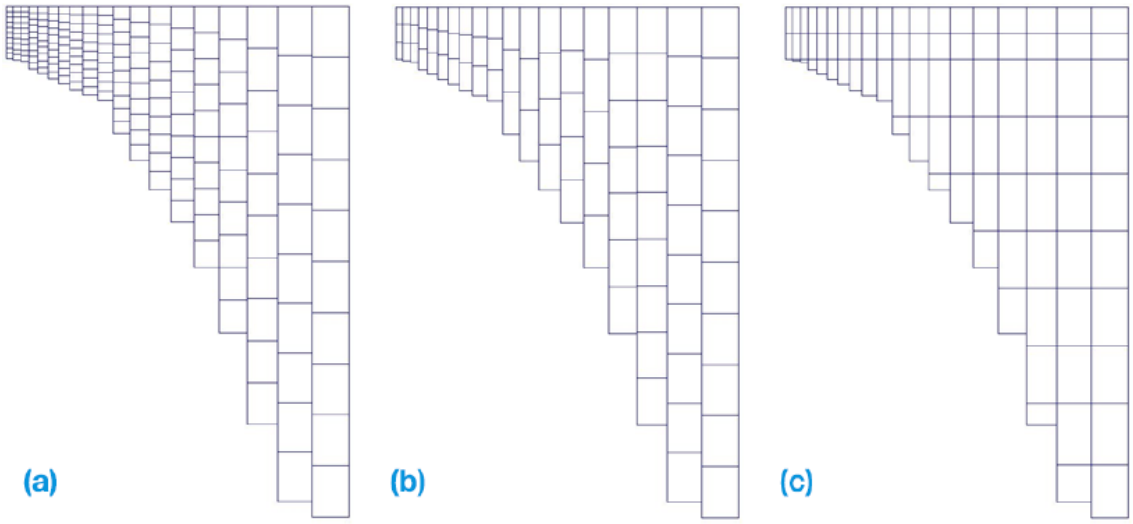

Figure 3-2. Vertical-layering options in EFDC+: (a) SIG, (b) SGZ-Specified Bottom, and (c) SGZ-Uniform Layering.

3.2.1.3 Fundamental Hydrodynamic Equations

Following the coordinate transformation, the governing equations are expressed in their final form for numerical solution. These equations include the horizontal momentum equations, the vertical hydrostatic relationship, the continuity equation, the equation of state, and the temperature and salinity transport equations. In this section, only the principal equations directly relevant to reservoir simulation are presented to retain the theoretical foundations of the model while avoiding unnecessary expansion of the text.

a) Horizontal Momentum Equations

These equations describe how the horizontal flow velocity changes in response to the forces acting on the water. The principal components governing these changes include temporal and spatial variations in velocity, water-surface slope and pressure gradients, the Coriolis force, bed friction, and turbulence-induced momentum diffusion. In simple terms, the horizontal momentum equation

represents the balance between the tendency of water to move and the forces that accelerate or decelerate it.

The momentum equation in the (x)-direction is written as follows. The momentum equation in the (y)-direction has a similar structure:

$$\frac{\partial}{\partial t}\left(m_x m_y H u\right) + \frac{\partial}{\partial x}\left(m_y H u u\right) + \frac{\partial}{\partial y}\left(m_x H v u\right) + \frac{\partial}{\partial z}\left(m_x m_y w u\right)$$

$$- m_x m_y f H v - \left(v\frac{\partial m_y}{\partial x} - u\frac{\partial m_x}{\partial y}\right) H v$$

$$= -m_y H \frac{\partial}{\partial x}(g\zeta + p + P_{atm}) - m_y\left(\frac{\partial h}{\partial x} - z\frac{\partial H}{\partial x}\right)\frac{\partial p}{\partial z}$$

$$+ \frac{\partial}{\partial x}\left(\frac{m_y}{m_x} H A_H \frac{\partial u}{\partial x}\right)$$

$$+ \frac{\partial}{\partial y}\left(\frac{m_x}{m_y} H A_H \frac{\partial u}{\partial y}\right) + \frac{\partial}{\partial z}\left(\frac{m_x m_y}{H} A_v \frac{\partial u}{\partial z}\right) - m_x m_y c_p D_p u\sqrt{u^2 + v^2}$$

$$+ S_u \qquad \text{3-2}$$

b) Vertical Hydrostatic Relationship

In the vertical direction, EFDC+ applies the hydrostatic assumption instead of solving the complete vertical momentum equation. This assumption means that vertical pressure is primarily determined by the weight of the overlying water column and that vertical accelerations are considered negligible compared with pressure and gravitational forces. Consequently, the vertical equation is simplified as follows:

$$\frac{\partial p}{\partial z} = -gH\frac{(\rho - \rho^0)}{\rho^0} \qquad \text{3-3}$$

In this equation, (p) represents the pressure component resulting from density variations, or the baroclinic pressure, in the transformed coordinate system; (z) is the dimensionless vertical coordinate in the sigma system; (g) is gravitational acceleration; (HH) is the total water-column depth; (ρ) is the local water density; and (ρ^0) is the reference water density.

This relationship is conceptually important because it shows that wherever density differences exist, the pressure distribution also changes. Consequently, temperature and salinity are not merely water quality variables; through their effects on density, they can influence the flow field and the stratification structure of the reservoir.

c) Continuity Equation

The continuity equation represents the conservation of mass for an incompressible fluid. Its physical meaning is that when the amount of water entering a computational cell exceeds the amount leaving it, the free-surface elevation or the volume of water stored in that cell increases. Conversely, when the outflow exceeds the inflow, the water level or stored volume decreases. Therefore, this equation is directly related to free-surface fluctuations, changes in reservoir volume, and the mass balance of the model.

In EFDC+, following the transformation of the vertical coordinate into the sigma system, the continuity equation is written as follows:

$$\frac{\partial}{\partial t}(m_x m_y \zeta) + \frac{\partial}{\partial x}(m_y H u) + \frac{\partial}{\partial y}(m_x H v) + \frac{\partial}{\partial z}(m_x m_y w) = S_h \qquad 3\text{-}4$$

In this equation, (ζ) is the free-surface elevation, (H) is the total water-column depth, (u) and (v) are the horizontal velocity components in the curvilinear (x)- and (y)-directions, and (w) is the vertical velocity component in the sigma-coordinate system. The parameters (m_x) and (m_y) are the horizontal-grid metric coefficients that account for the effects of the curvilinear coordinate transformation.

The term (S_h) represents mass sources and sinks within the computational cell, such as water entering or leaving through model boundaries, hydraulic structures, or other volumetric fluxes. Accordingly, the continuity equation ensures that simulated water-level variations remain consistent with the combined inflows, outflows, and changes in storage within the computational domain.

3.2.1.4 Equation of State

Water density is one of the key physical variables in the hydrodynamic simulation of reservoirs because its variations can lead to the development of density-driven currents, thermal stratification, and stable or unstable vertical mixing conditions. In simple terms, whenever temperature, salinity, or suspended-solids concentrations differ among various parts of a reservoir, water density also varies, and the resulting density gradients can influence the flow pattern. Therefore, in three-dimensional models such as EFDC+, density calculation constitutes an essential component of the model's physical core.

In its general form, water density is considered a function of pressure, salinity, temperature, and suspended-solids concentration:

$$\rho = \rho(p, S, T, C) \quad (3\text{-}5)$$

where (ρ) is water density, (p) is pressure, (S) is salinity, (T) is temperature, and (C) is the suspended-solids concentration. In many reservoir applications, temperature and salinity are the principal factors controlling density variations. These variations, particularly during the warm season, play a fundamental role in the formation and persistence of thermal stratification.

In EFDC+, the standard UNESCO equation of state is used to calculate water density as a function of temperature and salinity:

$$\begin{aligned} \rho = {} & 999.842594 + 6.793952 \times 10^{-2} T - 9.095290 \times 10^{-3} T^2 \\ & + 1.001685 \times 10^{-4} T^3 - 1.120083 \times 10^{-6} T^4 + 6.536332 \times 10^{-9} T^5 \\ & + (0.824493 - 4.0899 \times 10^{-3} T + 7.6438 \times 10^{-5} T^2 \\ & - 8.2467 \times 10^{-7} T^3 + 5.3875 \times 10^{-9} T^4) S \\ & + (-5.72466 \times 10^{-3} + 1.0227 \times 10^{-4} T - 1.6546 \times 10^{-6} T^2) S^{1.5} \\ & + 4.8314 \times 10^{-4} S^2 \end{aligned} \quad (3\text{-}6)$$

where (ρ) is the water density in ($\mathrm{kg/m^3}$), (T) is the water temperature in degrees Celsius, and (S) is salinity in parts per thousand (ppt).

In addition to temperature and salinity, suspended solids may alter the effective density of the fluid when their concentration in the water column is high. This effect is particularly important during flood events or the inflow of sediment-laden water into the reservoir. In the present study, however, density variations and stratification in Seymareh Reservoir are governed primarily by temperature and, to a lesser extent, salinity. Accordingly, the equation of state establishes the principal link between the hydrodynamic module and the temperature and salinity variables, thereby enabling the simulation of stratification, vertical mixing, and constituent transport within the water column.

3.2.1.5 Turbulence Modeling

Water flow in natural environments such as reservoirs is generally turbulent because of the combined effects of inflows, wind, density variations, bed irregularities, and complex reservoir geometry. Turbulence plays an important role in the horizontal and vertical mixing of water and thereby influences the distribution of temperature, salinity, dissolved oxygen, nutrients, and other water quality variables. Because direct simulation of all turbulence scales is computationally impractical, numerical models employ turbulence-closure methods to estimate the mean effects of turbulent eddies on the flow field.

In the vertical direction, EFDC+ applies the second-order Mellor–Yamada turbulence-closure model, in which turbulence intensity and mixing coefficients are calculated dynamically according to the stability conditions of the water column. In the present study, the modified Galperin formulation [54] was used for the turbulence stability function. In this approach, the vertical

turbulent viscosity and diffusivity coefficients are functions of turbulent kinetic energy, the turbulence length scale, and the Richardson number.

The Galperin stability function accounts for the influence of stable or unstable density stratification on the intensity of vertical mixing. Under stable stratification, vertical mixing is suppressed, whereas under unstable conditions, mixing intensity increases. This formulation also imposes a constraint on the Richardson number to prevent unrealistic growth of the turbulence length scale under stable conditions. This feature is particularly important for the simulation of deep reservoirs because, during periods of thermal stratification, reduced vertical mixing plays a major role in deep-water oxygen depletion and nutrient accumulation.

In the horizontal direction, EFDC+ provides the option of applying the Smagorinsky subgrid-scale formulation. This approach was also used to represent horizontal turbulence in the present study. In this method, the horizontal diffusivity coefficient is calculated based on the dimensions of the computational cells and the spatial gradients of flow velocity. The general relationship is expressed as follows:

$$A_H = C_s \Delta x \Delta y \sqrt{\left(\frac{\partial u}{\partial x}\right)^2 + \left(\frac{\partial v}{\partial y}\right)^2 + \frac{1}{2}\left(\frac{\partial u}{\partial y} + \frac{\partial v}{\partial x}\right)^2} \qquad 3\text{-}7$$

where (A_H) is the horizontal turbulent diffusivity coefficient, (C_s) is the Smagorinsky coefficient, (Δx) and (Δy) are the computational-cell dimensions, and (u) and (v) are the horizontal velocity components.

Conceptually, this relationship indicates that greater spatial variations in velocity within a particular region produce higher estimates of turbulence intensity and horizontal diffusivity. Therefore, compared with the use of a constant coefficient, this approach provides a more realistic representation of the effects of local flow variations on horizontal mixing.

3.2.1.6 Boundary Conditions and External Forcing

To simulate flow within a water body, the model must receive not only the governing equations but also the boundary conditions and external forces acting on the system. These conditions control model behavior at the domain boundaries and at the water surface and bed, and they play an important role in realistically reproducing the flow field, water-surface elevation, mixing, and constituent transport.

In EFDC+, boundary conditions and external forcing may include bed friction, wind stress at the water surface, atmospheric exchange, wave effects, open inflow and outflow boundaries, and hydraulic structures. Bed friction acts as a resisting force against water motion and influences flow velocities in the near-bed layers. Wind stress is also one of the principal drivers of surface currents and mixing in reservoirs and can contribute to the formation of surface circulation patterns and the

displacement of water masses. In large reservoirs, wind-generated waves may additionally affect bed shear stress and sediment resuspension.

Open boundaries are defined at locations where water enters or leaves the model domain. In the present study, the upstream model boundary was defined at the point where the main river enters the reservoir, and time series of discharge, temperature, salinity, and inflowing water quality variables were applied at this boundary. At the downstream end, water withdrawal from the reservoir was simulated through hydraulic structures defined near the dam. Therefore, the boundary conditions in this study did not serve only a numerical function; they also provided the principal framework for linking the model to actual operational, hydrological, and water quality data from Seymareh Reservoir.

3.2.1.7 Numerical Solution Method

The simultaneous solution of three-dimensional hydrodynamic equations, particularly over a large domain such as Seymareh Reservoir, is computationally complex and time-consuming. To improve computational efficiency while maintaining numerical stability, EFDC+ employs a mode-splitting method. In this approach, the hydrodynamic calculations are divided into two principal components: the external mode and the internal mode.

In the external mode, the equations are solved in a two-dimensional, depth-averaged form. The main objective of this component is to calculate variations in free-surface elevation and depth-averaged velocities throughout the model domain. Because this mode primarily represents water-level fluctuations and the rapid response of the system, it can be solved with greater computational efficiency.

In the internal mode, after the water-surface elevation has been determined, the three-dimensional velocity structure and depth-dependent variations in flow are calculated. This component is essential for representing processes such as thermal stratification, density-driven currents, vertical mixing, and constituent transport within the water column.

Combining the external and internal modes enables the model to retain the three-dimensional nature of the simulation while remaining computationally suitable for long-term model runs. In the present study, this feature made it possible to simulate ten-year reservoir operation scenarios.

3.2.1.8 Hydraulic Structures

Another practical capability of EFDC+ is the simulation of hydraulic structures within the computational domain. This capability enables the model to account for the effects of structures such as culverts, weirs, slide gates, orifices, and hydraulic barriers on the flow regime. In EFDC+, discharge through these structures may be defined using rating curves and stage–discharge tables or calculated directly using the model's internal hydraulic equations.

In the present study, the hydraulic-structure capability, specifically an orifice-type structure, was used to represent the selected outlets of Seymareh Dam. An orifice is suitable for this purpose because the discharge through it is a function of the opening geometry, discharge coefficient, and effective upstream and downstream heads.

In EFDC+, flow through an orifice may be calculated using different formulations depending on the upstream and downstream water levels. If the upstream water surface does not completely submerge the orifice, the flow is calculated in a manner similar to flow over a weir. If the downstream water level is above the orifice opening, the model applies the submerged-flow equation. When the upstream water level is above the orifice opening and the downstream level is below it, the flow is calculated as a free jet through the orifice. The principal equation presented in the EFDC+ Theory Document for this condition is:

$$Q = C_2 A\sqrt{2g(H_{HW} + 0.5B)} \qquad 3\text{-}8$$

where (Q) is the discharge through the orifice, (C_2) is the discharge coefficient, (A) is the area of the orifice opening, (g) is gravitational acceleration, (H_{HW}) is the upstream head relative to the center of the orifice, and (B) is the height of the orifice opening.

Overall, using orifice-type structures in this study ensured that the dam outlets were not represented merely as simple discharge boundaries. Instead, the withdrawal elevation and hydraulic conditions governing the outlets were also incorporated into the model. This was particularly important for the main objective of the research, namely evaluating the effects of withdrawal from different elevations on the reservoir's thermal structure and water quality.

3.2.1.9 Summary of the Hydrodynamic Module

This section described the principal foundations of the EFDC+ hydrodynamic module. By solving the governing equations of fluid motion, this module calculates free-surface elevation, the three-dimensional velocity field, turbulence, density effects, and flow exchange through boundaries and hydraulic structures. The outputs of the hydrodynamic module provide the primary basis for solving the transport of temperature, salinity, nutrients, dissolved oxygen, and other water quality variables.

Because processes such as thermal stratification, withdrawal from different elevations, and constituent transport within the water column are particularly important in Seymareh Reservoir, the accuracy of the hydrodynamic module plays a decisive role in the reliability of the water quality results. In the present study, the development of a three-dimensional computational grid, selection of an appropriate vertical-layering scheme, application of a turbulence model, specification of inflow and outflow boundary conditions, and representation of the dam outlets as orifice structures formed the principal basis of the reservoir hydrodynamic simulation.

3.2.2 Constituent Transport Model

After the three-dimensional flow field has been calculated by the hydrodynamic module, the next step in EFDC+ is to simulate the movement and temporal variations of dissolved or suspended constituents within the water column. This process is performed by the constituent transport model. The velocity field obtained from the hydrodynamic solution determines the transport pathways of variables such as temperature, salinity, suspended sediments, nutrients, dissolved oxygen, and other water quality constituents. Therefore, the constituent transport module serves as the link between the hydrodynamic and water quality modules of the model.

3.2.2.1 Governing Constituent Transport Equation

The theoretical basis of this module is the general advection–diffusion equation. This equation states that changes in the concentration of a constituent within a specified volume of water result from the interaction of three principal processes: transport with the water flow, turbulent diffusion, and internal or external sources and sinks. Advection, or mass transport, refers to the movement of a constituent in the direction of the flow, whereas diffusion represents the spreading of the constituent through turbulent mixing from regions of higher concentration toward regions of lower concentration. The source and sink term includes processes such as loading through model boundaries, settling, decomposition, biological growth, and chemical reactions.

The general transport equation in EFDC+ is written as follows:

$$\begin{aligned}&\frac{\partial}{\partial t}(m_x m_y HC)+\frac{\partial}{\partial x}(m_y HuC)+\frac{\partial}{\partial y}(m_x HvC)+\frac{\partial}{\partial z}(m_x m_y wC)\\&\qquad-\frac{\partial}{\partial z}(m_x m_y w_s c)\\&=\frac{\partial}{\partial x}\left(\frac{m_y}{m_x}HA_H\frac{dC}{dx}\right)+\frac{\partial}{\partial y}\left(\frac{m_x}{m_y}HA_H\frac{dC}{dy}\right)+\frac{\partial}{\partial z}\left(\frac{m_x m_y}{H}A_b\frac{dC}{dz}\right)+S_c\end{aligned}\qquad 3\text{-}9$$

In this equation, (C) is the constituent concentration; (u), (v), and (w) are the velocity components in the three coordinate directions; (H) is the total water-column depth; and (m_x) and (m_y) are the metric coefficients of the curvilinear coordinate system. In addition, (A_H) is the horizontal diffusivity coefficient, (A_b) is the vertical turbulent diffusivity coefficient, (w_s) is the particle settling velocity, and (S_c) is the general source and sink term. For dissolved constituents such as salinity and many chemical compounds, the settling term is generally zero, whereas it becomes important for particulate constituents and suspended sediments.

The terms on the left-hand side of the equation represent, respectively, the temporal change in concentration, horizontal and vertical transport by the flow, and the effect of settling. The terms on the right-hand side represent horizontal and vertical turbulent diffusion and the sources and sinks of the constituent. This equation provides the common basis for transporting many of the

variables investigated in the present study, including salinity, temperature, nutrients, dissolved oxygen, and other water quality constituents.

3.2.2.2 Numerical Solution of the Transport Equations

The simultaneous numerical solution of all components of the transport equation is complex because processes such as advection, diffusion, settling, and internal reactions have different characteristics and timescales. For this reason, EFDC+ employs a fractional-step method to solve the transport equations. In this approach, the original equation is divided into several simpler components, each of which is solved separately during a distinct computational step.

During the advection step, the constituent concentration is transported according to the velocity field calculated by the hydrodynamic module. For this component, EFDC+ applies the Multidimensional Positive Definite Advection Transport Algorithm (MPDATA), a stable and positive-definite numerical scheme. An important advantage of this method is that it prevents the generation of negative and physically unrealistic concentrations while simultaneously reducing numerical diffusion. This feature is particularly important when simulating water quality variables in regions characterized by steep concentration gradients.

In the subsequent steps, vertical processes such as settling and vertical diffusion are calculated. These components are generally solved implicitly to maintain numerical stability in the presence of strong vertical gradients. Finally, the effects of internal and external sources and sinks are applied to the constituent concentration. Depending on the variable being simulated, these sources and sinks may include boundary loads, water quality reactions, organic matter decomposition, algal growth, oxygen consumption or production, and exchange with the bed.

Overall, the fractional-step method enables the model to solve the different transport and reaction processes in a stable and computationally efficient manner. This feature is particularly important for the present study because simulating water quality in Seymareh Reservoir requires the simultaneous transport of several variables within a three-dimensional, stratified flow field.

3.2.3 Dye Module

EFDC+ includes a module for simulating a hypothetical constituent referred to as dye. This constituent is generally treated as a passive tracer, meaning that its presence does not affect water density, viscosity, or the hydrodynamic flow field. Instead, it is transported and dispersed solely with the water flow. The dye module therefore provides a useful tool for investigating transport and mixing patterns, water-mass pathways, residence time, and water age in aquatic systems.

Dye transport, similar to that of other dissolved constituents, is governed by the general advection–diffusion equation introduced in the previous section. When the dye is defined as conservative, it is affected only by advection and diffusion, and no internal reaction is considered for its production or removal. In contrast, when the dye is defined as nonconservative, temporal decay may also be included.

Dye decay can be defined using either a zeroth-order or a first-order formulation. Under zeroth-order decay, the constituent decreases at a constant rate:

$$\frac{dC}{dt} = -K \tag{3-10}$$

Under first-order decay, the rate of constituent reduction is proportional to its concentration:

$$\frac{dC}{dt} = -KC \tag{3-11}$$

When required, the effect of temperature on the decay rate can also be incorporated using a temperature-correction coefficient:

$$\frac{dC}{dt} = -K\theta\left(T - T_{ref}\right)C \tag{3-12}$$

where (C) is the dye concentration, (K) is the decay coefficient, (θ) is the temperature-correction coefficient, (T) is the water temperature, and (T_{ref}) is the reference temperature.

One important application of this module is the calculation of water age. Water age represents the time elapsed since a water mass entered the model domain. For this purpose, the tracer value is set to zero at the inflow boundary and subsequently increases with time within the domain:

$$\frac{dC}{dt} = 1 \tag{3-13}$$

Under this formulation, the value of (C) in each computational cell can be interpreted as an indicator of water age, or the time elapsed since the water mass entered the system. This indicator is useful for evaluating residence time, water-renewal intensity, and identifying zones characterized by prolonged water retention within reservoirs.

3.2.4 Temperature and Heat Transport Module

Temperature is one of the most important physical variables in reservoir simulation because its spatial and temporal distributions influence numerous hydrodynamic, chemical, and biological processes. From a physical perspective, vertical temperature differences cause density variations and the development of thermal stratification. This stratification can control the intensity of vertical mixing, oxygen transport to deeper waters, and nutrient redistribution. From a water quality perspective, temperature also affects the rates of biochemical reactions, including algal growth, organic matter decomposition, nitrification, and oxygen consumption. Therefore, accurate simulation of the temperature field is essential for representing water quality behavior in Seymareh Reservoir.

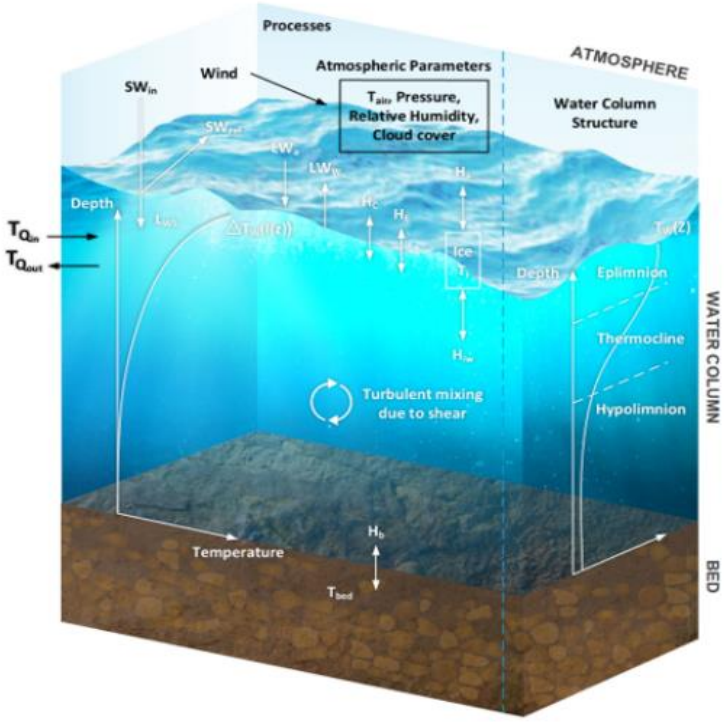

Figure 3-3. Conceptual overview of the temperature module.

The EFDC+ temperature module calculates the three-dimensional temperature distribution throughout the model domain by solving the general heat transport equation. The structure of this equation is similar to that of the general constituent transport equation, except that the transported variable is water temperature and its sources and sinks result from heat-exchange processes. The principal thermal processes represented in the model include surface heat exchange with the atmosphere, absorption of solar radiation within the water column, heat exchange with the bed, and heat entering or leaving the model domain through open boundaries and inflows and outflows.

3.2.4.1 Surface Heat Exchange

The most important process controlling water temperature is energy exchange across the air–water interface. This exchange is applied as a boundary condition at the model's surface layer and includes components such as longwave radiation, latent heat associated with evaporation, and sensible heat resulting from the temperature difference between the air and water. The general surface heat-flux relationship is expressed as follows:

$$-\frac{\rho c_p A_b}{H}\frac{\partial T}{\partial z} = H_L + H_E + H_C \qquad 3\text{-}14$$

where (ρ) is water density, (c_p) is the specific heat capacity of water, (A_b) is the vertical thermal diffusivity coefficient, (H) is the water-column depth, (T) is water temperature, (H_L) is the

longwave radiation flux, (H_E) is the latent heat flux, and (H_C) is the sensible heat flux. This relationship indicates that changes in the temperature of the surface-water layer depend on the sum of heat exchanges between the water and the atmosphere.

EFDC+ provides two principal approaches for calculating surface heat exchange: the full heat-balance method and the equilibrium-temperature method.

a) Full Heat-Balance Method

In this method, each component of the heat flux is calculated separately based on meteorological data and surface-water temperature. The principal components are as follows:

- Longwave radiation flux (H_L): a function of water temperature, air temperature, vapor pressure, and cloud cover.
- Latent heat flux (H_E): dependent on evaporation and the vapor-pressure difference between the water surface and the atmosphere.
- Sensible heat flux (H_C): influenced by the temperature difference between the air and water and by wind speed.

The principal relationships for these components are expressed as follows:

$$H_L = \epsilon\sigma(T_s + 273.15)^4\left(0.39 - 0.05\sqrt{e_a}\right)(1 + B_c C) + 4\epsilon\sigma(T_s + 273.15)^3(T_s - T_a) \quad 3\text{-}15$$

$$H_E = c_e \rho_a L E W_s (e_s - e_a)\frac{0.622}{P_a} \quad 3\text{-}16$$

$$H_C = c_h \rho_a c_p a W_s (T_s - T_a) \quad 3\text{-}17$$

where (T_s) is the surface-water temperature, (T_a) is the air temperature, (e_s) is the saturation vapor pressure at the water surface, (e_a) is the atmospheric vapor pressure, (W_s) is wind speed, (ρ_a) is air density, (P_a) is atmospheric pressure, (L) is the latent heat of evaporation, (ϵ) is emissivity, (σ) is the Stefan–Boltzmann constant, and (c_e) and (c_h) are the latent- and sensible-heat transfer coefficients, respectively.

b) Equilibrium-Temperature Method

In the equilibrium-temperature method, surface heat exchange is represented using a simpler relationship. The equilibrium temperature, (T_e), is defined as the temperature at which the net heat exchange between the water and atmosphere becomes zero. Accordingly, the net heat flux is assumed to be proportional to the difference between the surface-water temperature and the equilibrium temperature:

$$H_n = -K_{aw}(T_s - T_e) \quad \text{3-18}$$

where (H_n) is the net heat flux, (K_{aw}) is the surface heat-exchange coefficient, (T_s) is the surface-water temperature, and (T_e) is the equilibrium temperature. Under this formulation, when the surface-water temperature exceeds the equilibrium temperature, the water loses heat; when it is below the equilibrium temperature, the water gains heat.

The equilibrium temperature and heat-exchange coefficient are generally estimated using empirical relationships based on meteorological data:

$$T_e = \frac{I_{sw}}{23 + f(W)(\beta + 0.255)} + T_d \quad \text{3-19}$$

$$K = 23 + (\beta_w + 0.225)17W_2 \quad \text{3-20}$$

$$\beta_w = 0.255 - 0.0085T_w - 0.000204T_w^2 \quad \text{3-21}$$

This method is particularly useful for long-term reservoir simulations because it retains the principal effects of surface heat exchange while reducing the computational complexity associated with separately calculating all heat-flux components.

3.2.4.2 Shortwave Radiation Absorption and Light Attenuation

Shortwave solar radiation is one of the principal sources of energy entering a reservoir. A portion of this radiation is reflected at the water surface, while the remaining portion penetrates the water column and is gradually absorbed with increasing depth. The amount of radiation entering the water may be affected by factors such as shading, surface cover, atmospheric conditions, and, in some regions, ice cover. The effective shortwave radiation entering the water surface is generally represented in the model as follows:

$$I_{sw} = I_0 S_f \min\{\exp[-K_{e,me}(H_{rps} - H)], 1\} \min\{\exp[-K_{e,ic} H_{ic}], 1\} \quad \text{3-22}$$

where (I_{sw}) is the effective shortwave radiation entering the water, (I_0) is the incident radiation, (S_f) is the shading coefficient, ($K_{e,me}$) is the attenuation coefficient associated with surface cover or obstructions, (H_{rps}) and (H) are parameters related to water-surface conditions, ($K_{e,ic}$) is the ice attenuation coefficient, and (H_{ic}) is the ice thickness.

After radiation enters the water column, its intensity decreases with increasing depth. This process, known as light attenuation, is an important factor controlling both the vertical temperature

distribution and algal growth. The simplest representation of light attenuation is based on the Beer–Lambert law:

$$\mathrm{I(z)} = \mathrm{I}_{sw} \exp(-\zeta\, \mathrm{z}) \qquad \text{3-23}$$

where (I(z)) is the radiation intensity at depth (z), ($I_\{sw\}$) is the radiation entering the water surface, and (ζ) is the light-extinction or attenuation coefficient. A higher extinction coefficient causes radiation to be absorbed at shallower depths and reduces its penetration into the deeper layers.

In some applications, solar radiation is divided into two components with different attenuation characteristics. In the two-band attenuation model, one component is rapidly absorbed within the surface layers, whereas the other penetrates to greater depths. The general equation for this method is expressed as follows:

$$I(z) = I_{sw}\left[R\exp\left(z\zeta_f\right) + (1-R)\exp(z\zeta_s)\right] \qquad \text{3-24}$$

where (R) is the fraction of radiation subject to rapid attenuation, (ζ_f) is the rapid-attenuation coefficient, and (ζ_s) is the slow-attenuation coefficient. This approach provides a more realistic representation of differences in the penetration of various components of the solar spectrum through the water column.

An important capability of EFDC+ is its ability to relate the light-extinction coefficient to water quality variables. Under this approach, the extinction coefficient is not treated as a constant value but is calculated based on the concentrations of constituents such as suspended solids, particulate and dissolved organic carbon, chlorophyll-a, and aquatic vegetation. The general water quality–dependent light-extinction relationship is expressed as follows:

$$K_{ess} = K_{e,b} + K_{e,TSS}TSS + K_{e,POC}POC + K_{e,DOC}DOC + K_{e,chl}\sum Chl + K_{e,MAC}MAC \qquad \text{3-25}$$

where (K_{ess}) is the total light-extinction coefficient, ($K_{e,b}$) is the background extinction coefficient, (TSS) represents total suspended solids, (POC) is particulate organic carbon, (DOC) is dissolved organic carbon, (Chl) represents chlorophyll-a, and (MAC) is aquatic-plant biomass.

The importance of this relationship lies in the direct feedback it establishes between water quality and light penetration. For example, an increase in chlorophyll-a resulting from algal growth increases turbidity and reduces light penetration, which may subsequently limit algal growth in deeper layers. This process, known as self-shading, is particularly important in the analysis of biological and optical processes in reservoirs.

3.2.4.3 Heat Exchange with the Bed

Heat exchange between the bottom water layer and bed sediments is generally smaller than surface heat exchange. However, in long-term simulations and deep reservoirs, it may affect the temperature of the near-bed layers. This exchange depends on the temperature difference between the water and bed, the thermal properties of the sediments, and the intensity of near-bed flow. EFDC+ can represent this process as a heat flux between the water column and the bed and, when required, can also calculate bed temperature dynamically. This capability is useful for more accurately representing the thermal behavior of the hypolimnion and other deep reservoir layers.

3.2.4.4 Ice Formation and Melting

EFDC+ is capable of simulating the formation and melting of ice cover. This capability is primarily applicable to water bodies located in cold climates. When the surface-water temperature approaches the freezing point, the surface heat balance may result in ice formation, and the model calculates changes in ice thickness based on heat exchange at the air–ice and ice–water interfaces. However, this module is primarily thermodynamic and does not simulate the dynamic movement of ice masses. Given the climatic conditions of Seymareh Reservoir, this capability did not play a major role in the present study.

3.2.4.5 Water-Volume Loss Due to Evaporation

In addition to appearing as a latent heat flux in the energy balance, evaporation from the water surface can directly reduce the volume of water stored in the reservoir. EFDC+ can account for evaporation in the volumetric water balance. The evaporation rate may either be specified as model input or calculated from the latent heat flux. When calculated internally, the volume of evaporated water is determined from the latent heat component and applied as a volumetric outflow from the water surface.

In the present study, the option for direct volumetric water loss due to evaporation was deactivated. This choice was made because reservoir outflow was calculated directly from observed inflow discharge and changes in reservoir storage volume. Therefore, the net effects of factors such as evaporation, precipitation, possible seepage, and other secondary components of the water balance were implicitly reflected in the observed changes in reservoir volume and in the calculated outflow discharge. Consequently, activating volumetric evaporation separately in the model could have resulted in double-counting part of the water losses and introduced errors in the simulated water-surface elevation.

Nevertheless, the thermal effect of evaporation was not excluded because surface heat exchange, including latent heat flux, remained active in the model's thermal calculations. Therefore, evaporation was considered in terms of the energy balance and its effects on water temperature and thermal stratification, but it was not activated as an independent volumetric loss in the model water balance.

3.2.5 Sediment Transport Module

Sediment transport processes are important in reservoirs for several reasons. Sediments can affect bed morphology, effective reservoir storage capacity, water turbidity, and the cycling of nutrients and pollutants. Sediment particles, particularly fine-grained particles, can adsorb phosphorus and other compounds and remove them from the water column. Conversely, processes such as bed erosion and sediment resuspension can return these substances to the water column and consequently affect water quality. Therefore, the sediment transport module in EFDC+ is an important component for simulating systems in which interactions among flow, sediment, and water quality are significant.

EFDC+ provides both a standard sediment transport module and the advanced SEDZLJ module for sediment simulation. These modules are dynamically coupled with the hydrodynamic component of the model. In other words, the flow field and bed shear stress influence sediment erosion, transport, and deposition, while in morphodynamic studies, changes in bed morphology may also feed back into the flow field.

3.2.5.1 Governing Sediment Transport Equation

The transport of suspended sediment within the water column, similar to that of other constituents, is governed by the general transport equation. The principal difference between sediment and many dissolved constituents is that sediment particles settle under the influence of gravity. Therefore, the sediment settling velocity is included in the transport equation. The general mass-conservation equation for sediment class (j) is expressed as follows:

$$\frac{\partial}{\partial t}\left(m_x m_y H C_j\right) + \frac{\partial}{\partial x}\left(m_y H u C_j\right) + \frac{\partial}{\partial y}\left(m_x H v C_j\right) + \frac{\partial}{\partial z}\left(m_x m_y w C_j\right) - \frac{\partial}{\partial z}\left(m_x m_y w_{s,j} C_j\right) = \frac{\partial}{\partial z}\left(\frac{m_x m_y}{H} A_b \frac{\partial C_j}{\partial z}\right) + S_{s,j}^{E} + S_{s,j}^{E} \quad \text{3-26}$$

where (C_j) is the concentration of sediment class (j), $(w_{s,j})$ is the settling velocity of that sediment class, (A_b) is the vertical diffusivity coefficient, and $(S_{s,j}^{E})$ and $(S_{s,j}^{I})$ represent the external and internal sediment source and sink terms, respectively. The settling term indicates that, in addition to being transported by the flow and dispersed through turbulent mixing, sediment particles tend to move downward and leave the water column.

At the bed boundary, sediment exchange between the water column and the bed is defined as a net flux. This flux is determined by the difference between erosion from the bed and deposition onto the bed. Therefore, when the erosion rate exceeds the deposition rate, the suspended-sediment concentration in the water column increases. Conversely, when deposition is dominant, a portion of the particles is removed from the water column and stored in the bed.

3.2.5.2 Noncohesive Sediments

Noncohesive sediments include particles such as sand and gravel, whose behavior is governed primarily by particle size, density, settling velocity, and bed shear stress. The movement of these particles begins when the shear stress applied to the bed exceeds the critical shear stress for incipient motion. Once mobilized, the sediment may be transported either as bed load or suspended load.

In the bed-load mode, particles move close to the bed, generally through rolling, sliding, or short saltation movements. In the suspended-load mode, turbulence intensity and shear stress are sufficiently high to keep particles suspended within the water column and transport them with the flow.

In EFDC+, the exchange of noncohesive sediment with the bed may be calculated from the difference between the actual near-bed sediment concentration and the equilibrium sediment concentration. The general net bed-exchange flux is expressed as follows:

$$J_o = w_s(C_{eq} - C_{ne}) \qquad 3\text{-}27$$

where (J_o) is the net sediment-exchange flux at the bed, (w_s) is the settling velocity, (C_{eq}) is the equilibrium near-bed concentration, and (C_{ne}) is the actual near-bed concentration.

When (C_{eq}) exceeds (C_{ne}), conditions favor erosion or resuspension. Conversely, when (C_{ne}) exceeds (C_{eq}), deposition is the dominant process.

3.2.5.3 Cohesive Sediments

Cohesive sediments consist of fine-grained particles such as silt and clay. Their behavior is more complex than that of noncohesive sediments because electrochemical forces and flocculation processes affect their settling, erosion, and deposition. Under these conditions, settling velocity is not determined solely by particle size but also depends on sediment concentration, turbulence intensity, water chemistry, and floc formation.

For cohesive sediments, deposition generally occurs when the bed shear stress is lower than the critical shear stress for deposition. As the shear stress decreases, the likelihood of particle settling and attachment to the bed increases. In contrast, erosion occurs when the bed shear stress exceeds the critical shear stress for erosion. Under such conditions, part of the bed sediment is detached and reintroduced into the water column. This process may become particularly important during high-flow events, floods, or intensive mixing events.

From a water quality perspective, the behavior of cohesive sediments is particularly important because their high specific surface area enables them to transport nutrients and pollutants.

Consequently, their erosion and resuspension may affect phosphorus concentrations, turbidity, dissolved oxygen, and other water quality indicators.

3.2.5.4 SEDZLJ Module

In addition to the standard sediment module, EFDC+ includes the advanced SEDZLJ module. This module was developed for more detailed investigations of sediment transport and bed evolution. Instead of relying solely on general empirical relationships, it can use measured data describing sediment erodibility. Such data are commonly obtained using instruments such as SEDFlume, in which sediment samples are subjected to controlled shear stresses and their erosion rates are measured at different bed depths.

The principal advantage of SEDZLJ is its ability to more accurately represent vertical bed heterogeneity and variations in sediment resistance with depth. However, application of this module requires detailed field data on bed-sediment characteristics. It is therefore more suitable for specialized studies of morphology and sedimentation.

Within the context of the present study, introducing this capability is important because it demonstrates that EFDC+ supports advanced coupling among hydrodynamics, sediment transport, and water quality. Nevertheless, the primary focus of this research is the simulation of hydrodynamics, temperature, salinity, and water quality in Seymareh Reservoir.

3.2.6 Chemical Fate and Transport Module

The chemical fate and transport module in EFDC+ is used to simulate pollutants that, in addition to undergoing advection and diffusion within the water column, may partition among different phases of the aquatic environment. Many chemicals, such as heavy metals and persistent organic compounds, do not remain solely in the dissolved phase. Instead, a portion may sorb onto suspended particles, dissolved organic carbon, or bed sediments. Therefore, the transport pathways and persistence of these substances strongly depend on sorption, desorption, settling, resuspension, and exchange with the bed.

In EFDC+, this module is internally coupled with the hydrodynamic and sediment transport modules. The flow field controls pollutant transport, while suspended sediments and the sediment bed act as carrier or storage phases for chemical substances. Consequently, this module is particularly useful in studies concerned with the fate of particle-reactive contaminants.

In general, a chemical substance may be represented in three principal phases: the freely dissolved phase in water, the phase associated with dissolved organic matter such as DOC, and the phase sorbed onto suspended particles or sediments. The total chemical concentration can be expressed as the sum of the contributions from these phases:

$$C = C_w + \sum_j C_D^j + \sum_i C_S^i$$ Equation 3-28

where (C) is the total concentration of the chemical, (C_w) is its freely dissolved concentration, (C_D^j) represents the fraction associated with dissolved phases, and (C_S^i) represents the fraction sorbed onto solid particles or sediments.

To simplify the calculations, EFDC+ generally applies the equilibrium-partitioning assumption. Under this assumption, sorption and desorption among the different phases are considered sufficiently rapid that, at each time step, the distribution of the chemical among phases is determined using partition coefficients. Therefore, rather than solving separate transport equations for each phase, the mass fraction of the chemical in each phase is calculated. The mass fractions of the freely dissolved phase, the fraction associated with dissolved material, and the fraction sorbed onto solid particles can be expressed as follows:

$$f_w = \frac{C_w}{C} = \frac{\varphi}{\varphi + \sum_i p_i^S s_i + \sum_j p_j^D D_j}$$

$$f_D^j = \frac{C_D^j}{C} = \frac{p_j^D D_j}{\varphi + \sum_i p_i^S s_i + \sum_j p_j^D D_j}$$ Equation 3-29

$$f_S^i = \frac{C_S^i}{C} = \frac{p_i^S s_i}{\varphi + \sum_i p_i^S s_i + \sum_j p_j^D D_j}$$

In these equations, (f_w), (f_D^j), and (f_S^i) represent the mass fractions of the chemical in the freely dissolved phase, the phase associated with dissolved carrier materials, and the phase sorbed onto solid particles, respectively. In addition, (φ) represents porosity or the volumetric fraction of the aqueous phase, (s_i) is the concentration of solid particles, (D_j) is the concentration of dissolved carrier material, and (p_i^S) and (p_j^D) are the partition coefficients associated with the respective phases.

Using these mass fractions, chemical transport is simulated through an equation formulated in terms of the total concentration. The structure of this equation is similar to that of the general constituent transport equation; however, the settling term is applied only to the fraction of the chemical sorbed onto solid particles:

$$\frac{\partial}{\partial t}(mHC) + \frac{1}{m}\frac{\partial}{\partial x}\left(m_y HuC\right) + \frac{1}{m}\frac{\partial}{\partial y}(m_x vC) + \frac{\partial}{\partial z}\left(m_x m_y wC\right) - \frac{\partial}{\partial z}\left(m\sum_i w_S^i f_S^j C\right) = \frac{\partial}{\partial z}\left(\frac{mA_b}{H}\frac{\partial C}{\partial z}\right) - mH\gamma C$$

Equation 3-30

where (C) is the total chemical concentration, (w_S^i) is the settling velocity of the carrier particles, (f_S^i) is the fraction of the chemical sorbed onto those particles, (A_b) is the vertical diffusivity coefficient, and (γ) is the chemical decay or degradation rate. This equation indicates that the dissolved fraction is transported and dispersed with the flow, whereas the particle-associated fraction is additionally affected by settling and exchange with the bed.

Within the sediment bed, the chemical concentration may also change through processes such as deposition of carrier particles, bed erosion and resuspension, porewater exchange, molecular diffusion, bioturbation, and chemical or biological degradation. To simulate these processes, EFDC+ divides the sediment bed into several discrete layers and calculates the chemical mass balance within each layer. However, the complete representation of these processes is primarily relevant to specialized studies of contaminated sediments, heavy metals, and persistent organic compounds.

The present study focuses mainly on simulating hydrodynamics, temperature, salinity, dissolved oxygen, nutrients, and algal growth in Seymareh Reservoir. Therefore, the chemical fate and transport module is introduced as one of the supplementary capabilities of EFDC+ but does not play a primary role in the analyses conducted in this research. Introducing this module is nevertheless important because it demonstrates that the EFDC+ framework can also represent advanced interactions among flow, sediment, organic matter, and particle-reactive contaminants.

3.2.7 Eutrophication and Water Quality Module

Eutrophication, which results from the enrichment of aquatic environments with nutrients, particularly nitrogen and phosphorus compounds, is one of the most important water quality concerns in reservoirs. Increased nutrient concentrations can lead to excessive algal growth, reduced water transparency, pronounced fluctuations in dissolved oxygen, and, under more advanced conditions, the development of hypoxia or anoxia in deeper layers. This issue is particularly important in deep, stratified reservoirs because thermal separation of the water column can restrict oxygen exchange between surface and deep layers and create conditions favorable for nutrient release from the bed.

The EFDC+ water quality module was developed to simulate physical, chemical, and biological processes in the water column simultaneously. Based on an integrated eutrophication and water quality modeling framework, the module defines the principal components of the aquatic ecosystem as state variables and calculates their changes in response to physical transport,

biochemical reactions, exchange with the bed, algal growth and mortality, and nutrient cycling. Because the module is directly coupled with hydrodynamics and water temperature, variations in flow, thermal stratification, vertical mixing, and water temperature can influence both reaction rates and the spatial distribution of water quality variables.

In the present study, among the broad range of water quality variables available in EFDC+, only those most directly related to the principal research question—the effects of water-withdrawal elevation on the water quality of Seymareh Reservoir—were activated. These variables included labile particulate organic carbon, dissolved organic carbon, total phosphate, ammonium, nitrate/nitrite, dissolved oxygen, and one green-algae group. Nevertheless, to provide a complete overview of the module's capabilities, the principal EFDC+ water quality state variables are first introduced, after which the variables activated in the present study are described in greater detail.

3.2.7.1 State Variables in the Water Quality Module

In the EFDC+ water quality module, each water quality constituent is defined as a state variable. Spatial and temporal changes in the concentration of each state variable result from two main categories of processes: first, physical transport through flow and mixing, and second, biochemical reactions that may produce, consume, or transform the variable. Table 3-1 presents the principal water quality state variables available in EFDC+. The final column indicates whether each variable was used in the present study.

Table 3-1. Principal water quality state variables in EFDC+

No.	Water Quality State Variable	Symbol	Unit	Group	Status in the Present Study
1	Refractory particulate organic carbon	RPOC	mg/L	Organic carbon	Inactive
2	Labile particulate organic carbon	LPOC	mg/L	Organic carbon	Active
3	Dissolved organic carbon	DOC	mg/L	Organic carbon	Active
4	Refractory particulate organic phosphorus	RPOP	mg/L	Phosphorus	Inactive
5	Labile particulate organic phosphorus	LPOP	mg/L	Phosphorus	Inactive
6	Dissolved organic phosphorus	DOP	mg/L	Phosphorus	Inactive
7	Total phosphate	PO4t	mg/L	Phosphorus	Active
8	Refractory particulate organic nitrogen	RPON	mg/L	Nitrogen	Inactive
9	Labile particulate organic nitrogen	LPON	mg/L	Nitrogen	Inactive
10	Dissolved organic nitrogen	DON	mg/L	Nitrogen	Inactive

11	Ammonium	NH4	mg/L	Nitrogen	Active
12	Nitrate and nitrite	NO3, NO2	mg/L	Nitrogen	Active
13	Particulate biogenic silica	SiP	mg/L	Silica	Inactive
14	Available dissolved silica	SiA	mg/L	Silica	Inactive
15	Chemical oxygen demand	COD	mg/L	Other variables	Inactive
16	Dissolved oxygen	DO	mg/L	Other variables	Active
17	Total active metals	TAM	mol/m³	Other variables	Inactive
18	Fecal coliform bacteria	FCB	MPN/100 mL	Other variables	Inactive
19	Carbon dioxide	CO2	mg/L C	Other variables	Inactive
20	Aquatic plants and algae	Ba	mg/L C	Algae and macrophytes	One green-algae group was activated
21	Zooplankton	Z	mg/L C	Zooplankton	Inactive

As shown in Table 3-1, EFDC+ can simulate the principal cycles of carbon, nitrogen, phosphorus, silica, and oxygen, as well as algae, aquatic vegetation, zooplankton, and selected microbial and chemical indicators. However, the objective of the present study was not to represent every component of the aquatic ecosystem. Instead, the study focused on variables most directly associated with reservoir stratification, oxygen depletion, algal growth, and the water quality response to changes in withdrawal elevation. Accordingly, the activated variables included LPOC, DOC, PO4t, NH4, NO3/NO2, DO, and one green-algae group.

3.2.7.2 Mass-Conservation Equation in the Water Quality Module

The calculations performed by the water quality module are based on the mass-conservation equation for each state variable. This equation states that changes in the concentration of a variable within each computational cell result from its physical transport by flow and diffusion, together with production or consumption through water quality reactions. The general transport equation for a water quality variable is expressed as follows:

$$\frac{\partial}{\partial t}\left(m_x m_y HC\right)+\frac{\partial}{\partial x}\left(m_y HuC\right)+\frac{\partial}{\partial y}\left(m_x HvC\right)+\frac{\partial}{\partial z}\left(m_x m_y wC\right) = \frac{\partial}{\partial x}\left(\frac{m_y HA_x}{m_x}\frac{\partial C}{\partial x}\right)\frac{\partial}{\partial y}+\left(\frac{m_x HA_y}{m_y}\frac{\partial C}{\partial y}\right)+\frac{\partial}{\partial z}\left(m_x m_y \frac{A_z}{H}\frac{\partial C}{\partial z}\right) + m_x m_y HS_{CP} \quad \text{Equation 3-31}$$

where (C) is the concentration of the water quality state variable; (u), (v), and (w) are the velocity components; (H) is the total water-column depth; (m_x) and (m_y) are the grid metric coefficients; (A_x), (A_y), and (A_z) are the diffusivity coefficients in the respective coordinate directions; and (S_{CP}) is the general source and sink term.

The source and sink term constitutes the principal component of the water quality module and includes processes such as algal growth and mortality, organic matter decomposition, oxygen production and consumption, nitrification, nutrient uptake, and exchange with the bed.

In EFDC+, the water quality equation is generally solved using a stepwise procedure. First, the physical transport of the variable by the flow field and mixing is calculated. Changes caused by biochemical reactions are then applied. During the kinetic step, the change in the concentration of each variable can be expressed in the following simplified form:

$$\frac{\partial C}{\partial t_k} = SCK \qquad \text{Equation 3-32}$$

where (SCK) represents the sum of the production and consumption reactions associated with the state variable under consideration. This separation enables the effects of physical transport and water quality reactions to be calculated systematically and with numerical stability.

3.2.7.3 Algae, Macrophytes, and Zooplankton

Algae, or phytoplankton, are primary producers in aquatic ecosystems and play important roles in oxygen, nutrient, and carbon cycling. Algal growth consumes nitrogen and phosphorus and produces oxygen through photosynthesis. Conversely, algal respiration, mortality, and decomposition can consume oxygen and return organic matter and nutrients to the water column.

EFDC+ allows multiple algal groups with different characteristics to be defined. These groups may include cyanobacteria, diatoms, green algae, and other phytoplankton groups. Differences among these groups are represented through parameters such as growth rate, optimum growth temperature, nutrient requirements, settling velocity, and sensitivity to light or salinity. This capability enables the model to simulate competition among different biological groups under varying environmental conditions.

In addition to free-floating algae, EFDC+ can simulate macrophytes, including rooted aquatic vegetation, as well as epiphytes. This capability is particularly relevant to wetlands, shallow lakes, and other water bodies in which aquatic plants play important roles in nutrient cycling, sediment stabilization, and oxygen production. The model can also simulate zooplankton as primary consumers. Through grazing on algae, zooplankton can regulate algal biomass and contribute to nutrient recycling through excretion and the release of nutrient compounds.

Despite these capabilities, macrophytes and zooplankton were not activated in the present study. Owing to limited available data and to simplify the biological structure of the model, only one green-algae group was included to represent algal biomass and calculate chlorophyll-a. This choice was considered appropriate for the study objective, namely analyzing the responses of chlorophyll-a, dissolved oxygen, and nutrients to different water-withdrawal scenarios.

Changes in algal biomass are represented in the model as a balance among growth, metabolism, mortality, grazing or biological removal, settling, and external loading. The general algal-biomass equation is expressed as follows:

$$\frac{\partial B_x}{\partial t} = (P_x - BM_x - D_x)B_x - PR_x + \frac{\partial}{\partial Z}(WS_x B_x) + \frac{WB_x}{V} \quad \text{Equation 3-33}$$

where (B_x) is the biomass of algal group (x), (P_x) is the growth rate, (BM_x) is the basal metabolic rate, (D_x) is the mortality rate, (PR_x) represents removal through grazing or predation, (WS_x) is the settling velocity, (WB_x) is the external load, and (V) is the computational-cell volume.

Algal growth is calculated as the product of the maximum growth rate and a set of limiting functions:

$$P_x = PM_x f_1(N) f_2(I) f_3(T) f_4(S) \quad \text{Equation 3-34}$$

where (PM_x) is the maximum growth rate of algal group (x), $(f_1(N))$ is the nutrient-limitation function, $(f_2(I))$ is the light-limitation function, $(f_3(T))$ represents the effect of temperature, and $(f_4(S))$ represents the effect of salinity. In simple terms, even when the potential algal growth capacity is high, nutrient deficiency, insufficient light, unfavorable temperature, or unsuitable salinity can reduce the actual growth rate.

3.2.7.4 Organic Carbon Cycle

Organic carbon is represented in the water quality model in several forms to account for differences between rapidly degradable and slowly degradable fractions of organic matter. In the complete EFDC+ framework, organic carbon consists of refractory particulate organic carbon (RPOC), labile particulate organic carbon (LPOC), and dissolved organic carbon (DOC). RPOC generally represents the fraction of organic matter that decomposes slowly, whereas LPOC and DOC are more reactive and can influence oxygen consumption over shorter timescales.

In the present study, LPOC and DOC were activated. These two variables were used to represent a substantial portion of the biodegradable organic load within the water column. Microbial decomposition of LPOC and DOC can consume dissolved oxygen and thereby affect oxygen conditions throughout the water column, particularly in deeper layers.

Because BOD5 measurements were available in the observational dataset, while EFDC+ does not directly use BOD5 as a principal state variable, the measured BOD5 values were converted during data preparation into the corresponding organic-carbon components, namely LPOC and DOC. To

compare model outputs with the observed data, the simulated organic-carbon concentrations were subsequently converted back into equivalent BOD5 values. This approach preserved the internal structure of the model while allowing model performance to be evaluated using the parameter available in the field dataset.

3.2.7.5 Phosphorus Cycle

Phosphorus is one of the most important nutrients influencing algal growth in freshwater systems. In the complete EFDC+ framework, phosphorus is simulated in several organic and inorganic forms. These forms include refractory particulate organic phosphorus (RPOP), labile particulate organic phosphorus (LPOP), dissolved organic phosphorus (DOP), and total phosphate (PO4t). Organic forms of phosphorus can be converted into phosphate through decomposition and mineralization, while phosphate represents the principal form available for algal uptake.

In the present study, the primary focus was placed on PO4t. In the model, total phosphate represents the inorganic and bioavailable form of phosphorus used for algal growth. This variable may be supplied through upstream inflows, mineralization of organic compounds, and exchange with the bed, while it is also consumed through algal uptake. Consequently, variations in PO4t are directly associated with algal growth and changes in chlorophyll-a.

In stratified reservoirs, phosphorus dynamics are strongly influenced by oxygen conditions in the deep layers and near the bed. Oxygen depletion near the sediment–water interface can promote the release of phosphorus from sediments and increase phosphate concentrations in deeper waters. Therefore, phosphorus is not solely an externally supplied variable originating from the watershed; it may also be recycled internally through water–sediment exchange. This process is important when evaluating withdrawal scenarios at different elevations because changes in withdrawal elevation may affect mixing, deep-water oxygen conditions, and ultimately phosphorus availability.

3.2.7.6 Nitrogen Cycle

Nitrogen is another major nutrient required for algal growth. In the complete EFDC+ framework, the nitrogen cycle includes three organic forms and two inorganic forms. The organic forms consist of refractory particulate organic nitrogen (RPON), labile particulate organic nitrogen (LPON), and dissolved organic nitrogen (DON). Through decomposition and mineralization, these compounds may be transformed into inorganic nitrogen forms. The inorganic forms include ammonium (NH4) and nitrate/nitrite (NO3/NO2), which directly contribute to algal growth and oxygen cycling.

In the present study, the two principal inorganic nitrogen forms, NH4 and NO3/NO2, were activated and evaluated. Ammonium is a bioavailable form of nitrogen that can be taken up by algae and is generally produced through the mineralization of organic nitrogen, external loading, and sediment fluxes. It may be consumed directly by algae or converted into nitrate through nitrification under oxygenated conditions.

Nitrate and nitrite are represented in the model as oxidized forms of inorganic nitrogen. They are produced through nitrification and may subsequently be consumed by algae. Under oxygen-depleted conditions, a portion of the nitrate may also be removed from the water-column nitrogen cycle through denitrification. Nitrogen cycling is therefore directly connected to dissolved oxygen conditions, algal growth, and organic matter decomposition.

Conceptually, the nitrification rate is a function of ammonium concentration, dissolved oxygen, and temperature. When dissolved oxygen concentrations decrease, nitrification becomes limited. Consequently, nitrogen behavior in oxygen-depleted deep layers differs from that in oxygenated surface waters.

3.2.7.7 Other Water Quality Variables

In addition to the carbon, nitrogen, and phosphorus cycles, EFDC+ can simulate other variables, including silica, chemical oxygen demand, total active metals, fecal coliform bacteria, and carbon dioxide. Silica is important for simulating diatom growth because diatoms require silica to construct their cell walls. In the model, silica can be represented as particulate biogenic silica (SiP) and available dissolved silica (SiA).

Chemical oxygen demand (COD) represents a fraction of reduced or chemically oxygen-demanding substances that may consume dissolved oxygen. Total active metals (TAM) are used in the model to represent sorption sites for certain compounds, particularly phosphate and silica. Fecal coliform bacteria (FCB) can be used to simulate microbial contamination, while carbon dioxide (CO2) can be applied to investigate inorganic carbon cycling and processes related to respiration and photosynthesis.

These variables were not activated in the principal analyses of the present study because the research focused on dissolved oxygen, the principal nutrients, biodegradable organic carbon, and algae. Nevertheless, their inclusion among the available state variables demonstrates the broad capability of the EFDC+ water quality module for more comprehensive ecological and pollution studies in aquatic systems.

3.2.7.8 Dissolved Oxygen

Dissolved oxygen is one of the principal indicators of aquatic ecosystem health and constitutes one of the most important model-output variables in the present study. Dissolved oxygen concentration is determined by the balance between oxygen-producing and oxygen-consuming processes. Photosynthesis by algae is the principal source of oxygen production within the water column. In contrast, respiration by algae and other organisms, organic matter decomposition, nitrification, sediment oxygen demand, and the oxidation of reduced substances are among the main oxygen-consuming processes.

Conceptually, the dissolved oxygen balance can be expressed as follows:

$$\frac{\partial DO}{\partial t} = P_{\text{photo}} + R_{\text{reaer}} - R_{\text{resp}} - R_{\text{OM}} - R_{\text{nit}} - SOD$$ Equation 3-35

where (P_{photo}) is oxygen production through photosynthesis, (R_{reaer}) is oxygen exchange with the atmosphere through reaeration, (R_{resp}) is oxygen consumption through respiration, (R_{OM}) is oxygen consumption resulting from organic matter decomposition, (R_{nit}) is oxygen consumption caused by nitrification, and (SOD) is sediment oxygen demand.

In stratified reservoirs, dissolved oxygen concentrations are generally higher in the surface layer because of atmospheric exchange and photosynthetic activity. In deeper layers, however, particularly during warm and stable stratification periods, dissolved oxygen may decline substantially. This reduction is primarily caused by restricted vertical mixing combined with the continued consumption of oxygen in the lower layers. Accurate representation of dissolved oxygen is therefore essential for evaluating the effects of withdrawal scenarios at different elevations.

3.2.7.9 Sediment Diagenesis and Water–Sediment Fluxes

Bed sediments in reservoirs are not merely passive physical boundaries; they can also function as active biogeochemical environments. Organic matter deposited on the bed is decomposed through microbial activity, a process that may consume oxygen and produce or release nutrients. The collective physical, chemical, and biological processes occurring within the sediment bed are referred to as sediment diagenesis.

Sediment diagenesis is particularly important in stratified reservoirs because, during periods of oxygen depletion in deeper waters, conditions at the bed may become hypoxic or anoxic. Under these conditions, oxygen consumption at the sediment–water interface may increase, and the release of nutrients, particularly phosphorus and ammonium, may be intensified. These processes can alter water quality in the deeper layers and, following mixing or withdrawal from lower elevations, may also affect the quality of the released water.

EFDC+ provides several options for defining constituent exchange between the sediment bed and the water column. These fluxes may be specified as constant values, as temporally and spatially varying inputs, or calculated using the dynamic sediment-diagenesis model. In the present study, temporally and spatially varying fluxes were supplied as model inputs to represent sediment–water exchange. This approach was selected because it enabled seasonal and spatial patterns of constituent release or consumption at the sediment–water interface to be represented without activating the complete and more complex dynamic diagenesis model.

Under this approach, flux values for the selected variables are specified for different times and areas within the model. These fluxes may represent nutrient release from the bed, oxygen consumption by sediments, or the uptake of certain compounds by the sediment. In general, a positive flux indicates constituent transfer from the bed into the water column, whereas a negative

flux represents constituent removal from the water column and transfer into the bed. Conceptually, this method allows the seasonal influence of sediments on water quality, particularly during warm and oxygen-depleted periods, to be incorporated into the model.

One of the most important bed-related processes is sediment oxygen demand. This process represents the amount of oxygen consumed at the sediment–water interface during organic matter decomposition and the oxidation of reduced compounds. In general, sediment oxygen demand consists of two principal components: carbonaceous oxygen demand resulting from the oxidation of reduced compounds and organic matter decomposition, and nitrogenous oxygen demand associated with ammonium nitrification near the bed. This relationship can be expressed conceptually as follows:

$$SOD = CSOD + NSOD$$ Equation 3-36

where (SOD) is the total sediment oxygen demand, ($CSOD$) is the carbonaceous sediment oxygen demand, and ($NSOD$) is the nitrogenous sediment oxygen demand.

In the present study, incorporating water–sediment fluxes was important because Seymareh Reservoir may experience oxygen depletion in its deeper layers during stratification periods. This decline in dissolved oxygen is not only an important water quality consequence but may also influence nutrient release from the sediment bed. Therefore, the use of temporally and spatially varying fluxes enabled the potential effects of the bed on dissolved oxygen, ammonium, phosphate, and other water quality variables to be represented more realistically in the simulations.

3.2.7.10 Summary of the Water Quality Module

The EFDC+ water quality module enables the integrated simulation of processes related to eutrophication, nutrient cycling, dissolved oxygen, organic matter, algal biomass, silica, microbial indicators, and selected chemical processes. This broad capability makes the model suitable for a wide range of water quality analyses in rivers, lakes, reservoirs, and wetlands.

In the present study, among the full range of capabilities available in this module, the analysis focused on LPOC, DOC, PO4t, NH4, NO3/NO2, DO, and one green-algae group. This set of variables was considered sufficient and appropriately targeted for evaluating the effects of withdrawal scenarios at different elevations on the water quality of Seymareh Reservoir. In addition, temporally and spatially varying fluxes were defined at the sediment–water interface to account for the effects of sediments on nutrient release and oxygen consumption in the deeper layers. This framework provides the basis for analyzing the water quality results and comparing the reservoir operation scenarios presented in Chapter 4.

3.2.8 Supplementary Capabilities of EFDC+

3.2.8.1 Lagrangian Particle-Tracking Module

In addition to simulating constituent concentrations within an Eulerian framework, in which calculations are performed at fixed computational-grid cells, EFDC+ includes a Lagrangian particle-tracking module. Under this approach, the trajectory of each particle or discrete mass parcel is tracked independently within the three-dimensional flow field. Thus, rather than examining concentration changes at a fixed location, the model evaluates particle movement over time in response to flow, turbulence, and dispersion.

Particle movement in this module primarily consists of two components. The first is advection, through which a particle moves in different directions with the local water-flow velocity. These velocities are obtained from the hydrodynamic-module outputs. The second component is turbulence-induced dispersion, which is generally simulated using a random-walk method. Under this method, a stochastic displacement is added to the particle trajectory to represent the effects of turbulent eddies and flow fluctuations. The magnitude of this displacement depends on the turbulent diffusivity coefficients.

The particle-tracking module can be used to investigate pollutant transport pathways, estimate water or constituent travel times between different locations, analyze residence time, simulate the dispersal of aquatic eggs and larvae, and assess the transport of floating materials. Within the same framework, EFDC+ also provides an oil-spill modeling capability. In this application, each particle is treated as an oil parcel, and in addition to transport by currents and turbulent dispersion, the effects of wind, evaporation, and biodegradation on its trajectory and mass reduction are considered.

Despite the importance of this module in pollutant-transport and residence-time studies, the particle-tracking module was not used in the present research. This was because the main focus of the study was the simulation of hydrodynamics, temperature, salinity, dissolved oxygen, nutrients, and chlorophyll-a in Seymareh Reservoir.

3.2.8.2 Marine Hydrokinetic Module

The marine hydrokinetic module is a specialized EFDC+ capability developed to investigate the effects of devices that extract energy from water currents, such as river-current and tidal turbines. By extracting part of the kinetic energy from the flow, these devices can alter velocity, turbulence, and flow patterns in their surrounding areas. From a hydrodynamic perspective, their operation is represented as a momentum sink within the flow field, meaning that a portion of the flow momentum is removed at the location of the device.

In EFDC+, the effects of such equipment are simulated by introducing source and sink terms into the hydrodynamic and turbulence equations. On the one hand, energy extraction by the turbine reduces momentum and consequently decreases flow velocity in the computational cells

containing the device. On the other hand, the turbine and its supporting structure may generate a turbulent wake downstream, which is represented in the model through changes in turbulent kinetic energy and its dissipation rate.

This module is primarily applied in studies evaluating the environmental effects of energy generation from water currents. For example, it can be used to assess changes in flow velocity, mixing, sediment transport, pollutant dispersion, and water quality around turbine arrays. Because no hydrokinetic structures were simulated in Seymareh Reservoir in the present study, this module was not activated and is introduced only as one of the supplementary capabilities of EFDC+.

3.2.8.3 Shellfish Aquaculture Module

The shellfish aquaculture module in EFDC+ is designed to simulate the physical and biological interactions between shellfish or bivalve farms and the surrounding aquatic environment. Shellfish are filter-feeding organisms that process large volumes of water and remove suspended organic particles, phytoplankton, and particulate organic matter (POM) from the water column. Their presence can therefore influence water clarity, algal concentrations, organic matter cycling, and constituent fluxes to the bed.

In this module, shellfish growth is calculated using an energy- or biomass-balance approach. Conceptually, net growth is equal to the energy assimilated from food minus the energy consumed through respiration and other metabolic activities. The principal processes represented by the module include filtration, digestion, assimilation, respiration, organic-matter deposition to the bed, growth, and reproduction. Filtration rates depend on factors such as shellfish size, temperature, salinity, dissolved oxygen, and suspended-solids concentration. Under unfavorable conditions, such as excessive suspended-solids concentrations or oxygen depletion, shellfish feeding activity decreases.

This module is directly coupled with the water quality module. Shellfish act as consumers of phytoplankton and particulate organic matter, while fecal material and metabolic products return organic matter and nutrients to the bed and water column. Therefore, in studies of coastal waters, wetlands, and aquaculture areas, this module can be used to evaluate the effects of shellfish farming on water quality and eutrophication.

In the present study, this module was not activated because of the reservoir-based nature of the study area and the absence of shellfish aquaculture in Seymareh Reservoir. It is therefore introduced solely to provide a more complete overview of the capabilities available in EFDC+.

3.3 Model Development and Preparation

Following the introduction of the theoretical foundations and principal capabilities of EFDC+, this section describes the practical stages involved in developing and preparing the three-dimensional model of Seymareh Reservoir. These stages include introducing the study area; describing the dam, reservoir, and operational structures; preparing hydrological and water quality data; defining

initial and boundary conditions; generating the bathymetry and computational grid; and specifying the principal model-run settings. The purpose of this section is to present the practical model-implementation framework clearly so that the calibration results and management scenarios discussed in Chapter 4 are based on a transparent and traceable modeling procedure.

3.3.1 Description of the Study Area

Seymareh Reservoir, the study area of the present research, is located on the Seymareh River in Ilam Province in southwestern Iran. The dam site is situated in a mountainous region of the Zagros Mountains, upstream of Darreh Shahr. As a result, the reservoir has formed within an environment characterized by complex topography, a deep valley, and considerable lateral slopes. These conditions play an important role in the reservoir's hydrodynamic behavior, mixing patterns, and the vertical and longitudinal distributions of water quality variables.

The Seymareh River is one of the principal tributaries of the Karkheh River system and is formed by the confluence of the Qarah Su and Gamasiab rivers. The watershed upstream of the reservoir covers a substantial area, and in addition to the main Seymareh River, several tributaries contribute to the reservoir inflow. Consequently, the inflow regime results from interactions among the climatic and hydrological conditions of different sub-watersheds and exhibits considerable temporal and spatial variability in both quantity and quality.

Because Seymareh Reservoir is large and relatively deep, it provides favorable conditions for the development of seasonal thermal stratification, vertical differences in temperature and density, and consequent variations in the distribution of water quality parameters throughout the water column. Therefore, the reservoir represents an important and appropriate system for three-dimensional hydrodynamic and water quality modeling.

3.3.2 Characteristics of the Dam, Reservoir, and Operational Structures

Seymareh Dam is a double-curvature concrete arch dam constructed on the Seymareh River for hydropower generation, regulation of surface-water flows, and meeting downstream water demands. The dam has a height of 180 m from the foundation, a crest length of 202 m, and a crest elevation of 730 m above sea level. The normal reservoir water level is 720 m, while the reported maximum water level is 731.45 m above sea level. At an elevation of 731.5 m, the total reservoir volume is 3,251 million m^3. The reservoir volume at the normal water level is 2,473 million m^3, of which 810 million m^3 constitutes active storage. The reservoir surface area at the normal water level is estimated to be 62.7 km^2. These characteristics indicate that Seymareh Reservoir is a large and deep reservoir; consequently, the location and elevation of water withdrawal may influence its thermal structure, vertical mixing, and the distribution of water quality parameters within the water column.

Several principal structures have been constructed within the Seymareh dam and hydropower complex for water conveyance and release. The power-plant intake is located at an elevation of

665 m above sea level. Its associated pressurized headrace tunnel is located on the left bank of the river and has a length of 1,545.92 m, an internal diameter of 11 m, and a design discharge capacity of 460 m^3/s. In addition, two low-level outlets, each measuring 9 × 5.8 m, are located within the dam body at elevations of 620 and 640 m above sea level. Their reported discharge capacities are 591 and 528 m^3/s, respectively.

Although the low-level outlet at an elevation of 620 m is included among the operational structures of the dam, it was not incorporated into the present model. The simulations focused only on the outlets at elevations of 665 and 640 m. This selection was made because reproducing the actual operating conditions of the hydropower plant was prioritized during model calibration, and the outlet at 665 m directly represented these conditions. The outlet at 640 m was subsequently incorporated as a deep-water outlet under the different operational scenarios to evaluate the effects of withdrawal from deeper reservoir layers and its potential role in managing the thermal and water quality conditions of the lower layers.

To simplify the numerical implementation, the two selected outlets at elevations of 665 and 640 m were represented as equivalent rectangular gates, each with an effective width of 10 m. In EFDC+, both outlets were then defined using the hydraulic-structure capability, specifically as orifice-type structures. Accordingly, two independent orifices were created in the model at elevations of 665 and 640 m, and the opening and closing of each structure were controlled using separate time series. During model calibration, only the outlet at 665 m was active, whereas the outlet at 640 m was added during the scenario-based simulations.

3.3.3 Operational Data and Hydrodynamic Boundary Conditions

The operational data used in this study included daily inflow discharge, reservoir water-surface elevation, and daily reservoir storage volume. These data were obtained directly from the study center located at Seymareh Dam and were available for the period from 2013 to 2025. The model calibration period extended from June 2016 to February 2017, while a ten-year period from March 2014 to March 2024 was selected for the analysis of reservoir operation scenarios. Daily inflow data had originally been prepared in separate files for each water year. Following collection, the records were combined into a continuous dataset and arranged in chronological daily order.

In EFDC+, the main reservoir inflow was defined as an open boundary at the computational cell corresponding to the location where the main river enters the reservoir. Because data were available only for the principal inflow, this river branch was used as the upstream boundary of the model.

Because daily reservoir outflow data were not directly available, the outflow discharge was calculated using the reservoir volume balance. Accordingly, the daily outflow discharge was obtained from the following equation:

$$Q_{\text{out},t} = Q_{\text{in},t} - \frac{V_t - V_{t-1}}{\Delta t}$$ Equation 3-37

where ($Q_{\text{in},t}$) is the daily inflow discharge, ($Q_{\text{out},t}$) is the daily outflow discharge on day (t), (V_t) is the reservoir storage volume on day (t), (V_{t-1}) is the reservoir storage volume on the preceding day, and (Δt) is the time interval, equal to one day. Whenever the calculated outflow discharge was negative, it was set to zero to prevent the introduction of physically unrealistic values. Compared with an estimate based solely on the difference in water-surface elevation, this method has a more appropriate physical basis because it directly incorporates the actual change in reservoir storage into the calculation.

3.3.4 Operational Scenarios and Implementation of Outlets in the Model

After calculating the daily reservoir outflow discharge, this discharge was distributed during the long-term simulations between the two modeled outlets located at elevations of 665 and 640 m according to three operational scenarios. Under Scenario 1, the entire outflow discharge was released through the outlet at 665 m, while the outlet at 640 m remained inactive. This scenario represents an operational condition in which reservoir releases are primarily routed through the hydropower outlet. Under Scenario 2, 30% of the outflow discharge was assigned to the outlet at 640 m and 70% to the outlet at 665 m. Under Scenario 3, the outflow discharge was divided equally between the two elevations. These two combined-withdrawal scenarios were defined to investigate the effects of withdrawing part of the flow from deeper reservoir layers and to evaluate its potential consequences for thermal structure and water quality.

In addition to the flow-distribution ratios, an operational constraint was imposed on the outlet at 665 m. Because this outlet corresponds to the hydropower intake, whenever the reservoir water-surface elevation fell below 670 m, the outlet at 665 m was assumed to be closed, and the entire outflow discharge was routed through the outlet at 640 m. This condition was introduced to represent the operational limitation of withdrawal through the 665-m outlet at low reservoir levels. During model calibration, only the outlet at 665 m was active to reproduce the actual hydropower operating conditions as closely as possible, whereas the outlet at 640 m was included only in the long-term management scenarios.

The classical rectangular-orifice flow equation was used to convert the target discharge assigned to each outlet into a physical gate opening. In the present study, both modeled outlets at elevations of 665 and 640 m were represented as equivalent rectangular gates, and the effective gate opening was calculated using the following equation:

$$h = \frac{Q}{C_d\, b\, \sqrt{2gH}}$$ Equation 3-38

where (h) is the effective gate opening, (Q) is the discharge through the outlet gate, (C_d) is the discharge coefficient, (b) is the effective gate width, (g) is gravitational acceleration, and (H) is the upstream hydraulic head relative to the outlet invert elevation. In this study, (C_d) was set to 0.6, and an effective width of 10 m was specified for both outlets.

To make the calculated gate openings more consistent with actual reservoir behavior, the calculation algorithm was not limited to a single fixed equation but was also made dependent on the trend in reservoir water-level variation. During periods of declining water level, the gate opening was calculated directly using the orifice-flow equation. During periods of rising water level or relative water-level stability, however, the effective hydraulic head was corrected by accounting for the elevation of the centroid of the gate opening, thereby providing a more realistic estimate of the required opening. In addition, an adjustment factor of 0.98 was applied in the final calculations to improve consistency between the calculated values and the expected behavior of the operational system.

Because the outlet at 665 m is associated with the hydropower-generation system, it was assumed, to represent actual plant operation more realistically, that this outlet would operate only during peak-demand hours, from 18:00 to 24:00. Accordingly, the calculated daily gate-opening time series for this outlet was converted into an hourly time series, such that the hydropower gate remained closed during most of the day and opened only during the peak-demand period. To preserve the total daily release volume, the required opening was concentrated within the operating hours.

However, to prevent unrealistically large gate openings, a safety constraint was also imposed. Whenever the required opening exceeded the allowable limit, the outlet at 665 m was operated continuously over the entire day using the corresponding average daily opening rather than being restricted to the designated hourly operating period. Furthermore, whenever the water-surface elevation fell below the outlet invert elevation, the gate opening was set to zero.

After these time series had been generated, the gate-opening values were specified as inputs to the hydraulic structures in the model. Two independent orifice-type structures were created in EFDC+ for the outlets at elevations of 665 and 640 m, and the opening and closing of each outlet were controlled using the corresponding time series. During calibration, only the time series associated with the 665-m outlet was used. In the scenario-based simulations, however, time series for both outlets were generated and introduced into the model according to the specified flow-distribution ratios.

This approach enabled a more realistic representation of hydropower operation during the calibration period while also allowing different withdrawal strategies from the intermediate and deep reservoir layers to be evaluated over the ten-year simulation period.

3.3.5 Extraction and Processing of Outflow Water Quality Data

In EFDC+, hydraulic structures such as orifices, weirs, culverts, and gates are defined as part of the hydrodynamic calculations, and the model can calculate the discharge passing through these structures using hydraulic equations. In addition, the constituent-transport and water quality modules are internally coupled with the hydrodynamic field and calculate constituent concentrations throughout the water column. However, in the model outputs used in the present study, the quality of water passing through the orifice-type structures was not provided directly as an outflow water quality time series. Therefore, the quality of the released water had to be calculated from the vertical profiles in the outlet cell together with the gate-opening conditions. The EFDC+ theoretical documentation [55] also indicates that hydraulic structures are calculated within the hydrodynamic component, whereas constituent transport and water quality are simulated throughout the water column. Accordingly, combining these two components during post-processing provides a reasonable method for extracting outflow water quality.

An initial attempt was made to define a virtual downstream cell along the outlet pathway so that water quality after passage through the structure could be extracted directly from the adjacent downstream cell. However, because of the concentrated nature of flow through the orifices, the considerable difference between the outlet elevations, and wetting and drying conditions in the virtual downstream cell, this configuration resulted in numerical instability. Therefore, to avoid numerical errors and maintain the stability of the long-term simulations, the virtual downstream cell was omitted, and outflow water quality was calculated during post-processing using the vertical profiles in the outlet cell.

For this purpose, vertical profiles of hydrodynamic and water quality variables were extracted at 10-day intervals from the terminal model cell in which the outlet structures at elevations of 665 and 640 m were defined. The extracted variables included temperature, salinity, dissolved oxygen, phosphate, ammonium nitrogen, nitrate nitrogen, chlorophyll-a, dissolved organic carbon, labile particulate organic carbon, velocity, and discharge. An effective withdrawal-depth range was specified around each outlet elevation. The elevation range of 663–667 m was used for the structure located at 665 m, while the range of 638–642 m was used for the structure located at 640 m.

The vertical-profile data were subsequently combined with the gate-operation file. This file contained the opening values of the gates at elevations of 640 and 665 m for each day under each scenario. During data processing, when the opening of a gate was zero, the corresponding outlet was excluded from the calculation of outflow water quality. For the outlet at 640 m, the daily opening value was used. For the outlet at 665 m, considering that the hydropower outlet operated during peak-demand hours, the opening corresponding to the evening period of that day was used as the representative value.

The representative value of each parameter within the withdrawal zone of an outlet was not selected from a single depth. Instead, a weighted average of the values within the effective withdrawal range was calculated. In this averaging procedure, sampling points closer to the central elevation of the outlet and associated with greater effective discharge and velocity were assigned larger weights. The final value of each parameter in the released water was then calculated by combining the values corresponding to the two outlet structures at elevations of 665 and 640 m, weighted according to the effective discharge contribution of each outlet:

$$C_{\text{out}} = \frac{Q_{\text{eff},665} C_{665} + Q_{\text{eff},640} C_{640}}{Q_{\text{eff},665} + Q_{\text{eff},640}} \quad \text{Equation 3-39}$$

where (C_{out}) is the final value of the parameter in the outflow, (C_{665}) and (C_{640}) are the values of the same parameter within the withdrawal zones of the outlets located at elevations of 665 and 640 m, respectively, and ($Q_{\text{eff},665}$) and ($Q_{\text{eff},640}$) are the effective discharges of the two outlets after accounting for their gate openings. When only one outlet was active, the water quality value associated with that outlet was taken as the final outflow water quality.

This method enabled outflow water quality to be calculated according to the actual withdrawal elevation, the temporal variation in gate openings, and the effective discharge contribution of each outlet. Consequently, the outflow results used to analyze the operational scenarios in Chapter 4 provide a more realistic representation of the combined water withdrawn from the intermediate and deep layers of the reservoir.

3.3.6 Water Quality, Salinity, and Temperature Data for the Reservoir Inflow

To define the water quality boundary conditions at the reservoir inflow, data from the study conducted by Simin Dehghan Madiseh, entitled “Assessment of Water and Sediment Quality in Seymareh Dam Lake Using Biological and Chemical Quality Indices” [56], were used. In that study, monthly sampling was conducted from June 2016 to February 2017 at five stations, including one inflow station, three stations within the reservoir, and one outflow station. The report also presented various physical and chemical water quality parameters, including temperature, dissolved oxygen, BOD5, total dissolved solids (TDS), electrical conductivity (EC), nitrate, total phosphorus, phosphate, ammonia, ammonium, silicate, and pH.

Although Station 1 was identified as the lake inflow station in the reference study, data from Station 2 were used in the present research to define the water quality of the model inflow. This station was selected because its location was closer to the computational cell used as the inflow boundary in the model (Figure 3-4).

Figure 3-4. Geographic locations of the sampling stations in Seymareh Reservoir [56]

Because the data in the reference study were primarily presented as monthly graphs, the required parameter values were extracted by directly reading the graphs and were subsequently reconstructed as model-input files. These data were available only for selected months between June 2016 and February 2017. Therefore, values for months without observations were estimated using linear interpolation to complete the inflow time series. For the ten-year scenario simulations, the reconstructed monthly pattern for 2016–2017 was adopted as the baseline annual pattern and repeated throughout the entire simulation period. All these data were applied to the same principal inflow open boundary so that the upstream model boundary simultaneously included inflow discharge and the associated water quality parameters.

Continuous measurements of reservoir inflow temperature were also unavailable for the entire simulation period. Therefore, inflow water temperature was estimated using a heat-balance model for the incoming flow. Meteorological variables, including air temperature, dew-point temperature, wind speed, relative humidity, and solar radiation, together with inflow discharge, were incorporated into the calculations. The estimation was based on the balance among the principal heat fluxes, including net radiation, sensible heat exchange with the atmosphere, back radiation from the water surface, and evaporative heat loss. Water temperature was estimated over time for an assumed river reach upstream of the reservoir and was subsequently specified as the temperature boundary condition at the inflow open boundary. This method allowed inflow

temperature to vary consistently with seasonal conditions and hydrological and meteorological fluctuations rather than being represented by a constant value.

One of the important water quality parameters available in the observational dataset was five-day biochemical oxygen demand (BOD5). However, BOD5 is not directly defined as a state variable in the EFDC+ water quality module. Instead, the model uses organic-matter variables such as DOC, LPOC, and RPOC. Therefore, before the boundary conditions were applied, the BOD5 values were converted into the corresponding model constituents.

The conversion of observed water quality data into the state variables required by EFDC+ has also been applied in other studies. For example, in the EFDC-NIER model, observed water quality parameters such as BOD, total organic carbon (TOC), dissolved oxygen, nutrients, and chlorophyll-a were converted into model variables including DOC, LPOC, RPOC, and other components of the carbon, nitrogen, and phosphorus cycles [57]. The conversion procedure used in the present study was performed as follows:

$$CBOD_5 = BOD_5 \times R_{CBOD} \quad \text{Equation 3-40}$$

$$CBOD_u = \frac{CBOD_5}{1 - e^{-5k_{BOD}}} \quad \text{Equation 3-41}$$

$$TOC = \frac{CBOD_u}{R_{O_2/C}} \quad \text{Equation 3-42}$$

$$DOC = TOC \times F_D \quad \text{Equation 3-43}$$

$$LPOC = TOC \times (1 - F_D) \times F_L \quad \text{Equation 3-44}$$

$$RPOC = TOC \times (1 - F_D) \times (1 - F_L) \quad \text{Equation 3-45}$$

In the preceding equations, the conversion coefficients were specified as follows:

(R_{CBOD}): the conversion factor from (BOD_5) to ($CBOD_5$), set to 0.85 [58];

(k_{BOD}): the biochemical decomposition reaction-rate coefficient, set to ($0.23\ \mathrm{day}^{-1}$) [59];

($R_{O_2/C}$): the stoichiometric oxygen-to-carbon ratio, set to 2.67 [55];

(F_D): the fraction of dissolved organic carbon in total organic carbon, set to 0.70 [60]; and

(F_L): the labile fraction of particulate organic carbon, set to 0.833 [61].

Because the RPOC fraction was negligible, it was not included in the final boundary-condition specification, and the incoming organic load was represented primarily by DOC and LPOC. To compare the model outputs with the observational data, the same conversion procedure was

applied in reverse so that the simulated organic-carbon concentrations could be converted back into equivalent (BOD_5) values.

3.3.7 Initial Conditions of the Model

To initiate the simulations, the model initial conditions were defined separately for the calibration period and the long-term operational scenarios. The calibration simulation began on May 30, 2016, while the long-term scenario simulations began on March 21, 2014. The initial reservoir water-surface elevation was specified as 704.37 m above sea level at the beginning of the calibration period and 652.3 m above sea level at the beginning of the long-term simulations.

The initial water-temperature field was defined using tabulated data obtained from the study center located at Seymareh Dam. These data were available as vertical temperature profiles. Following interpolation, the initial temperature field was reconstructed across the different vertical layers of the model. Thus, temperature initialization was based on observational data, avoiding the assumption of a uniform temperature throughout the water column.

For salinity and the other water quality parameters during the calibration period, values obtained from the graphs for June 2016 were used. Parameter values at depths of 0, 20, 40, 60, and 80 m were extracted from the available graphs. Interpolation was then applied to assign an initial vertical profile of each variable over the entire water-column depth. This method was used for the principal water quality parameters, including salinity, dissolved oxygen, and nutrient compounds, so that the initial model conditions would correspond as closely as possible to the actual reservoir conditions at the beginning of the calibration period.

The same reconstructed profiles were also used to define the initial temperature and water quality conditions for the long-term scenario simulations. In other words, the initial values of these variables were assigned based on the information extracted for June 2016. However, as in the calibration simulation, the initial temperature field for the long-term scenarios was determined from the observational tables provided by the Seymareh Dam study center. This approach allowed the initial conditions, particularly for variables sensitive to stratification and vertical mixing, to be defined using the available data while preserving their vertical continuity.

Overall, the initial conditions of the model variables were specified as vertical profiles rather than as spatially uniform values throughout the reservoir. This was particularly important for temperature, salinity, and water quality parameters because the reservoir's vertical structure and the differences between surface and deep-water conditions can substantially influence the evolution of the simulation during its initial days.

3.3.8 Bed Topography, Computational Domain, and Model Grid

To represent the geometry of Seymareh Reservoir accurately, bathymetric data provided by the Iran Water and Power Resources Development Company were used to construct the digital bed-elevation model. The data were supplied as AutoCAD files containing (x), (y), and (z) points.

Following processing, they were used to generate the reservoir-bed topography and assign bed elevations and water depths to the model cells. A continuous topographic surface was generated from the point data using the kriging interpolation method in Surfer. The computational domain extended from the upstream boundary at the location where the main river enters the reservoir to the downstream boundary near Seymareh Dam.

To assess the quality of the generated bed topography, a longitudinal bed profile was extracted along the main reservoir axis. Figure 3-5 presents the topographic map of Seymareh Reservoir together with the path used to extract the longitudinal profile. The red line indicates the profile path extending from the upstream end of the reservoir to the dam, while the arrow at the end of the path identifies the dam location.

As observed in the longitudinal profile, the bed elevation generally decreases along the main reservoir axis from upstream toward the dam, with the deepest part of the reservoir forming near the dam. However, two localized increases in bed elevation are visible at approximate distances of 10,000 and 15,000 m from the beginning of the profile. These peaks resulted from localized topographic constrictions, the relatively wide spacing of the bathymetric survey points, and interpolation limitations in these areas. They were therefore examined as part of the geometric quality control of the model.

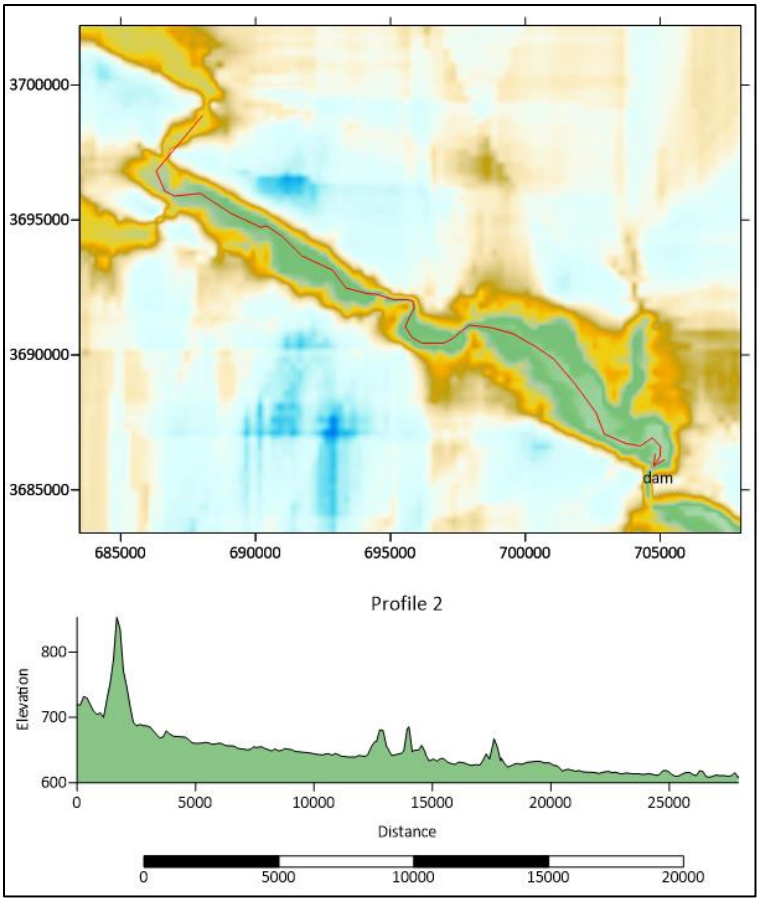

Figure 3-5. Topographic map of Seymareh Reservoir and the longitudinal profile extracted along the main reservoir axis from the upstream end to the dam site.

To prevent the formation of unrealistic irregularities along the principal flow path, the computational cells in these sections were modified within the modeling environment. These modifications were made to preserve the continuity of the reservoir's longitudinal bed slope and ensure that the principal deep channel extended logically from the upstream area toward the dam. As a result, the final model topography not only remained consistent with the available bathymetric data but also exhibited more acceptable hydrodynamic behavior and avoided creating artificial barriers to the transport of flow, heat, and constituents.

A horizontal orthogonal grid was used to simulate the three-dimensional hydrodynamic and water quality processes in Seymareh Reservoir. The bed elevation of each cell was assigned based on the processed reservoir topography. Initially, a relatively fine grid with cell dimensions of 100 × 100 m was generated and used as the reference grid for assessing grid resolution. Figure 3-6 presents an example of the generated two-dimensional grid and the bed elevations assigned to the computational cells. This grid adequately represented the spatial variations in bed elevation and the geometric details of the reservoir, and a one-month simulation was conducted using it.

However, the model runtime was very long, particularly for extended simulations, making it computationally impractical for the ten-year scenario simulations.

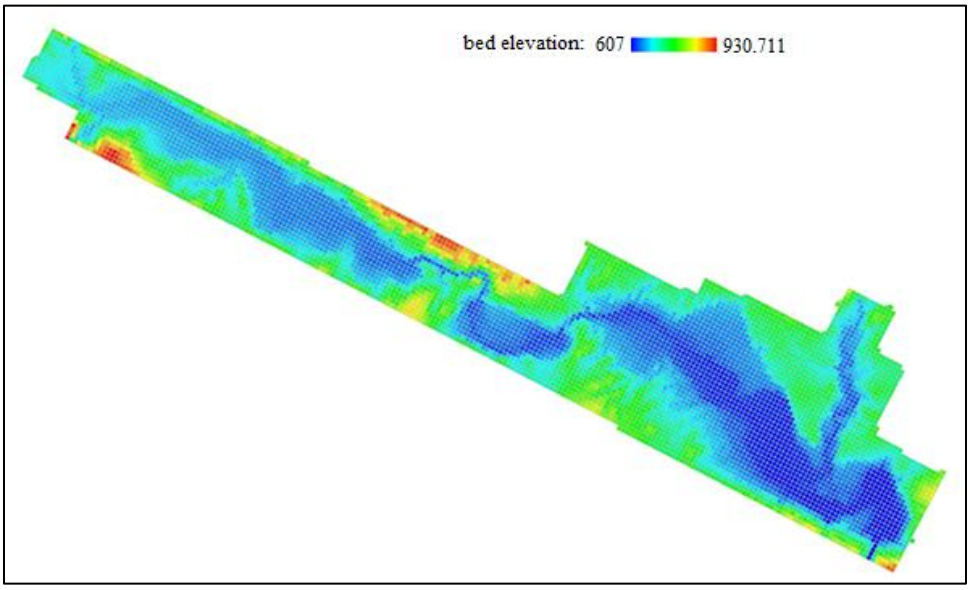

Figure 3-6. Reference two-dimensional computational grid of Seymareh Reservoir and the bed elevations assigned to the model cells.

Therefore, during the subsequent stages of model preparation, the cell dimensions were gradually increased, and the results obtained with the coarser grids were compared with those of the 100 × 100 m reference grid. The objective was to identify a grid that could reduce computational time while reproducing the principal bed structure, variations in bed elevation, and the general patterns of hydrodynamic variables with only negligible differences from the reference-grid results.

Based on this assessment, a grid with cell dimensions of 350 × 350 m, shown in Figure 3-7, was selected as the final configuration. Its results did not differ substantially from those obtained with the reference grid, while the computational speed increased considerably. This grid was therefore adopted as an appropriate balance between numerical accuracy and computational efficiency for both model calibration and the long-term simulations.

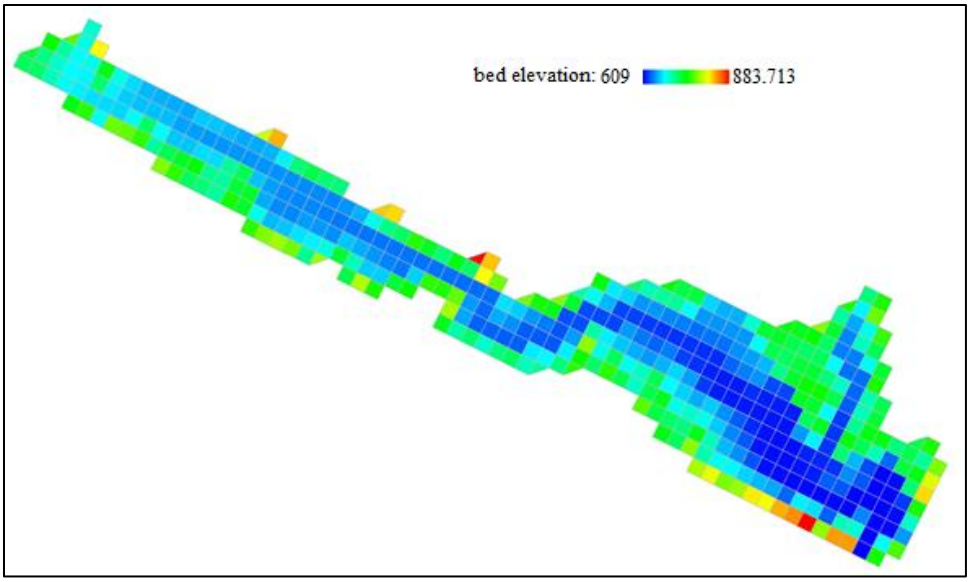

Figure 3-7. Two-dimensional computational grid used for Seymareh Reservoir and the bed elevations assigned to the model cells.

In the vertical direction, the model was configured using 40 uniform SGZ layers. The relative thickness of each layer within the water column was set to 0.025, corresponding to a vertical resolution of approximately 2 m in the deeper parts of the reservoir. This vertical configuration provided an appropriate representation of the reservoir's vertical structure and was considered suitable for simulating depth-dependent variations in temperature, salinity, and other water quality parameters. The same horizontal and vertical grid configuration was used, without substantial modification, during both model calibration and the long-term scenario simulations, allowing results from the different periods to be compared within a consistent numerical framework.

In the final calibration simulation, the model was run from May 30, 2016, to January 29, 2017, corresponding to the field-sampling period. A time step of 8 s was used for the hydrodynamic calculations, while a time step of 120 s was adopted for the biochemical reactions. In the numerical model settings, a two-time-level integration method and a central-difference scheme were used to solve the momentum equations. The Smagorinsky model was applied to represent horizontal turbulence, while a scheme based on the Galperin stability functions was used for vertical turbulence. In addition, the cell wetting and drying mechanism was activated to represent variations in water level and fluctuations in the inundated area more realistically within shallow and nearshore regions.

3.3.9 Meteorological Data and External Forcing

Energy and mass exchanges between the water surface and the atmosphere, which constitute major driving forces of the system, were simulated using hourly meteorological data. These data included solar radiation, air temperature, wind speed and direction, relative humidity, and cloud cover. The

information was used to define surface heat exchange, estimate thermal variations within the reservoir, and calculate the temperature of the river inflow.

The hydrodynamic and water quality boundary conditions also included the reservoir inflows and outflows. Time series of river inflow discharge and water temperature were derived from data provided by the study center located at Seymareh Dam and from supplementary information used in the heat-balance calculations. In addition, the concentrations of water quality parameters in the inflow, including chlorophyll-a, nitrate, ammonia, phosphate, and other water quality variables, were defined based on the field measurements reported by Dehghan Madiseh [56].

3.4 Model Calibration Process

After completing the model geometry, computational grid, initial and boundary conditions, and the incorporation of hydrological, meteorological, and water quality data, the model performance had to be evaluated and adjusted to reproduce the actual behavior of the reservoir. Model calibration in the present study was performed to reduce discrepancies between the simulated results and observational data and involved the stepwise adjustment of parameters affecting hydrodynamics, temperature, and water quality. This stage was essential because the results of the management scenarios can be considered reliable only when the model reproduces the observed reservoir conditions during the baseline period with acceptable accuracy.

3.4.1 Calibration Method and Target Variables

Following model development and data entry, a detailed and iterative calibration procedure was conducted to minimize the differences between the simulated results and field observations. The observational data used in this process were obtained from the field study conducted by Dehghan Madiseh [56] at Seymareh Reservoir.

Model calibration was performed sequentially so that the interactions among hydrodynamic, thermal, and water quality processes could be considered in a controlled manner during parameter adjustment. First, the performance of the hydrodynamic and temperature components was evaluated and adjusted using the reservoir water-surface elevation, stratification structure, and vertical temperature profiles. After ensuring that the flow field and thermal regime were represented satisfactorily, the water quality module was calibrated. This approach was selected because water quality processes, including dissolved oxygen dynamics, nutrient cycling, and algal growth, are strongly influenced by the hydrodynamic and thermal conditions of the reservoir.

The calibration period extended from May 30, 2016, to January 29, 2017, corresponding to the available field-sampling period. The observational data used at this stage included vertical profiles of temperature, salinity, and the principal water quality parameters at depths of 0, 20, 40, 60, and 80 m. Temperature, chlorophyll-a, dissolved oxygen, nitrate, ammonia, phosphate, and BOD5 were considered the principal calibration variables.

Water quality calibration was conducted using a guided trial-and-error procedure focused on the model's sensitive parameters. Only parameters considered conceptually most influential on the model response in Seymareh Reservoir were modified. These included algal growth and respiration coefficients, light- and nutrient-limitation parameters, nitrification coefficients, parameters governing organic matter decomposition, and coefficients associated with oxygen exchange. The final parameter values were selected according to two principles: first, they had to remain within the ranges reported in reference sources and model documentation; and second, they had to improve the overall agreement between the model results and field observations across different depths and months.

For organic matter, the field data were available as BOD5, whereas EFDC+ represents organic loading through organic-carbon state variables. Therefore, following the procedure described in Section 3-2-5, the BOD5 values were converted into organic-carbon components, particularly DOC and LPOC, before being introduced into the model. During calibration assessment, the corresponding model outputs were converted back into equivalent BOD5 values so that comparison with the observational data could be conducted using the same measured parameter.

3.4.2 Key Calibration Parameters and Their Scientific Ranges

Table 3-2 summarizes the most important parameters optimized during the calibration process. Only parameters that had a substantial influence on the final model response are included, while purely numerical settings and insensitive parameters have been excluded.

Table 3-2. Key Model Calibration Parameters, Selected Values, and Recommended Scientific Ranges

No.	Parameter	Brief Description	Value Used in the Model	Scientific Range/Calibration Guidance
1	AHO	Horizontal diffusivity coefficient	1 m²/s	Approximately 0.1–10 m²/s
2	AVO	Background vertical viscosity	(10^{-5}) m²/s	(10^{-6})–(10^{-4}) m²/s
3	ABO	Background vertical diffusivity coefficient	(10^{-6}) m²/s	(10^{-7})–(10^{-5}) m²/s
4	$WQKEB$	Background light-extinction coefficient	0.25 m^{-1}	Approximately 0.1–1.0 m^{-1}
5	$WQKETSS$	Light-extinction coefficient due to suspended solids	0.05 $(m^{-1})/(g,m^{-3})$	Approximately 0.01–0.10 $(m^{-1})/(g,m^{-3})$
6	PM_g	Maximum green-algae growth rate	1.2 day^{-1}	Approximately 0.5–3.0 day^{-1}
7	BMR_g	Basal metabolic rate of green algae	0.05 day^{-1}	Approximately 0.01–0.10 day^{-1}
8	PRR_g	Grazing/mortality rate of green algae	0.02 day^{-1}	Approximately 0.01–0.50 day^{-1}
9	KHN_g	Nitrogen half-saturation concentration for green-algae growth	0.1 mg/L	Approximately 0.01–0.30 mg/L

10	KHP_g	Phosphorus half-saturation concentration for green-algae growth	0.1 mg/L	Approximately 0.001–0.05 mg/L
11	TM_{g1}	Lower limit of the optimum temperature range for green-algae growth	17 °C	Approximately 15–20 °C
12	TM_{g2}	Upper limit of the optimum temperature range for green-algae growth	26 °C	Approximately 25–30 °C
13	$AOCR$	Oxygen-to-carbon ratio for photosynthesis	2.67 g O_2/g C	Generally close to 2.67
14	PM_d	Maximum diatom growth rate	2.5 day(^{-1})	Approximately 1.0–3.0 day(^{-1})
15	BMR_d	Basal metabolic rate of diatoms	0.01 day^{-1}	Approximately 0.005–0.10 day^{-1}
16	PRR_d	Grazing/mortality rate of diatoms	0.35 day^{-1}	Approximately 0.05–0.50 day^{-1}
17	$rNitM$	Maximum nitrification rate	0.1 day^{-1}	Approximately 0.05–1.00 day^{-1}
18	$KHNitDO$	Dissolved oxygen half-saturation concentration for nitrification	0.6 mg/L	Approximately 0.3–1.0 mg/L
19	$KHNitN$	Ammonium half-saturation concentration for nitrification	0.35 mg/L	Approximately 0.1–1.0 mg/L
20	KCD	COD decomposition rate	0.1 day^{-1}	Approximately 0.05–0.50 day^{-1}
21	KRO	Reaeration coefficient	1 day^{-1}	Approximately 0.5–5.0 day^{-1}

As shown in Table 3-2, model calibration focused on a set of key parameters that had the greatest influence on reproducing the reservoir's thermal structure, algal growth, nutrient cycling, and dissolved oxygen dynamics.

3.4.3 Model Performance Evaluation Criteria

Model performance during calibration was evaluated through direct comparison of vertical profiles, temporal variations in the parameters, and the model's ability to reproduce the seasonal behavior of the reservoir. Particular attention was given to the model's capacity to reproduce thermal stratification, oxygen depletion in the deeper layers, temporal and vertical variations in nutrient concentrations, and trends in algal biomass.

In addition to graphical analysis and conceptual agreement, commonly used statistical indices were employed to quantify model accuracy. These indices included the root mean square error (RMSE), mean absolute error (MAE), and Nash–Sutcliffe efficiency coefficient (NSE). The results of these statistical evaluations are presented in Chapter 4 in the section describing the calibration results.

4 Results and Discussion

4.1 Introduction

This chapter presents and analyzes the results of the three-dimensional hydrodynamic and water quality simulations of Seymareh Reservoir conducted using EFDC+. The results are organized so that the model's performance in reproducing the physical behavior of the reservoir, including water-surface elevation and thermal structure, is evaluated first. The results for the biogeochemical and water quality parameters are then assessed. The study period extended from June 2016 to January 2017 and included both thermal stratification during the warm months and the weakening of stratification and transition toward reservoir mixing during the colder months.

4.2 Calibration and Analysis of the Hydrodynamic and Temperature Model

Water-surface elevation and temperature are two key variables for evaluating the hydrodynamic performance of the model. Water-surface elevation indicates the model's ability to reproduce the reservoir volume balance and the consistency among inflow, outflow, and changes in storage. Temperature is the principal factor controlling density variations and the formation of thermal stratification in the reservoir. It also regulates the rates of many chemical and biological water quality processes. Therefore, before analyzing the water quality results, the model's ability to reproduce water-level fluctuations and the reservoir's thermal regime must be evaluated.

4.2.1 Water-Surface Elevation and Reservoir Volume Balance

The first step in evaluating model performance was to assess its ability to reproduce fluctuations in the reservoir water-surface elevation. Water level represents the overall outcome of the reservoir volume balance, and errors in its simulation may affect storage volume, hydraulic residence time, withdrawal depth, and ultimately the concentrations of water quality parameters. Figure 4-1 compares the time series of the simulated and observed water-surface elevations at Seymareh Dam during the calibration period. The corresponding statistical error indices are presented in Table 4-1

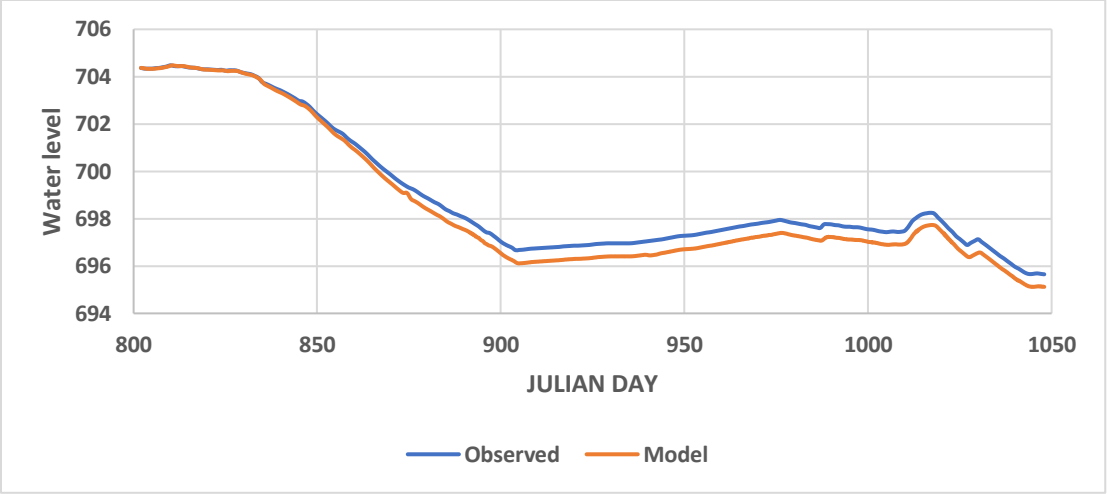

Figure 4-1. Observed and EFDC+-simulated water-surface elevations in Seymareh Reservoir during the calibration period.

Table 4-1. Statistical error indices for the EFDC+-simulated water-surface elevation in Seymareh Reservoir during the calibration period.

Statistical Index	**Value**
Number of data points ((n))	247
Mean absolute error (MAE)	0.41 m
Root mean square error (RMSE)	0.46 m
Normalized mean absolute error (NMAE)	0.058%
Normalized root mean square error (NRMSE)	0.065%

As shown in Figure 4-1, the model successfully reproduced the overall declining trend and fluctuations in reservoir water-surface elevation during the calibration period. During the early part of the simulation, the agreement between the observed and simulated values was very close, and the model accurately followed the gradual decline in water level. After approximately simulation day 900, the simulated values were slightly lower than the observations during most intervals. Nevertheless, the differences remained limited, and the overall pattern of water-level variation was preserved.

According to Table 4-1, the model reproduced water-level fluctuations with very high accuracy, with normalized errors below 0.1%. This strong agreement resulted from the development and implementation of the intelligent outlet-management algorithm described in Chapter 3.

4.2.2 Analysis of Vertical Profiles and Thermal Stratification

In this section, the vertical temperature profiles simulated by the model are compared with the observational data collected at the field-sampling stations in Seymareh Reservoir. Figure 4-2 illustrates the variations in temperature profiles during different months.

- **July—establishment of summer thermal stratification:** The profile corresponding to mid-July indicates that Seymareh Reservoir had entered a period of distinct thermal stratification. The surface-water temperature reached approximately 29.6 °C, whereas temperatures in the deeper layers, particularly at depths greater than 80 m, decreased to approximately 17.3 °C. This temperature difference of nearly 12 °C between the surface and deep waters indicates the formation of a pronounced thermal gradient within the water column. Such a gradient increases density stability and restricts complete vertical mixing between the surface and deeper layers.

- **August—maximum stability of thermal stratification:** During August, thermal stratification reached its most stable condition. Although the standard deviation of the model results was slightly higher in this month than in the other months, the model successfully reproduced the thermocline depth within approximately 30–40 m below the water surface.

- **Autumn and winter—autumn turnover period:** With the transition toward December and January, cooling of the overlying air and decreasing solar radiation reduced the temperature of the surface layer. The model results for January and February indicate a weakening of thermal stratification and a tendency toward increasingly uniform vertical temperature profiles, suggesting the onset of complete mixing within the reservoir.

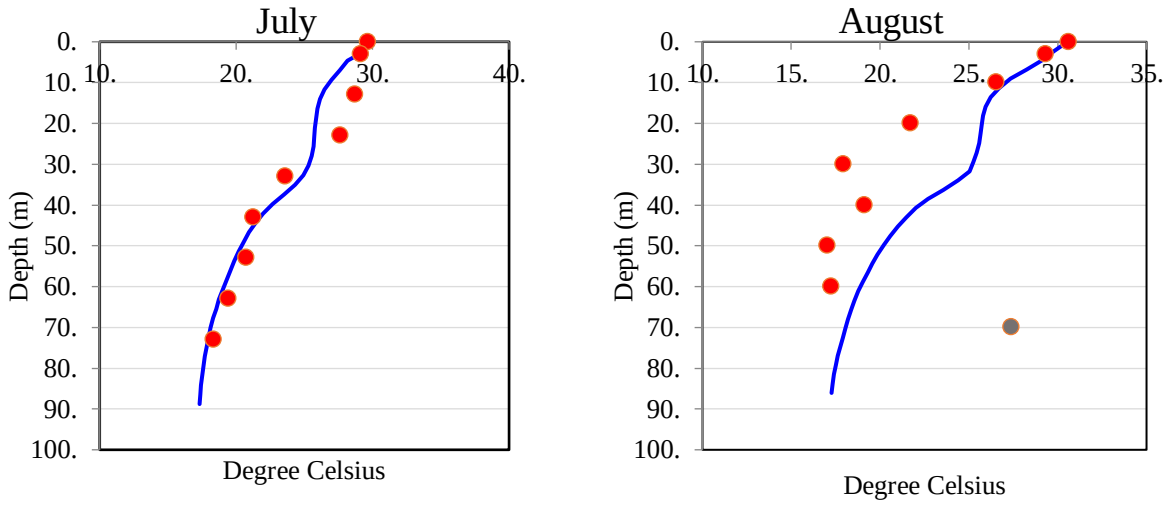

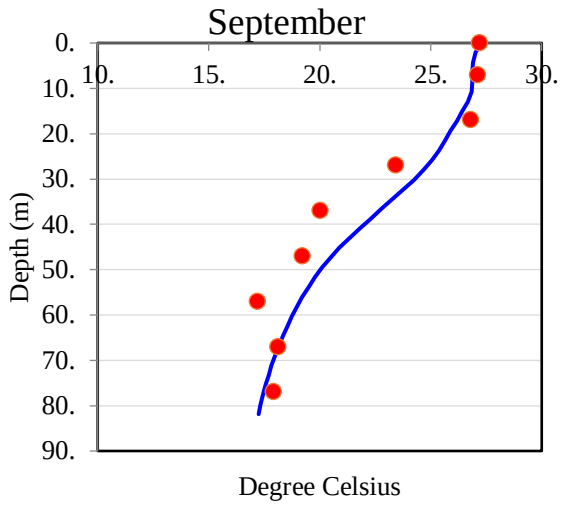
September
0.
10.
20.
30.
40.
50.
60.
70.
80.
90.
Depth (m)
10.
15.
20.
25.
30.
Degree Celsius

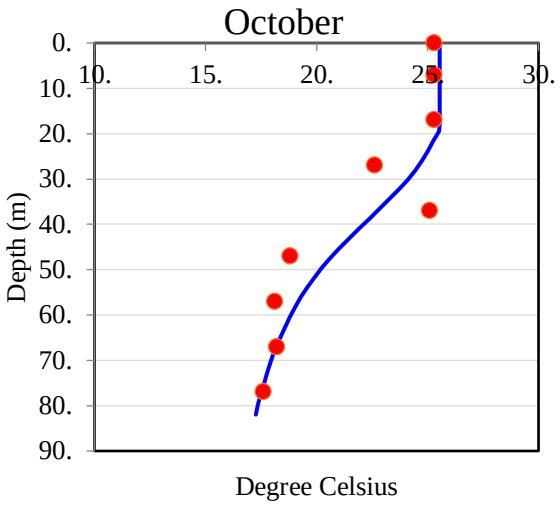
October
0.
10.
20.
30.
40.
50.
60.
70.
80.
90.
Depth (m)
10.
15.
20.
25.
30.
Degree Celsius

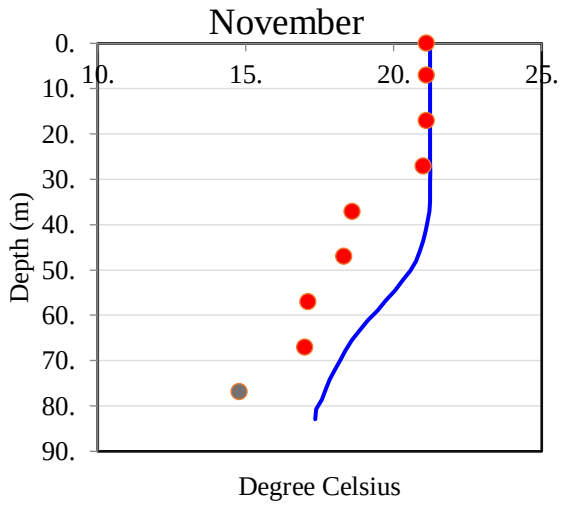
November
0.
10.
20.
30.
40.
50.
60.
70.
80.
90.
Depth (m)
10.
15.
20.
25.
Degree Celsius

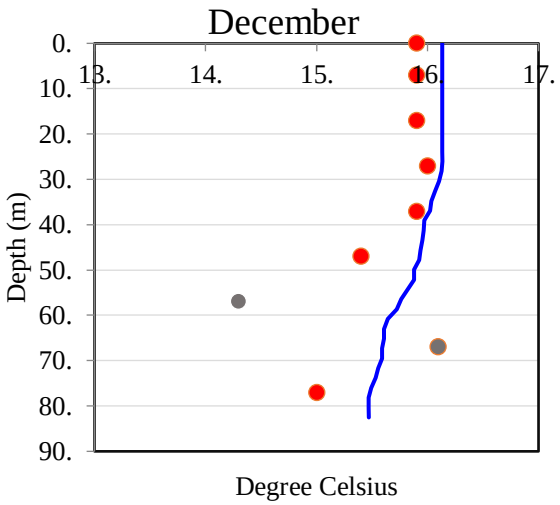
December
0.
10.
20.
30.
40.
50.
60.
70.
80.
90.
Depth (m)
13.
14.
15.
16.
17.
Degree Celsius

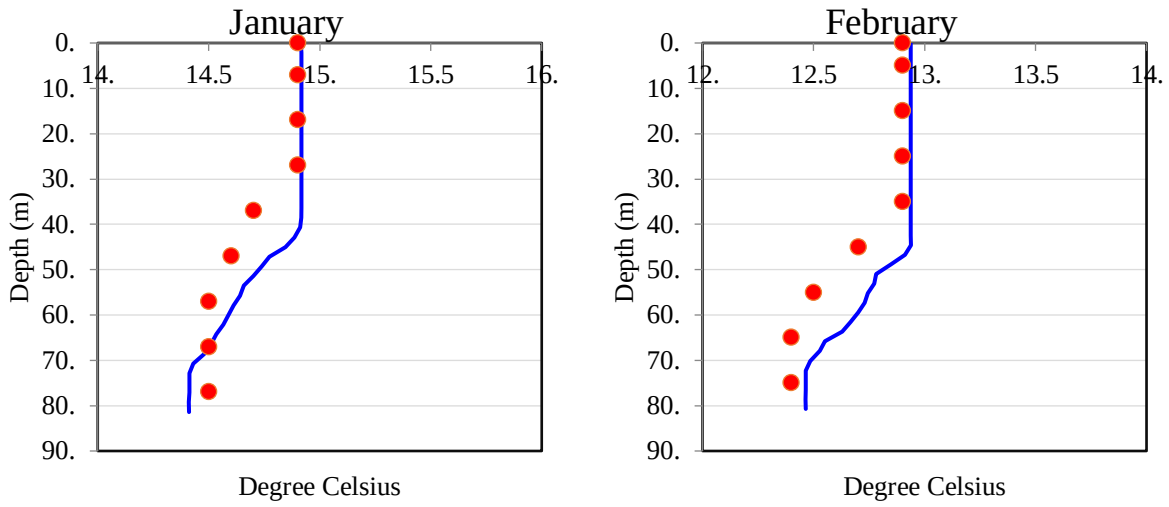

Figure 4-2. Vertical temperature profiles from July to February during the calibration period of the EFDC+ model for Seymareh Reservoir.

4.2.3 Statistical Evaluation of EFDC+ Accuracy in Temperature Simulation (Error Analysis)

To quantitatively assess the ability of EFDC+ to reproduce the thermal structure of Seymareh Reservoir and to confirm the reliability of the hydrodynamic results, five established statistical indices were used: mean absolute error (MAE), root mean square error (RMSE), Nash–Sutcliffe efficiency (NSE), normalized mean absolute error (NMAE), and normalized root mean square error (NRMSE). The results of this evaluation for the different sampling periods are presented in Table 4-2.

Table 4-2. Statistical evaluation of EFDC+ accuracy in simulating water temperature.

Statistical Index	July	August	Septem ber	Octobe r	Novem ber	Decem ber	Januar y	Februa ry	Mean
MAE (°C)	0.87	2.63	0.97	0.91	1.23	0.28	0.07	0.10	0.88
RMSE (°C)	1.16	3.43	1.31	1.27	1.66	0.32	0.11	0.13	1.17
NSE	0.93	0.57	0.89	0.86	0.08	0.15	0.65	0.61	0.59
NMAE_m ean(%)	3.61	11.74	4.44	4.18	6.32	1.79	0.51	0.81	4.18
NRMSE_ mean(%)	4.80	15.28	5.98	5.83	8.56	2.02	0.73	1.05	5.53

- **Analysis of the Statistical Results**

According to Table 4-2, the mean MAE and RMSE values for the entire period were 0.88 and 1.17 °C, respectively. The mean NMAE and NRMSE values were 4.18% and 5.53%, respectively, indicating that the model errors in reproducing reservoir water temperature were within an acceptable range.

In July, September, and October, NSE values exceeded 0.85, demonstrating the model's satisfactory ability to reproduce the thermal structure during the stratified period. The greatest errors occurred in August, which may be attributed to the sensitivity of the model to the precise location of the thermocline and to surface heat-exchange conditions during the peak of summer.

4.3 Calibration and Analysis of Water Quality Parameters

After confirming the satisfactory performance of the hydrodynamic model, the EFDC+ water quality module was activated to simulate the biogeochemical conditions of Seymareh Reservoir. This section examines the complex processes associated with nutrient cycling, dissolved oxygen dynamics, and algal growth.

4.3.1 Calibration and Analysis of Dissolved Oxygen

Dissolved oxygen is one of the most critical water quality parameters in reservoirs and is widely recognized as an indicator of aquatic ecosystem health. Dissolved oxygen concentrations in Seymareh Reservoir are governed by interactions between physical processes, including thermal stratification and surface reaeration, and biogeochemical processes, including algal photosynthesis, respiration, and organic matter decomposition.

a) Analysis of Vertical Profiles and Oxygen Stratification

The vertical profiles presented in Figure 4-3 indicate that Seymareh Reservoir develops pronounced oxygen stratification during the warm months. As shown by the July and August data, dissolved oxygen concentrations in the surface layer remained relatively high, ranging from approximately 10.8 to 12.6 mg/L, because of atmospheric exchange and algal photosynthetic activity. With increasing depth and passage through the thermocline, however, dissolved oxygen concentrations declined sharply.

In October, dissolved oxygen at a depth of 80 m decreased to 3.7 mg/L in the observations and 2.9 mg/L in the simulation. This reduction in deep-water oxygen concentrations can be attributed to two principal factors:

1. **Thermal barrier:** The strong thermal stratification demonstrated in Section 4-2 restricts oxygen transfer from the surface layer to deeper waters.
2. **Biological consumption:** The decomposition of settled organic matter and bacterial respiration in the deeper layers consume the available oxygen. In the absence of sufficient vertical mixing, these processes lead to the development of hypoxic conditions.

b) Turnover Period and Vertical Homogenization of Dissolved Oxygen

The model results for February clearly represent the autumn–winter turnover process. During this month, dissolved oxygen concentrations throughout the reservoir, from the surface to a depth of 80 m, became nearly uniform at approximately 11 mg/L. The close agreement between simulated and observed values at all depths confirms the model's ability to reproduce mass-transfer processes and complete reservoir mixing during the colder months.

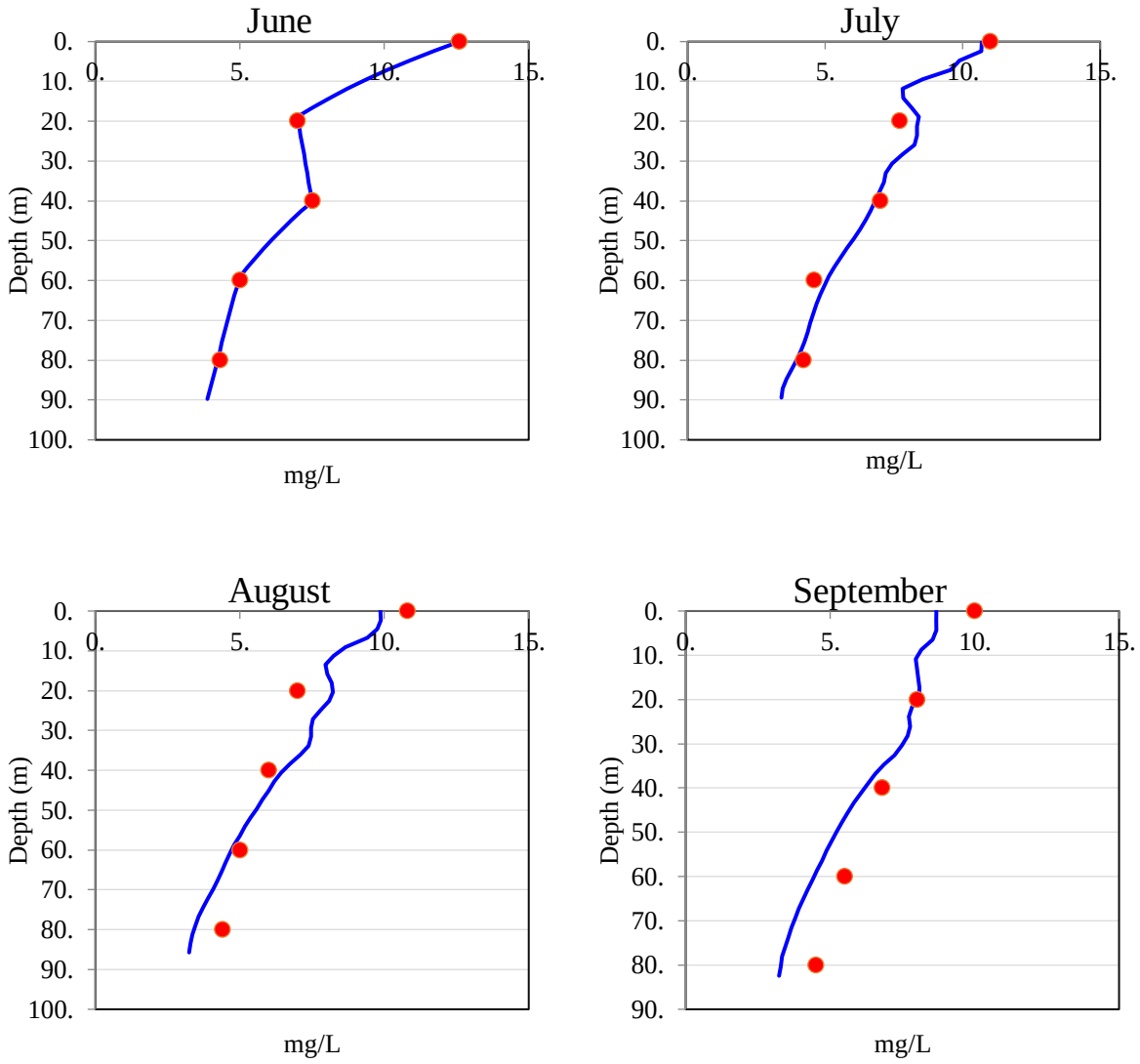

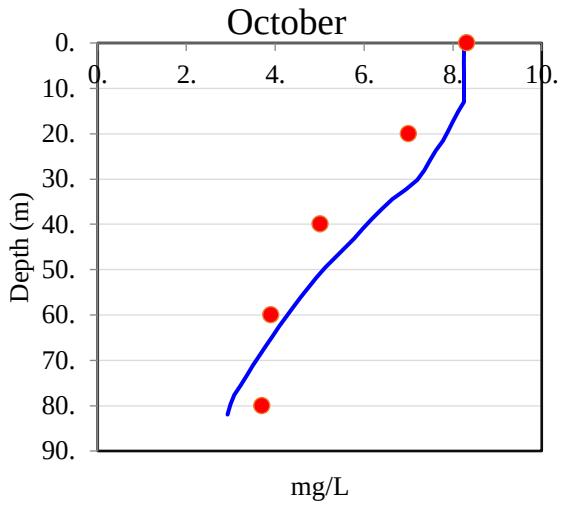
October
0.
10.
20.
30.
40.
50.
60.
70.
80.
90.
Depth (m)
0.
2.
4.
6.
8.
10.
mg/L

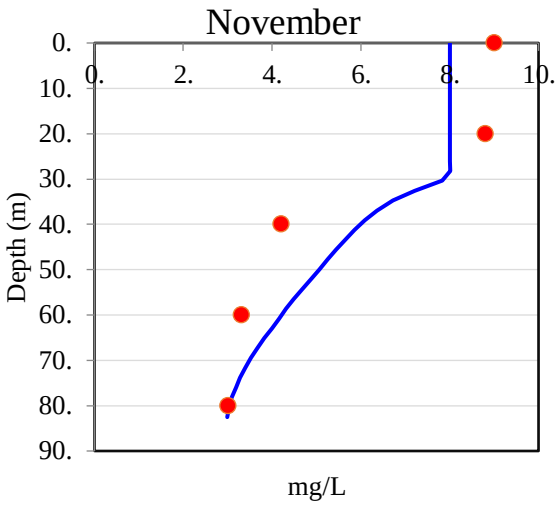
November
0.
10.
20.
30.
40.
50.
60.
70.
80.
90.
Depth (m)
0.
2.
4.
6.
8.
10.
mg/L

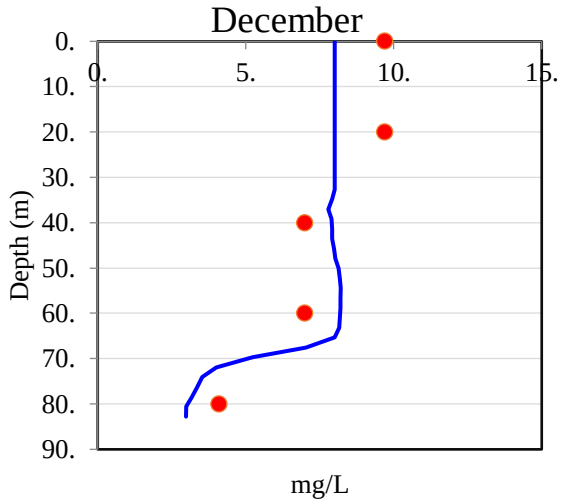
December
0.
10.
20.
30.
40.
50.
60.
70.
80.
90.
Depth (m)
0.
5.
10.
15.
mg/L

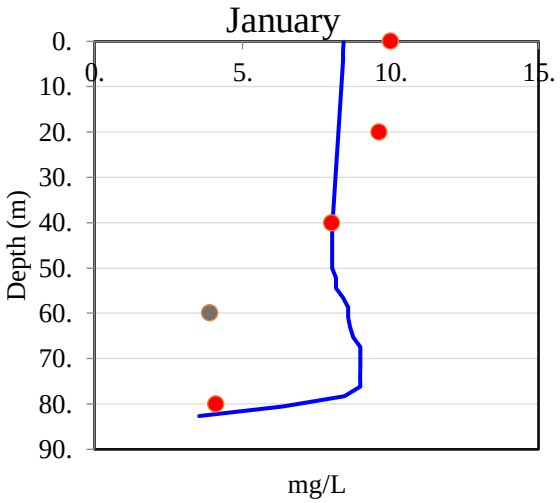
January
0.
10.
20.
30.
40.
50.
60.
70.
80.
90.
Depth (m)
0.
5.
10.
15.
mg/L

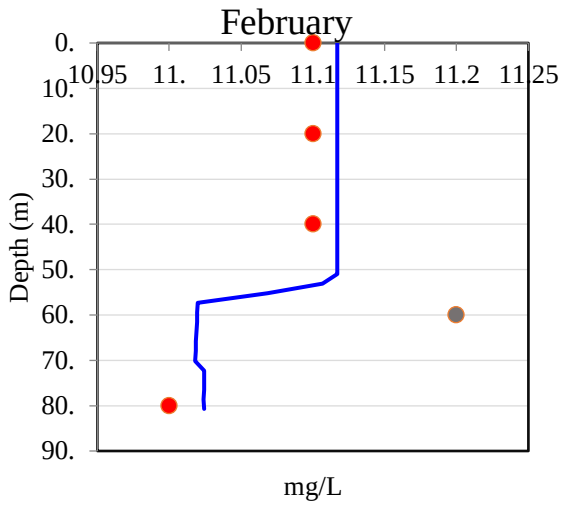

Figure 4-3. Comparison of the vertical dissolved oxygen profiles simulated by EFDC+ from June to February with the field observations.

c) Statistical Evaluation of Model Accuracy in Simulating Dissolved Oxygen

The statistical results obtained by comparing the simulated and observed values are presented in Table 4-3. These results demonstrate the model's overall accuracy in reproducing vertical variations in dissolved oxygen throughout the simulation period.

Table 4-3. Statistical evaluation of EFDC+ accuracy in simulating dissolved oxygen.

Statistical Index	June	July	August	September	October	November	December	January	February	Mean
MAE (mg/L)	0.03	0.37	0.78	0.84	0.61	0.91	1.31	1.42	0.02	0.70
RMSE (mg/L)	0.04	0.41	0.85	0.97	0.71	1.06	1.35	1.71	0.02	0.79
NSE	1.00	0.97	0.86	0.75	0.84	0.84	0.58	0.46	0.81	0.79
NMAE_mean (%)	0.39	5.41	11.79	12.11	11.00	16.00	17.47	17.95	0.17	10.25
NRMSE_mean (%)	0.54	5.96	12.85	13.95	12.73	18.81	18.01	21.55	0.17	11.62

According to Table 4-3, the mean RMSE for the entire simulation period was 0.79 mg/L. In June, the model achieved a Nash–Sutcliffe efficiency coefficient of 1.00, indicating complete agreement with the specified initial reservoir conditions. In February, the lowest normalized error, 0.17%, was recorded, demonstrating the model's excellent ability to reproduce the nearly oxygen-saturated conditions associated with complete reservoir mixing.

4.3.2 Calibration and Analysis of Organic Load (BOD5)

BOD5, as an indicator of biodegradable organic loading, plays an important role in interpreting dissolved oxygen conditions in the reservoir. Increased organic matter concentrations can intensify oxygen consumption through microbial decomposition, particularly in deep and weakly mixed layers. Therefore, examining variations in BOD5 together with dissolved oxygen, nutrients, and chlorophyll-a provides a more comprehensive representation of the reservoir's biogeochemical conditions.

a) Analysis of Vertical Organic-Load Profiles

The vertical variations in BOD5 throughout the water column are presented in Figure 4-4. According to the July profile, the BOD5 concentration reached its maximum value near the water surface, at approximately 9.5 mg/L. This pattern, which was also successfully reproduced by the model, may be attributed to the production of dissolved and particulate organic matter by algal biomass within the surface layer.

Toward the deeper parts of the reservoir, as clearly observed in the September profile, the organic-load concentration decreased to approximately 1.5–4 mg/L. This decline reflects the mineralization of organic matter during settling, a process that contributes to oxygen consumption in the lower layers.

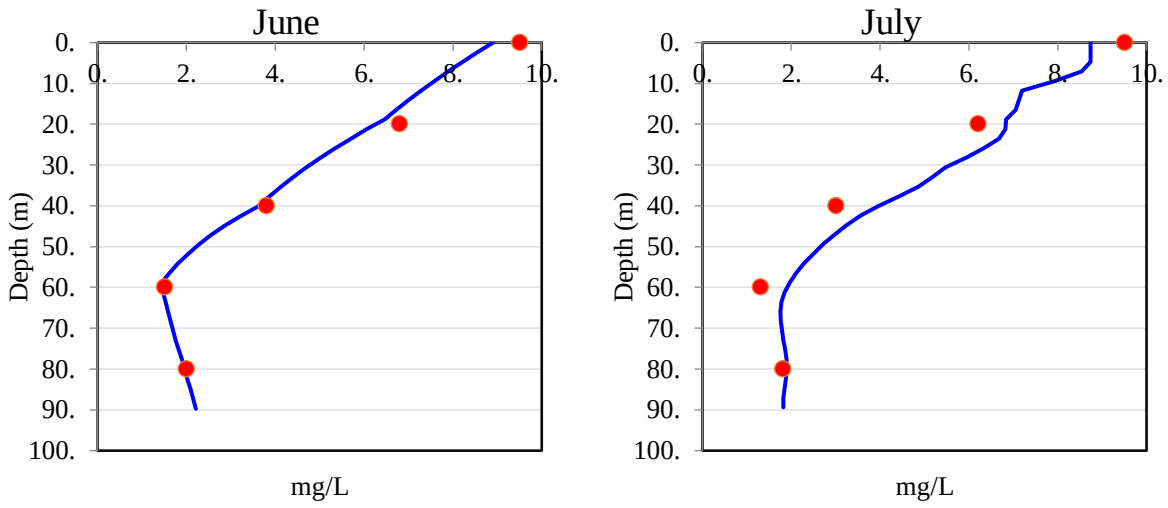

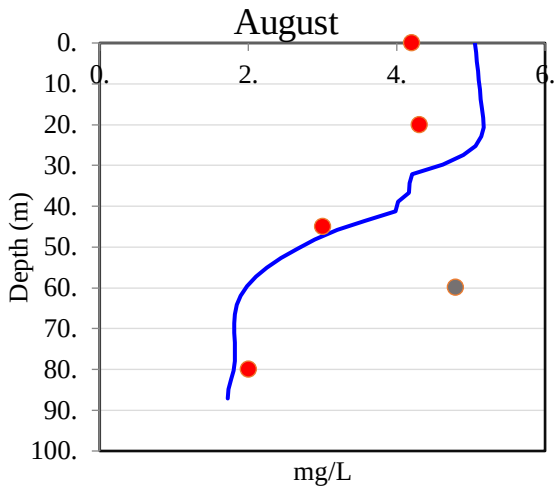
August
0.
10.
20.
30.
40.
50.
60.
70.
80.
90.
100.
Depth (m)
0.
2.
4.
6.
mg/L

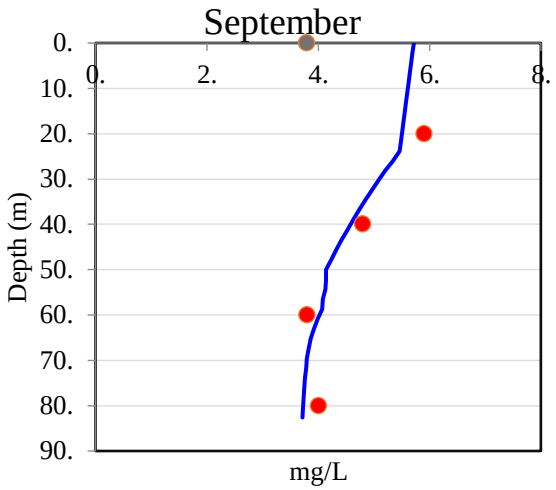
September
0.
10.
20.
30.
40.
50.
60.
70.
80.
90.
Depth (m)
0.
2.
4.
6.
8.
mg/L

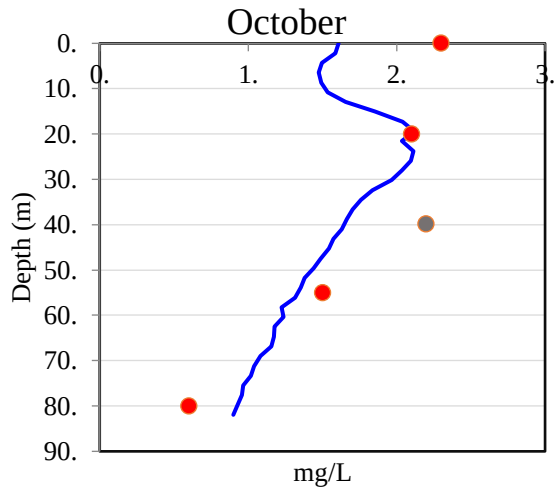
October
0.
10.
20.
30.
40.
50.
60.
70.
80.
90.
Depth (m)
0.
1.
2.
3.
mg/L

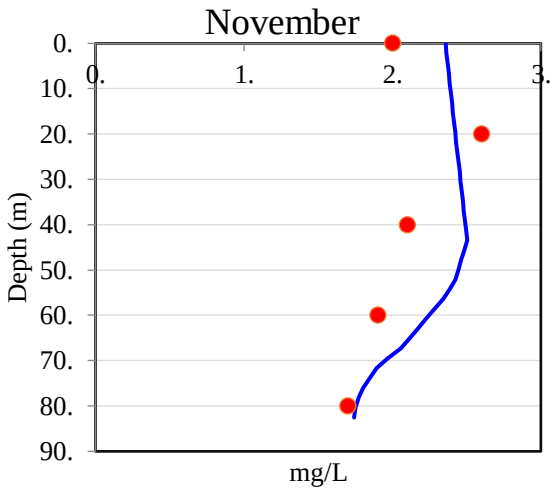
November
0.
10.
20.
30.
40.
50.
60.
70.
80.
90.
Depth (m)
0.
1.
2.
3.
mg/L

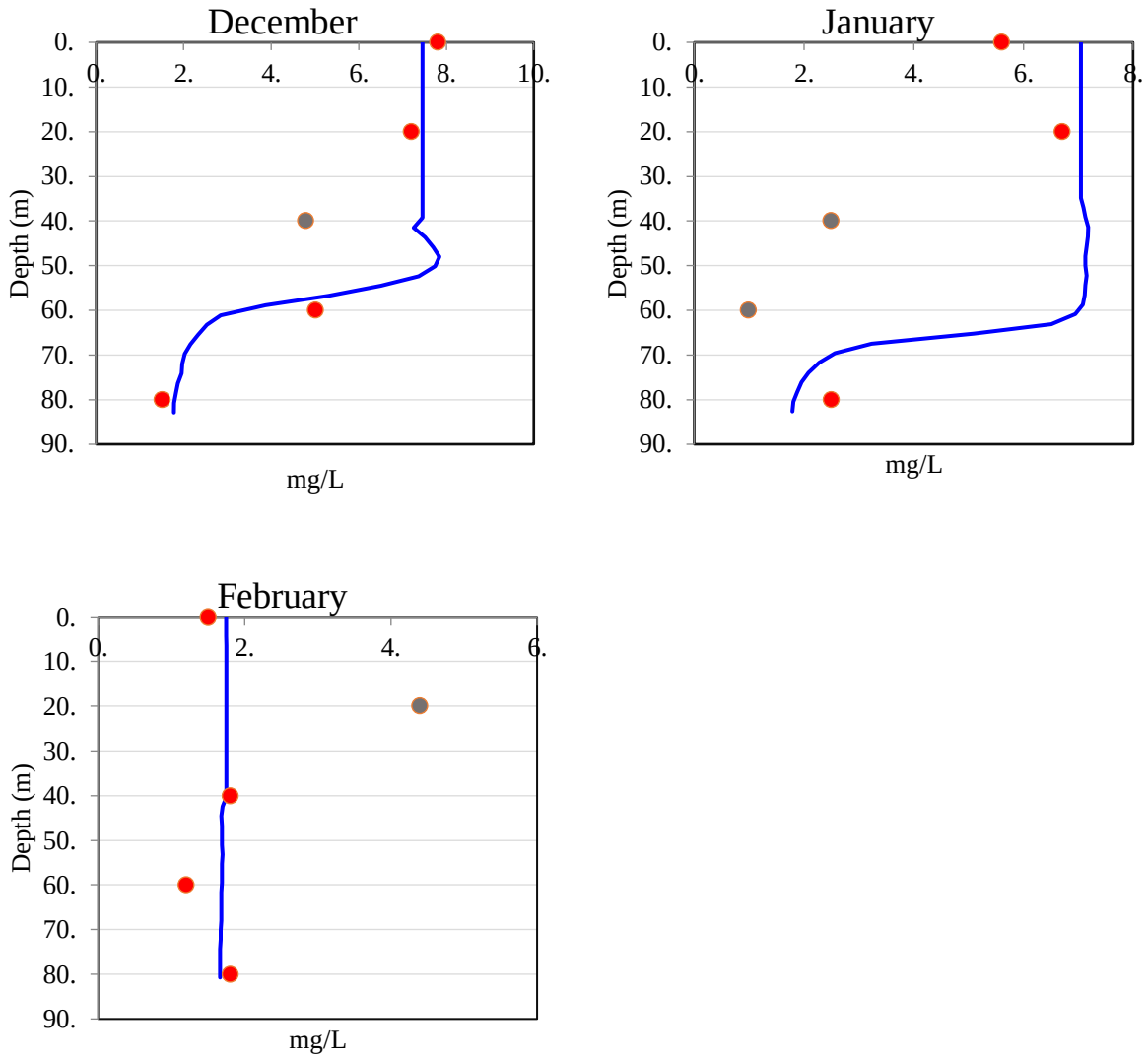

Figure 4-4. Comparison of the vertical BOD5 profiles simulated by EFDC+ from June to February with the field observations during the calibration period.

b) Statistical Evaluation and Error Analysis of BOD5 Simulation Using EFDC+

The results obtained from the comparison of simulated and observed values are presented in Table 4-4. According to this table, the mean RMSE for the entire simulation period was 0.53 mg/L, indicating that the model reproduced organic-carbon dynamics with good accuracy. In addition, the homogenization of the vertical profiles in February indicates a more uniform distribution of organic load throughout the reservoir following complete mixing associated with seasonal turnover.

Table 4-4. Statistical evaluation of EFDC+ accuracy in simulating BOD5.

Statistical Index	June	July	August	September	October	November	December	January	February	Mean
MAE (mg/L)	0.281	0.62	0.57	0.28	0.30	0.27	0.63	0.83	0.23	0.44
RMSE (mg/L)	0.368	0.68	0.64	0.28	0.39	0.30	0.86	0.95	0.28	0.53
NSE	0.985	0.95	0.54	0.88	0.65	0.04	0.88	0.72	-0.30	0.59
NMAE_mean (%)	5.950	14.03	16.77	5.97	18.34	12.88	11.77	16.77	14.66	13.02
NRMSE_mean (%)	7.790	15.50	19.01	6.15	24.06	14.33	16.02	19.20	18.01	15.56

4.3.3 Calibration and Analysis of Nitrogen Compounds

Nitrogen, as one of the principal nutrients, plays a key role in eutrophication and algal growth in Seymareh Reservoir. In the present EFDC+ application, the simulated nitrogen variables included ammonium nitrogen and nitrate nitrogen. Nitrification, defined as the conversion of ammonium nitrogen to nitrate nitrogen under aerobic conditions, and denitrification, defined as the reduction of nitrate under hypoxic or anaerobic conditions, were simulated dynamically as functions of dissolved oxygen concentration.

a) Analysis of Vertical Ammonium-Nitrogen Profiles and Hypoxic Conditions

The vertical variations in ammonium-nitrogen concentration presented in Figure 4-5 demonstrate the close relationship between this parameter and dissolved oxygen conditions in the deeper layers of the reservoir. According to the October profile, ammonium-nitrogen concentrations were very low in the surface layer. In the deeper layers, however, particularly at a depth of 80 m, the concentration increased substantially and reached approximately 0.65 mg/L.

This accumulation in the hypolimnion resulted from declining dissolved oxygen concentrations and the consequent limitation of nitrification. Under these conditions, ammonium nitrogen produced through the decomposition of organic matter may accumulate in the deep-water layers and near the sediment bed. In contrast, within the surface layers, a portion of the available ammonium nitrogen is consumed by algae and other microorganisms.

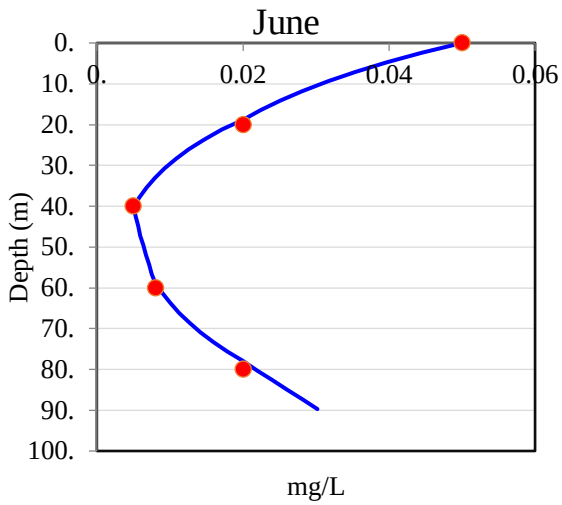
June
0.
10.
20.
30.
40.
50.
60.
70.
80.
90.
100.
Depth (m)
0.
0.02
0.04
0.06
mg/L

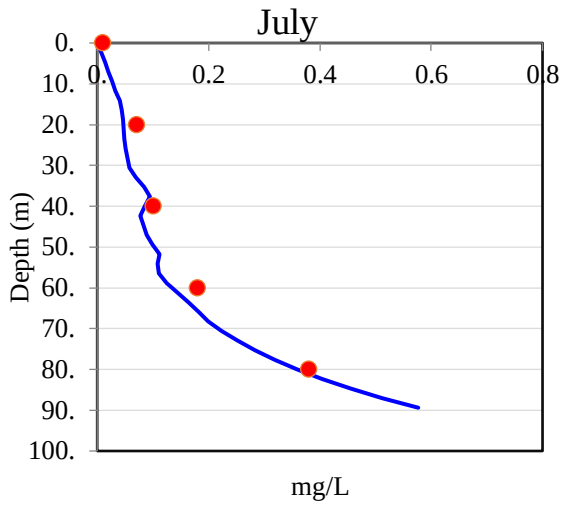
July
0.
10.
20.
30.
40.
50.
60.
70.
80.
90.
100.
Depth (m)
0.
0.2
0.4
0.6
0.8
mg/L

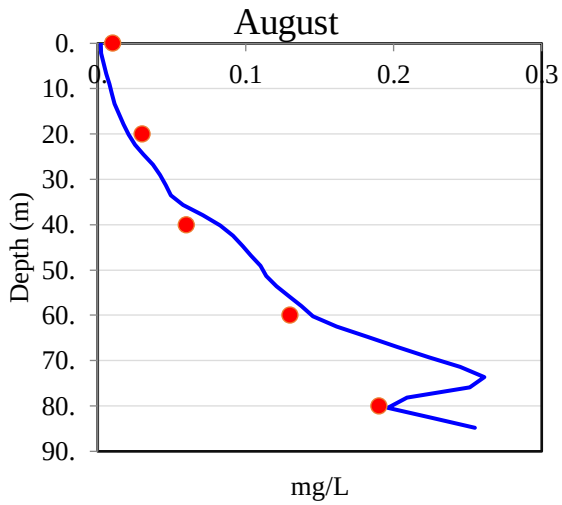
August
0.
10.
20.
30.
40.
50.
60.
70.
80.
90.
Depth (m)
0.
0.1
0.2
0.3
mg/L

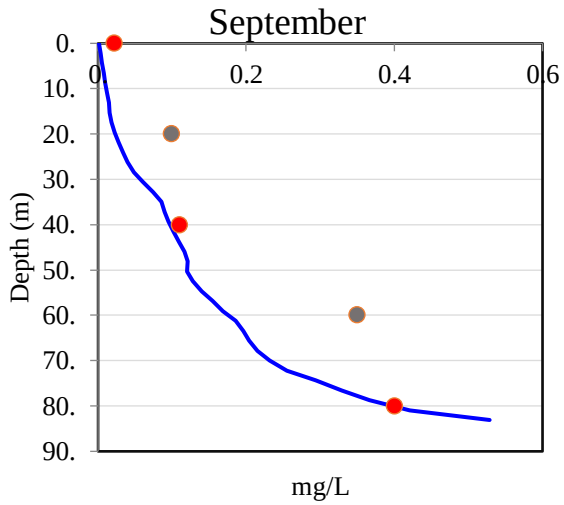
September
0.
10.
20.
30.
40.
50.
60.
70.
80.
90.
Depth (m)
0.
0.2
0.4
0.6
mg/L

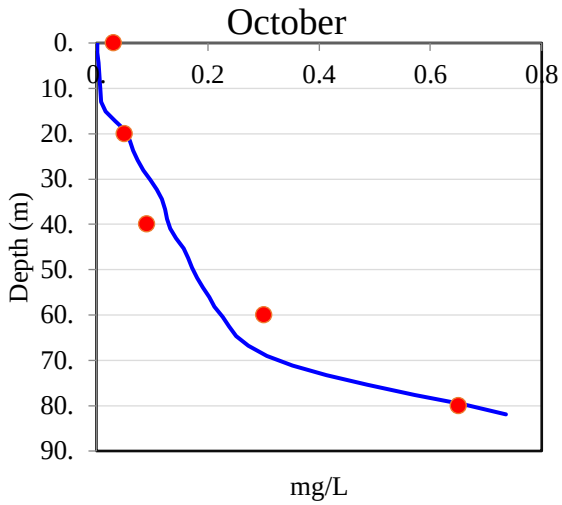
October
0.
10.
20.
30.
40.
50.
60.
70.
80.
90.
Depth (m)
0.
0.2
0.4
0.6
0.8
mg/L

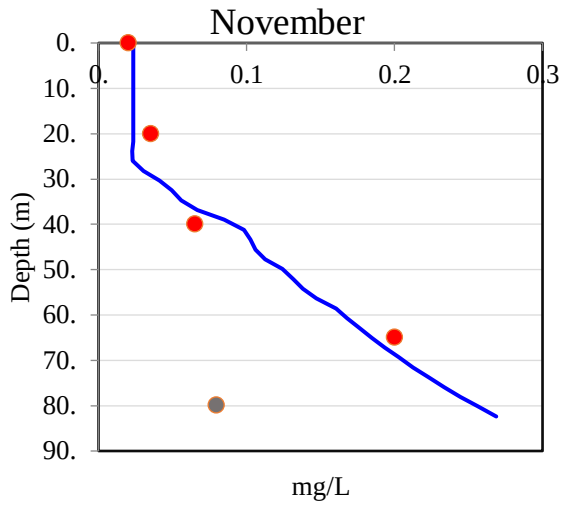
November
0.
10.
20.
30.
40.
50.
60.
70.
80.
90.
Depth (m)
0.
0.1
0.2
0.3
mg/L

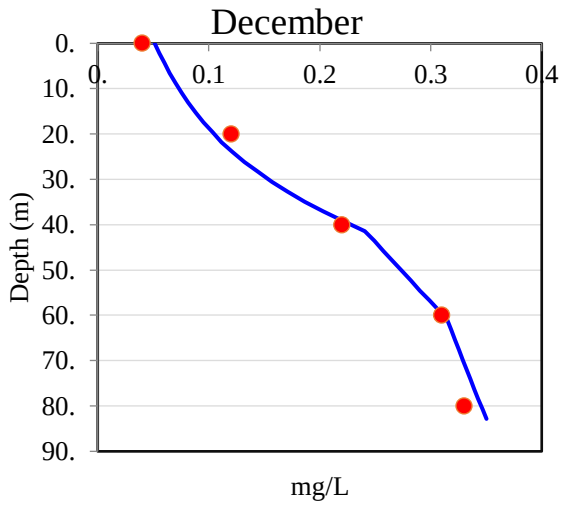
December
0.
10.
20.
30.
40.
50.
60.
70.
80.
90.
Depth (m)
0.
0.1
0.2
0.3
0.4
mg/L

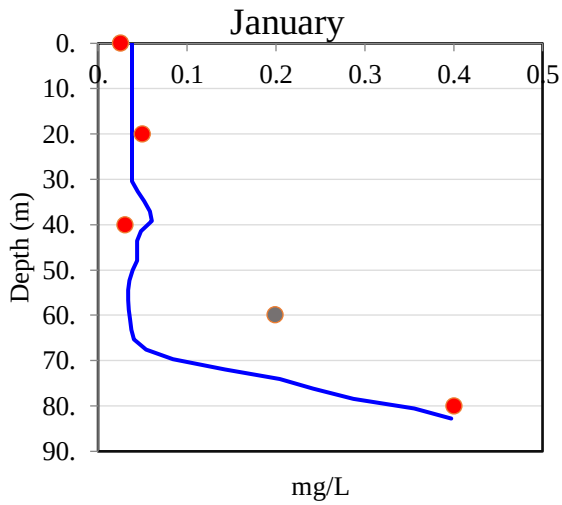
January
0.
10.
20.
30.
40.
50.
60.
70.
80.
90.
Depth (m)
0.
0.1
0.2
0.3
0.4
0.5
mg/L

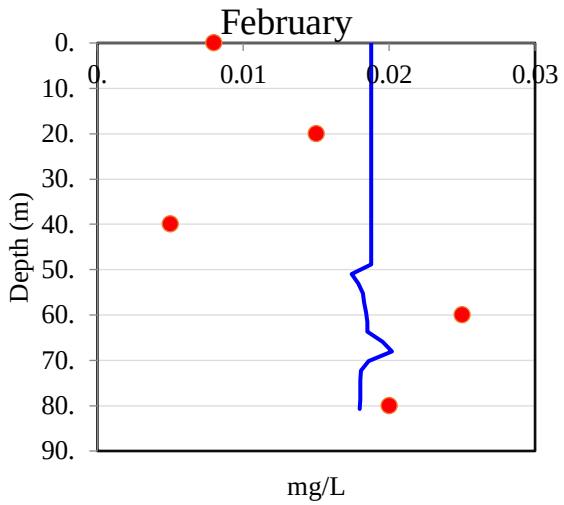

Figure 4-5. Comparison of the vertical ammonium-nitrogen profiles simulated by EFDC+ from June to February with field observations during the calibration period.

b) Analysis of Vertical Nitrate-Nitrogen Profiles and the Nitrification Process

The pattern of nitrate-nitrogen variation within the water column, shown in Figure 4-6, differs from that of ammonium nitrogen. In most months, such as in the July profile, nitrate-nitrogen concentrations remain relatively high in the surface and intermediate layers where sufficient oxygen is available, with values of approximately 15 to 18 mg/L. This pattern indicates active nitrification and the conversion of ammonium nitrogen to nitrate nitrogen within the aerobic layers of the reservoir.

With increasing depth and decreasing dissolved oxygen concentration, nitrate-nitrogen shows a declining trend. For example, in the January profile, nitrate-nitrogen decreases from about 14.5 mg/L at the surface to about 5.7 mg/L at a depth of 80 m. This reduction in the deeper layers may be attributed to the limitation of aerobic conditions and the enhancement of denitrification in low-oxygen environments, a process in which nitrate is consumed as an electron acceptor and is thereby reduced within the water column.

Finally, in February, coinciding with the occurrence of complete mixing, the nitrate-nitrogen profile becomes more uniform throughout the water column, as shown in the corresponding profile, and its concentration stabilizes at about 12.7 mg/L. This pattern indicates a more homogeneous distribution of nutrients following reservoir turnover and a reduction in the vertical separation between the surface and deep layers.

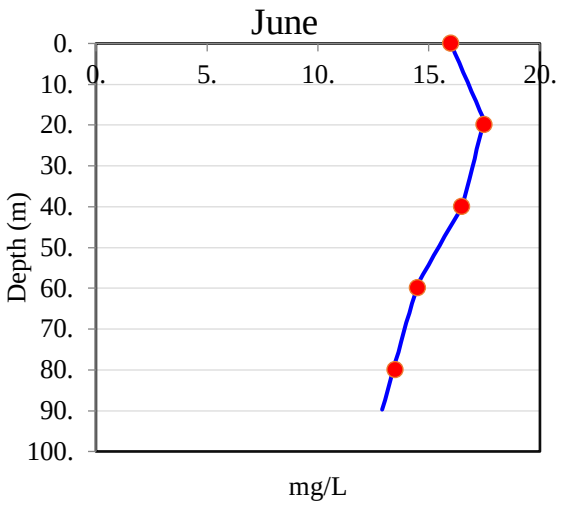
June
0.
10.
20.
30.
40.
50.
60.
70.
80.
90.
100.
Depth (m)
0.
5.
10.
15.
20.
mg/L

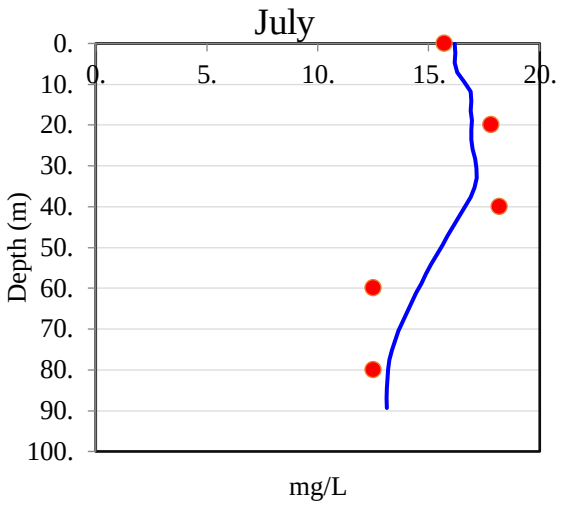
July
0.
10.
20.
30.
40.
50.
60.
70.
80.
90.
100.
Depth (m)
0.
5.
10.
15.
20.
mg/L

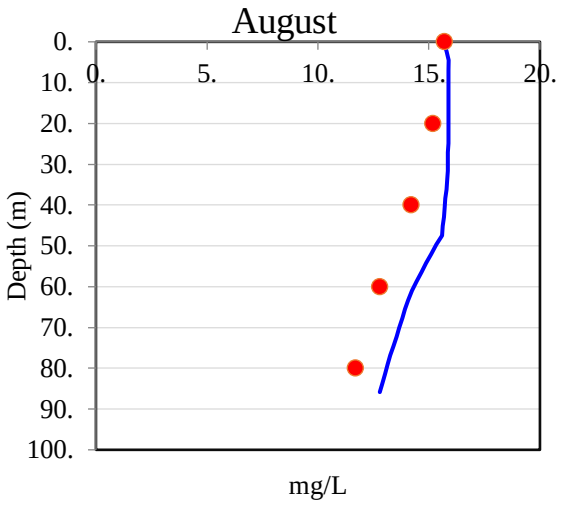
August
0.
10.
20.
30.
40.
50.
60.
70.
80.
90.
100.
Depth (m)
0.
5.
10.
15.
20.
mg/L

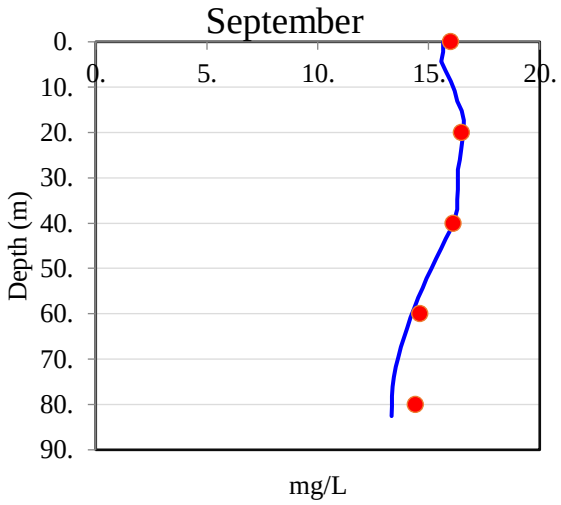
September
0.
10.
20.
30.
40.
50.
60.
70.
80.
90.
Depth (m)
0.
5.
10.
15.
20.
mg/L

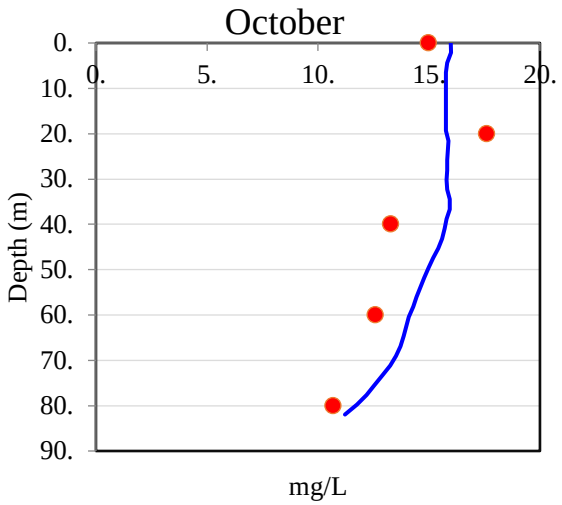
October
0.
10.
20.
30.
40.
50.
60.
70.
80.
90.
Depth (m)
0.
5.
10.
15.
20.
mg/L

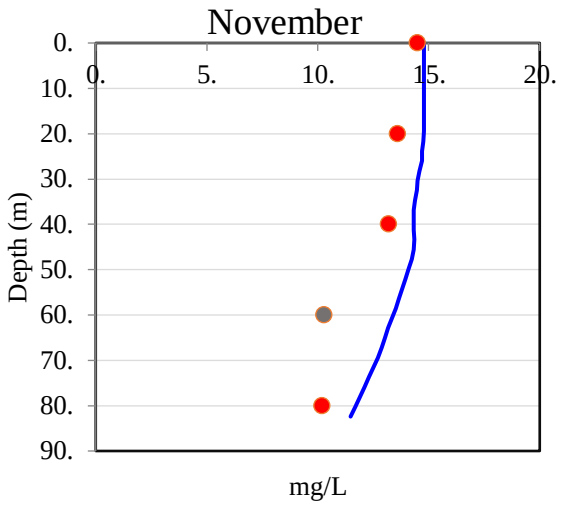
November
0.
10.
20.
30.
40.
50.
60.
70.
80.
90.
Depth (m)
0.
5.
10.
15.
20.
mg/L

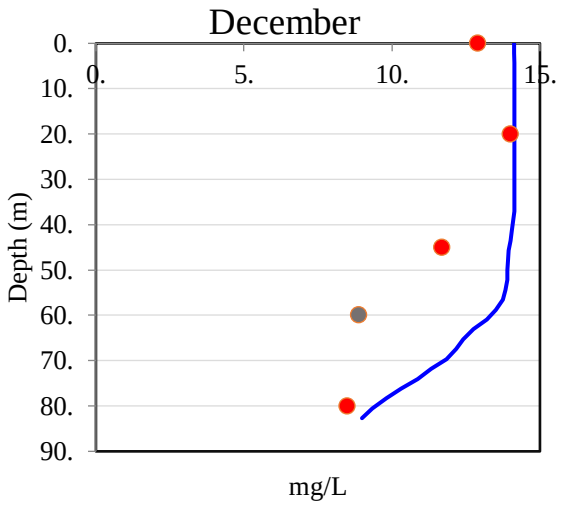
December
0.
10.
20.
30.
40.
50.
60.
70.
80.
90.
Depth (m)
0.
5.
10.
15.
mg/L

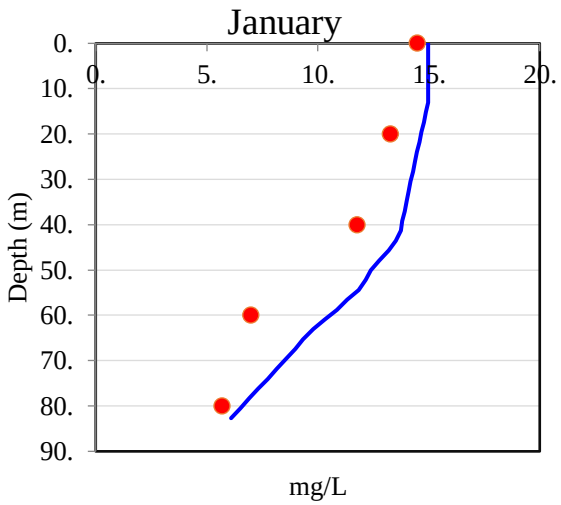
January
0.
10.
20.
30.
40.
50.
60.
70.
80.
90.
Depth (m)
0.
5.
10.
15.
20.
mg/L

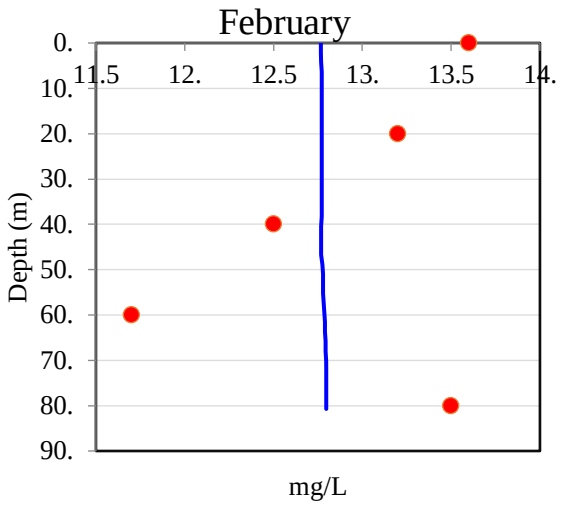

Figure 4-6. Comparison of the vertical nitrate-nitrogen profiles simulated by EFDC+ from June to February with field observations during the calibration period.

c) Statistical Evaluation and Error Analysis of Nitrogen Compounds

The accuracy of the model in reproducing ammonium-nitrogen and nitrate-nitrogen concentrations was evaluated using the statistical indices presented in Tables 4-5 and 4-6. According to Table 4-5, the mean Nash–Sutcliffe efficiency coefficient for ammonium nitrogen was 0.83, indicating very good agreement between the model results and the observed variations in this parameter. For nitrate nitrogen, the mean RMSE was 1.10 mg/L. Considering the range of nitrate concentrations within the reservoir, this value indicates acceptable model performance.

Table 4-5. Statistical evaluation of EFDC+ accuracy in simulating ammonium nitrogen.

Statistical Index	June	July	August	September	October	November	December	January	February	Mean
MAE (mg/L)	0.001	0.022	0.01	0.01	0.03	0.01	0.01	0.03	0.01	0.02
RMSE (mg/L)	0.001	0.025	0.01	0.01	0.04	0.01	0.01	0.04	0.01	0.02
NSE	0.996	0.96	0.96	0.99	0.97	0.96	0.99	0.95	-0.34	0.83
NMAE_mean(%)	3.450	15.33	14.51	6.68	15.03	12.65	5.03	22.55	50.47	16.17
NRMSE_mean(%)	4.880	17.33	15.84	8.02	18.50	16.39	5.67	27.83	58.62	19.23

Table 4-6. Statistical evaluation of EFDC+ accuracy in simulating nitrate nitrogen.

Statistical Index	June	July	August	September	October	November	December	January	February	Mean
MAE (mg/L)	0.044	1.12	1.03	0.37	1.55	1.02	1.14	1.65	0.66	0.96
RMSE (mg/L)	0.059	1.27	1.19	0.53	1.65	1.12	1.37	1.97	0.72	1.10
NSE	0.998	0.73	0.36	0.62	0.50	0.52	0.55	0.68	-0.03	0.55
NMAE_mean(%)	0.280	7.34	7.42	2.38	11.22	7.94	9.70	15.81	5.15	7.47
NRMSE_mean(%)	0.380	8.28	8.55	3.40	11.89	8.70	11.66	18.85	5.62	8.59

4.3.4 Calibration and Analysis of Phosphorus Compounds

Phosphorus is a key nutrient in reservoir ecosystems, and its concentration can directly influence primary productivity and algal growth. In EFDC+, phosphorus cycling is controlled by processes such as adsorption to and desorption from suspended particles, settling of phosphorus-containing compounds, mineralization of organic phosphorus, and phosphate release from bed sediments under low-oxygen conditions. In the present study, total phosphate was calibrated and analyzed as the principal indicator of phosphorus cycling.

a) Analysis of Vertical Phosphate Profiles and Governing Processes

The vertical distribution of total phosphate in Seymareh Reservoir is presented in Figure 4-7. Examination of these profiles indicates that phosphate concentrations did not follow a completely constant or uniform pattern during the simulation period but varied in response to seasonal conditions, water-column mixing, and biological activity.

In October, phosphate concentrations increased throughout a substantial portion of the water column compared with the summer months, reaching approximately 0.54–0.60 mg/L. This increase may be associated with reduced algal activity during autumn and the consequent reduction in phosphorus uptake by algae. In contrast, during the warmer months, particularly in the surface layers, some of the available phosphorus may be consumed through algal growth. Phosphate variations are therefore closely related to the biological dynamics of the reservoir.

In the February profile, the observational data show a vertical gradient, with phosphate concentrations decreasing from approximately 0.64 mg/L at the surface to about 0.25 mg/L at a depth of 80 m. The model also reproduced the general declining trend with depth. This behavior may reflect the combined effects of mixing, settling of particle-bound phosphorus, and changes in phosphorus exchange with the sediment bed toward the end of the simulation period.

During most months, including July and September, phosphate concentrations in the intermediate layers remained relatively stable, and no substantial differences were observed between the simulated and measured values. This indicates that the parameters governing phosphorus cycling, including mineralization rates and the partitioning coefficients controlling phosphate distribution between dissolved and particulate phases, generally reproduced the dominant behavior of phosphorus within the water column.

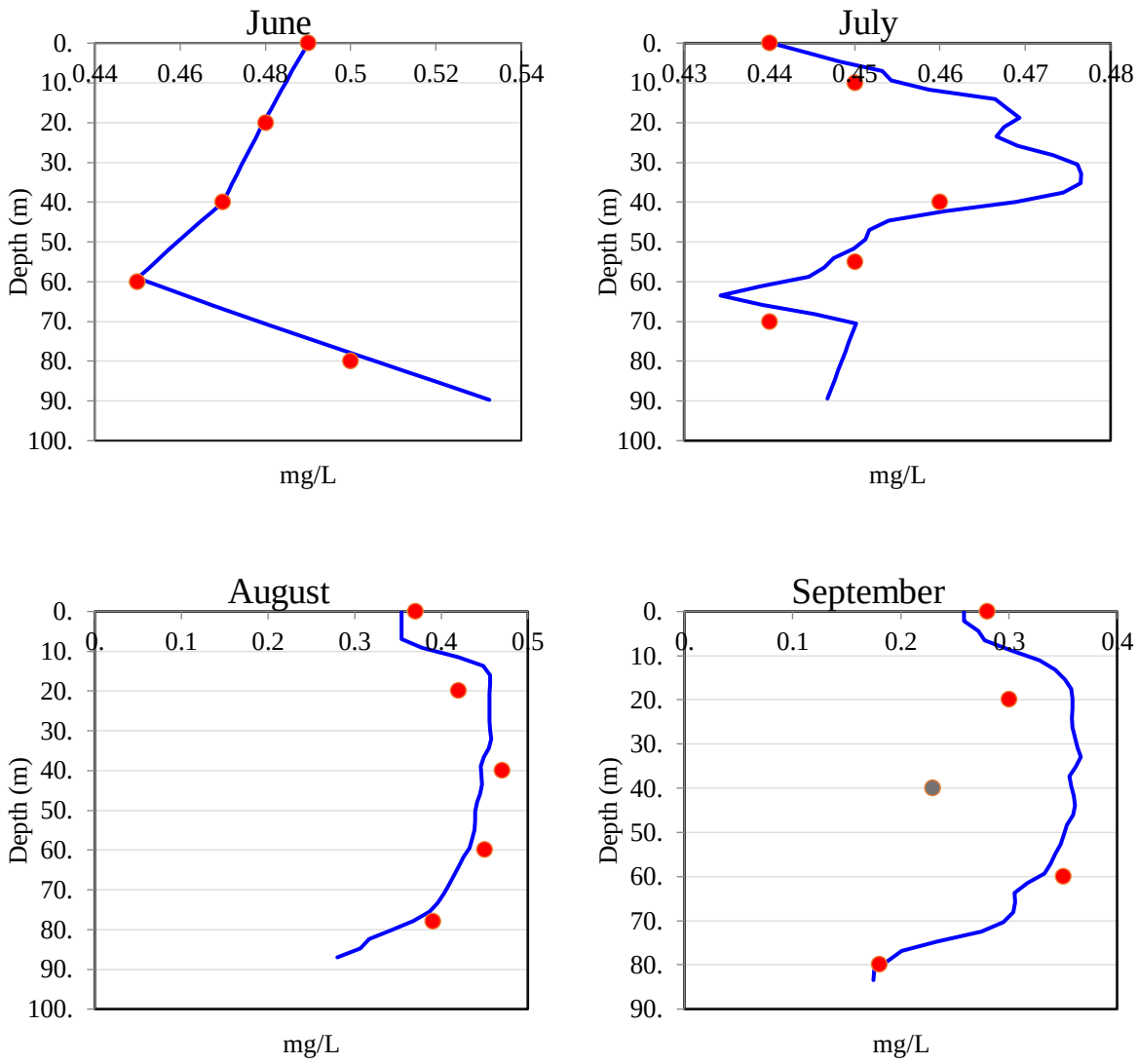

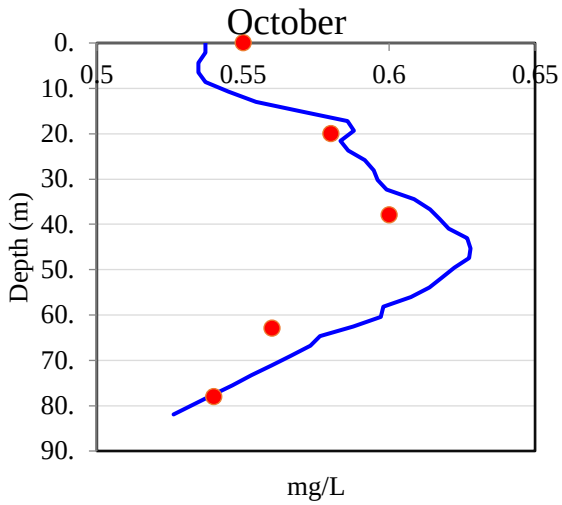
October
0.
10.
20.
30.
40.
50.
60.
70.
80.
90.
Depth (m)
0.5
0.55
0.6
0.65
mg/L

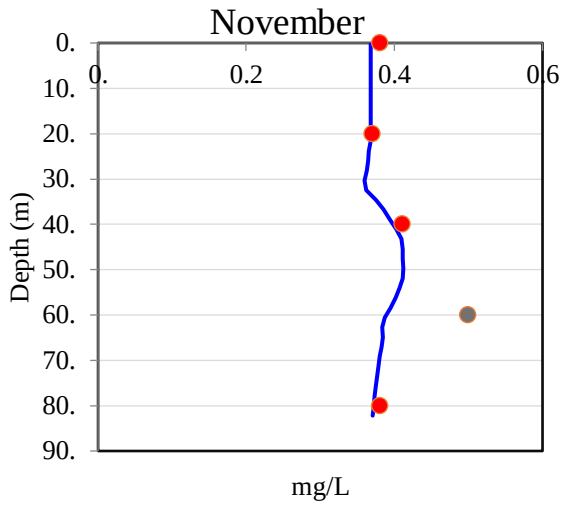
November
0.
10.
20.
30.
40.
50.
60.
70.
80.
90.
Depth (m)
0.
0.2
0.4
0.6
mg/L

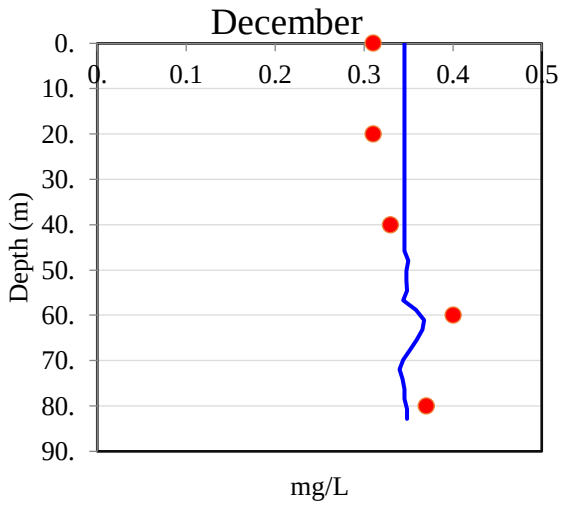
December
0.
10.
20.
30.
40.
50.
60.
70.
80.
90.
Depth (m)
0.
0.1
0.2
0.3
0.4
0.5
mg/L

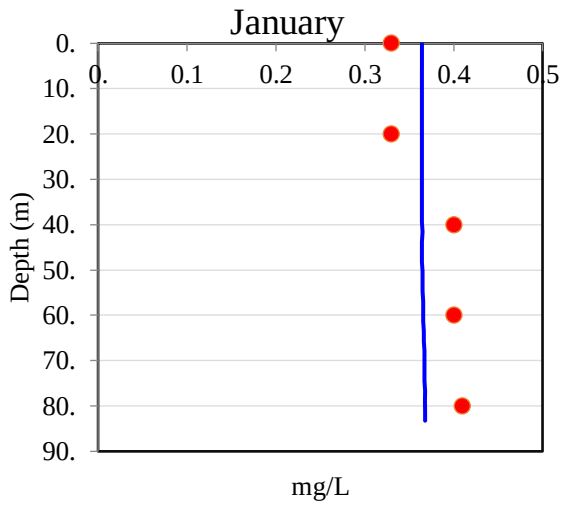
January
0.
10.
20.
30.
40.
50.
60.
70.
80.
90.
Depth (m)
0.
0.1
0.2
0.3
0.4
0.5
mg/L

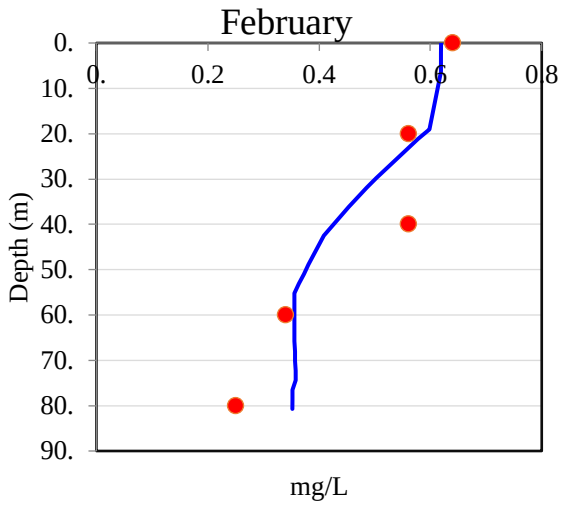

Figure 4-7. Comparison of the vertical total-phosphate profiles simulated by EFDC+ from June to February with field observations during the calibration period.

b) Relationship of Phosphorus with Dissolved Oxygen and Algae

The satisfactory reproduction of phosphate variations provides an essential basis for analyzing algal behavior and dissolved oxygen dynamics. During warm months such as July, the persistence of a surface-layer phosphate concentration of approximately 0.44 mg/L indicates that phosphorus was not completely depleted and remained available to support algal growth.

In the deeper layers, phosphate variations are related to dissolved oxygen conditions and constituent exchange with the sediment bed. Under low-oxygen conditions, phosphorus release from sediments may increase and influence phosphate concentrations in the lower layers. Phosphorus dynamics should therefore be interpreted together with the dissolved oxygen and chlorophyll-a results because the overall reservoir response results from interactions among nutrient cycling, thermal stratification, and biological activity.

c) Statistical Evaluation of Model Accuracy in Simulating Phosphorus

The statistical indices obtained from the comparison of simulated and observed values are presented in Table 4-7. The results indicate good agreement between the model and field data, with a low mean RMSE of 0.03 mg/L over the entire simulation period. The mean normalized indices, NMAE and NRMSE, were 5.83% and 6.70%, respectively, confirming that the overall model error remained below 10%.

Table 4-7. Statistical evaluation of EFDC+ accuracy in simulating total phosphate.

Statistical Index	June	July	August	September	October	November	December	January	February	Mean

MAE (mg/L)	0.002	0.005	0.02	0.03	0.01	0.01	0.03	0.04	0.06	0.02
RMSE (mg/L)	0.003	0.006	0.02	0.03	0.01	0.01	0.03	0.04	0.08	0.03
NSE	0.974	0.299	0.55	0.71	0.52	0.61	0.26	0.05	0.73	0.52
NMAE_mean(%)	0.370	1.18	5.68	9.48	2.21	2.18	8.52	9.97	12.88	5.83
NRMSE_mean(%)	0.580	1.40	5.91	12.00	2.64	2.42	8.88	10.01	16.49	6.70

4.3.5 Calibration and Analysis of Algae (Chlorophyll-a)

Chlorophyll-a, as the principal indicator of algal biomass, is one of the most important biological variables used to evaluate water quality conditions in reservoirs. Variations in this parameter result from the combined effects of physical and biogeochemical processes and are influenced by factors such as solar radiation intensity, water temperature, water-column transparency, and nutrient concentrations, particularly nitrogen and phosphorus. Therefore, satisfactory calibration of chlorophyll-a can demonstrate the model's ability to reproduce primary-production dynamics and the biological response of Seymareh Reservoir.

a) Analysis of Vertical Profiles and Temporal Variations in Chlorophyll-a

The vertical distribution of chlorophyll-a concentrations in Seymareh Reservoir is presented in Figure 4-8. Examination of these profiles shows that the highest chlorophyll-a concentrations generally occurred in the surface layers and declined rapidly with increasing depth. This pattern is consistent with the dependence of algal growth on light availability. Because light penetration through the water column is limited, conditions for photosynthesis and algal growth become progressively less favorable at greater depths.

In June, the maximum chlorophyll-a concentration was observed at the water surface and was approximately 10 µg/L. This value indicates increased algal activity at the beginning of the warm season, which may have resulted from favorable water temperatures, increased solar radiation, and the availability of nutrients in the surface layer. The model successfully reproduced this surface maximum and accurately represented the decline in chlorophyll-a concentration with depth.

During warm months such as July, chlorophyll-a concentration decreased from approximately 3.4 µg/L at the surface to values approaching zero at a depth of 60 m. This behavior demonstrates the role of light limitation in controlling algal growth in the lower layers. The satisfactory reproduction of this vertical gradient indicates that the model's light-extinction coefficients and their relationship with water quality were appropriately configured to represent the reduction in light availability with depth and its effect on algal biomass.

As the cold season approached, chlorophyll-a concentrations declined. In January, the surface concentration decreased to approximately 0.6 µg/L. Lower water temperatures, shorter day length, and reduced solar radiation intensity were among the principal factors responsible for the decline in algal activity during this period. The model results indicate that this seasonal reduction was reproduced satisfactorily and that the model successfully followed the decline in algal biomass during the colder months.

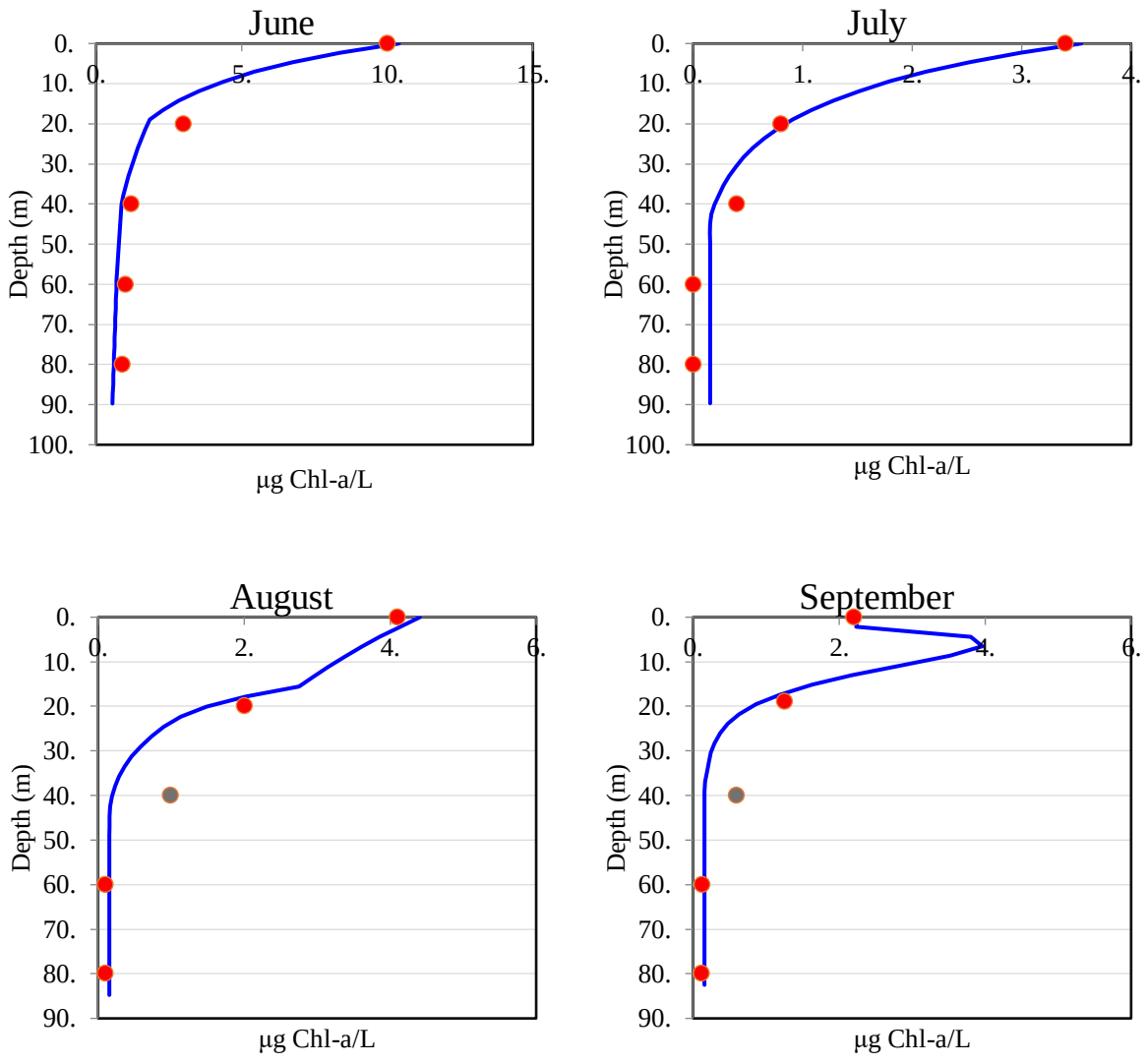

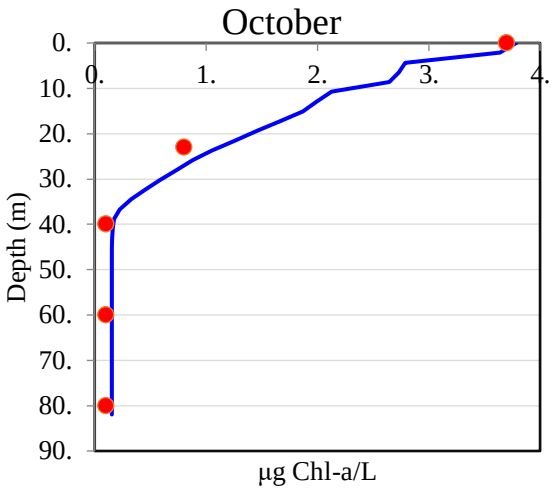
October
0.
10.
20.
30.
40.
50.
60.
70.
80.
90.
Depth (m)
0.
1.
2.
3.
4.
µg Chl-a/L

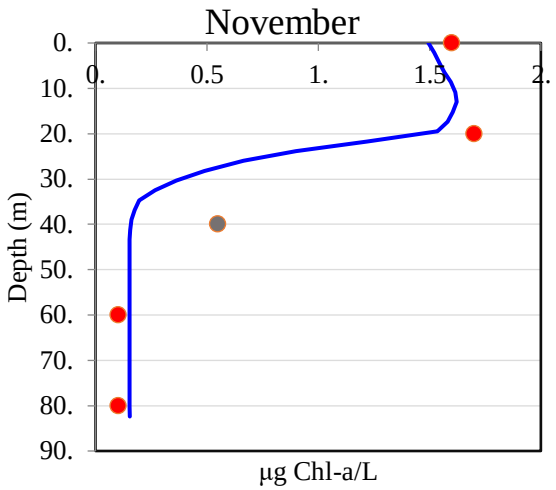
November
0.
10.
20.
30.
40.
50.
60.
70.
80.
90.
Depth (m)
0.
0.5
1.
1.5
2.
µg Chl-a/L

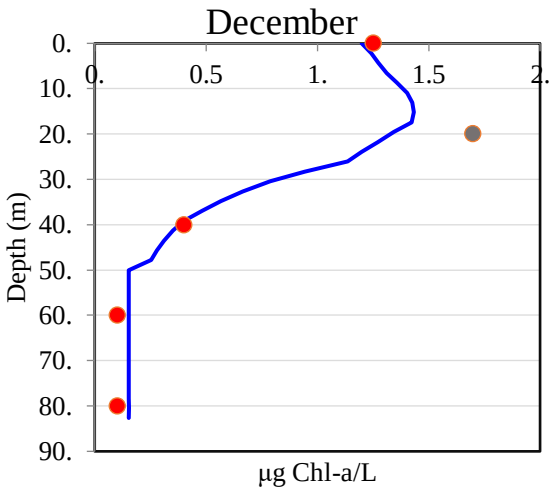
December
0.
10.
20.
30.
40.
50.
60.
70.
80.
90.
Depth (m)
0.
0.5
1.
1.5
2.
µg Chl-a/L

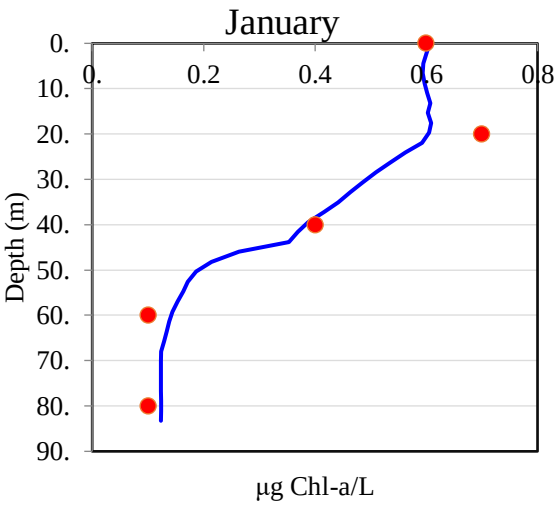
January
0.
10.
20.
30.
40.
50.
60.
70.
80.
90.
Depth (m)
0.
0.2
0.4
0.6
0.8
µg Chl-a/L

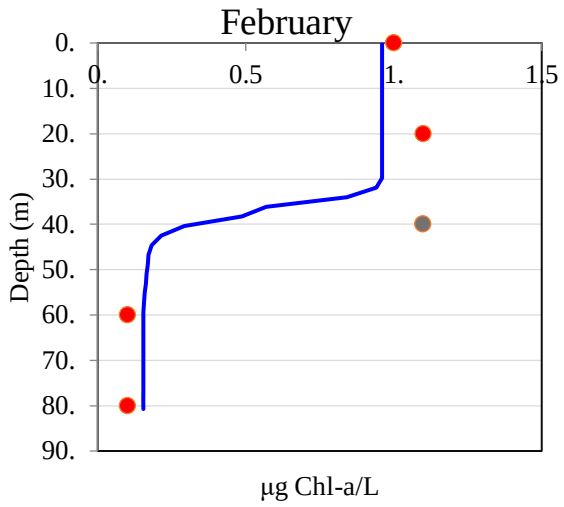

Figure 4-8. Comparison of the vertical chlorophyll-a profiles simulated by EFDC+ from June to February with field observations during the calibration period.

b) Overall Interpretation of Algal Conditions in the Reservoir

The chlorophyll-a calibration results indicate that EFDC+ successfully reproduced the biological response of the reservoir in relation to thermal conditions, light availability, and nutrient concentrations. The concentration of chlorophyll-a in the surface layers is consistent with the thermal stratification structure of the reservoir. During the warm season, the surface layer functions as the principal zone of primary production, while thermal separation restricts effective mixing between this layer and deeper waters.

From a water quality perspective, the chlorophyll-a concentrations indicate that Seymareh Reservoir may range from mesotrophic to moderately eutrophic conditions during certain periods. This is particularly important from a management perspective during months when surface chlorophyll-a concentrations increase, as it indicates the reservoir's potential for enhanced algal production under favorable temperature, light, and nutrient conditions.

c) Statistical Evaluation of Model Accuracy in Simulating Algae

The statistical indices obtained from the comparison of simulated and observed chlorophyll-a concentrations are presented in Table 4-8. The results indicate that the model reproduced the temporal and vertical variations in chlorophyll-a with satisfactory accuracy. The mean NSE for the entire simulation period was 0.97, demonstrating very good model performance in simulating variations in algal biomass.

The mean RMSE for the entire period was 0.19 µg/L. The highest model accuracy was observed in October and December, when NSE reached 0.99, indicating the model's ability to reproduce the

seasonal decline in algal biomass following the warm-season growth period. Although the normalized error indices were approximately 15–19% in some months, the consistently high NSE values indicate that the model successfully reproduced the overall temporal trend and vertical distribution of chlorophyll-a.

Table 4-8. Statistical evaluation of EFDC+ accuracy in simulating chlorophyll-a.

Statistical Index	June	July	August	September	October	November	December	January	February	Mean
MAE (µg Chl-a/L)	0.510	0.13	0.23	0.11	0.12	0.11	0.04	0.04	0.07	0.15
RMSE (µg Chl-a/L)	0.624	0.15	0.30	0.16	0.16	0.13	0.05	0.05	0.08	0.19
NSE	0.968	0.98	0.97	0.97	0.99	0.97	0.99	0.96	0.97	0.97
NMAE_ (%) mean	15.84	15.15	14.55	11.74	12.13	12.78	9.55	9.82	12.46	12.67
NRMSE_ (%) mean	19.37	16.15	18.82	17.05	16.17	15.33	10.06	12.91	14.23	15.57

4.4 Flow-Distribution Scenarios in the Long-Term Simulations

To investigate the effects of withdrawal from different reservoir elevations on its physical structure and water quality, three operational scenarios were defined for the long-term simulation period. Under Scenario 1, the entire outflow discharge was withdrawn from the outlet at an elevation of 665 m. Under Scenario 2, 70% of the outflow discharge was released from the 665-m outlet and 30% from the 640-m outlet. Under Scenario 3, the total withdrawal was divided equally between the two elevations, with 50% released from the 665-m outlet and 50% from the 640-m outlet.

The total outflow discharge was kept constant in all scenarios, and only the distribution of flow between the two withdrawal elevations was changed. Therefore, the differences observed among the scenarios did not result from changes in the total release volume but instead reflected the effects of withdrawal elevation on internal circulation, the vertical distribution of temperature, dissolved oxygen, nutrients, and biological indicators within the reservoir. In this respect, the scenarios made it possible to evaluate whether withdrawing part of the flow from a lower elevation could improve reservoir water quality without changing the total operational release.

When interpreting the results, it should be noted that changing the withdrawal elevation may produce simultaneous and sometimes opposing effects. Withdrawal from a lower elevation may increase the involvement of deep-water layers, partially reduce thermal stability, and improve dissolved oxygen conditions at depth. Conversely, it may increase nutrient concentrations within

the water column or in the released water. Therefore, the scenarios cannot be evaluated adequately using a single parameter; thermal, oxygen-related, nutrient, biological, and outflow indicators must be considered together.

4.4.1 Effects of the Scenarios on Reservoir Thermal Structure and Stratification

The simulation results showed that changing the withdrawal proportions at different elevations affected the thermal structure of the reservoir. As illustrated in Figure 4-9, during the warm season, Scenario 1 produced a more pronounced temperature difference between the surface and deep layers. Under this scenario, surface-water temperature remained higher during the warm months, while the deep-water temperature was lower, resulting in stronger thermal separation within the water column.

In contrast, under Scenarios 2 and 3, the allocation of part of the withdrawal to the 640-m outlet reduced the temperature difference between the surface and deep layers. The mean surface-to-bottom temperature difference during the warm season decreased from approximately 15 °C under Scenario 1 to approximately 10 °C under Scenarios 2 and 3. Thus, both scenarios involving withdrawal from the lower outlet caused a substantial weakening of thermal stratification.

However, the difference between Scenarios 2 and 3 was relatively small, and both produced nearly similar reductions in the thermal stability of the water column. In other words, increasing the proportion withdrawn from the 640-m outlet from 30% to 50% did not produce a substantial additional reduction in stratification.

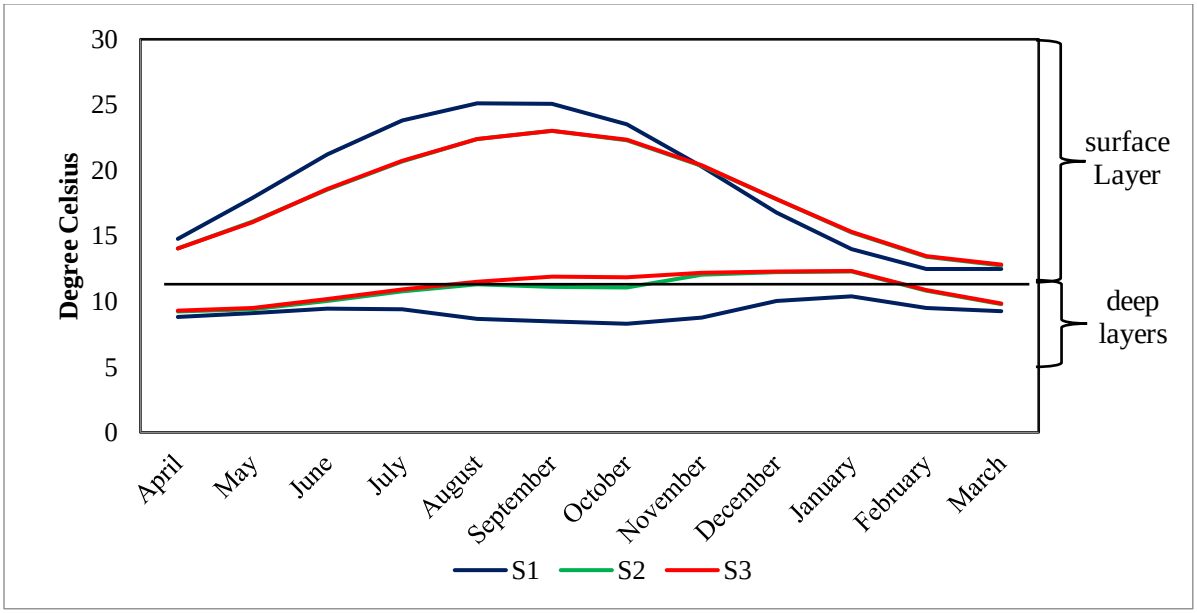

Figure 4-9. Thermal structure of Seymareh Reservoir based on the EFDC+ results under the selective-withdrawal scenarios.

The reduction in the surface-to-bottom temperature difference under Scenarios 2 and 3 resulted from simultaneous changes in both parts of the water column. Under these scenarios, the surface layer was cooler than under Scenario 1, whereas the deep layer became warmer. This pattern indicates that withdrawal from the lower elevation increased the involvement of deeper layers in reservoir release and internal circulation, thereby reducing thermal separation between the surface and deep waters. Therefore, the principal effect of Scenarios 2 and 3 was not merely a reduction in surface-water temperature but also a relatively more uniform temperature distribution throughout the water column.

During the cold season, the reservoir's thermal behavior differed from that observed during the warm season. Unlike the warm period, when surface-water temperature was higher under Scenario 1 than under the other two scenarios, Scenario 1 produced slightly lower surface temperatures during some winter months.

This difference can be attributed to the seasonal change in the dominant thermal processes within the reservoir. During the warm season, solar radiation and surface heating are the principal mechanisms responsible for the formation of a warm surface layer. Withdrawal from a lower elevation reduces stratification stability and consequently lowers surface-water temperature. During the cold season, however, the reservoir surface is affected by atmospheric cooling, and heat exchange with the atmosphere becomes the dominant process. Under these conditions, surface water cools rapidly, and the temperature difference between the surface and deeper layers decreases.

The deeper layers, owing to their greater thermal inertia, experience slower temperature variations and may retain more heat than the surface water. Therefore, under Scenarios 2 and 3, in which the deeper layers are more effectively connected to the withdrawal-induced circulation, surface-water temperatures remained slightly higher than under Scenario 1 during some cold months.

Despite these seasonal differences, the surface-to-bottom temperature difference indicates that Scenarios 2 and 3 also reduced thermal separation during the cold season. The mean temperature difference between the surface and deep layers decreased from approximately 4.45 °C under Scenario 1 to approximately 3.7 °C under Scenarios 2 and 3. Therefore, although stratification was considerably weaker in winter than in summer, withdrawal from the lower elevation still contributed to a relatively more uniform water column. Importantly, the difference between Scenarios 2 and 3 remained negligible during the cold season, and both scenarios generated nearly identical thermal responses.

Overall, the results indicate that withdrawal from a lower elevation reduces the intensity of reservoir thermal stratification but does not eliminate stratification completely. During the warm season, the surface-to-bottom temperature difference remained considerable under Scenarios 2 and

3; therefore, the reservoir retained its stratified behavior even under combined-withdrawal conditions.

From a management perspective, this result indicates that changing the withdrawal elevation can reduce thermal stability and provide conditions for a relative improvement in vertical exchange, but it is not sufficient by itself to produce complete homogenization of the water column. Therefore, the effects of changing the withdrawal elevation should be interpreted together with the responses of dissolved oxygen, nutrients, and biological indicators.

4.4.2 Effects of the Scenarios on Dissolved Oxygen in the Water Column

Dissolved oxygen is one of the most important indicators of reservoir water quality, and its variations are simultaneously influenced by temperature, stratification intensity, atmospheric exchange, photosynthetic production, oxygen consumption by organic matter, and vertical mixing conditions. Therefore, following the analysis of thermal structure, dissolved oxygen provides an important measure of the extent to which changes in withdrawal elevation influence the environmental conditions of the water column.

According to Figure 4-10, surface dissolved oxygen in the near-dam region exhibited a distinct monthly pattern. Under Scenario 1, dissolved oxygen concentrations during the early months of the year, particularly May and June, were higher than those under Scenarios 2 and 3. This pattern is consistent with the higher surface chlorophyll-a concentrations observed during the same period and may indicate the contribution of photosynthetic activity to surface oxygen production. During the remainder of the year, however, the differences among the scenarios decreased, and in some months, Scenarios 2 and 3 produced dissolved oxygen concentrations equal to or greater than those under Scenario 1.

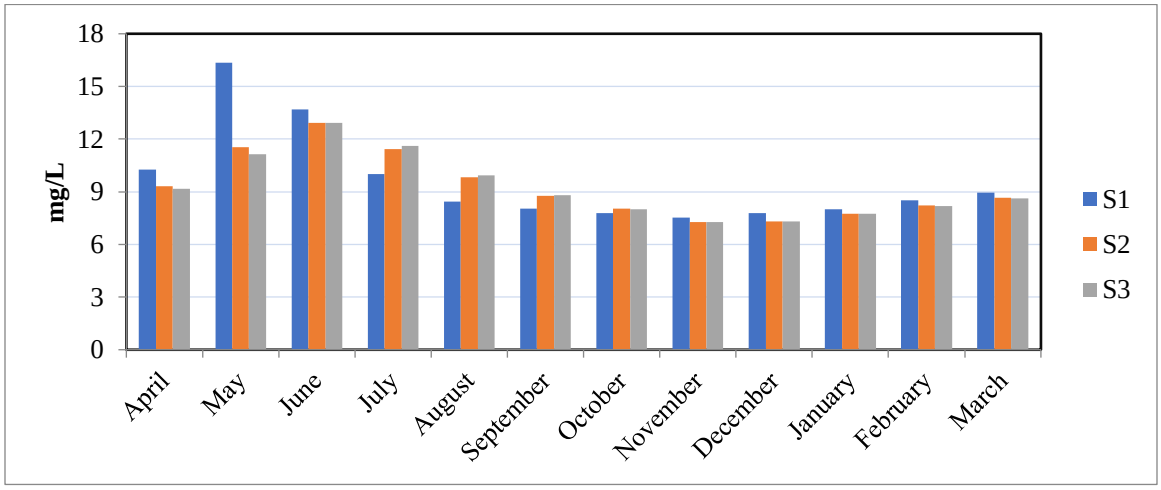

Figure 4-10. Surface dissolved oxygen concentrations in Seymareh Reservoir under the three selective-withdrawal scenarios, based on the ten-year mean EFDC+ results.

At the seasonal scale, the mean surface dissolved oxygen concentration during the warm season was approximately 10.7 mg/L under Scenario 1, whereas it increased to approximately 11.4 and 11.5 mg/L under Scenarios 2 and 3, respectively. Therefore, although Scenarios 2 and 3 reduced surface chlorophyll-a concentrations, this reduction did not result in lower surface dissolved oxygen.

This behavior can be attributed to the combined effects of several factors, including lower surface-water temperature and the resulting increase in oxygen solubility, reduced surface organic loading, and the relative weakening of thermal stratification. Consequently, the net effect of withdrawal from the lower elevation was a relative improvement in oxygen conditions within the surface layer.

As shown in Figure 4-11, a general improvement in dissolved oxygen under Scenarios 2 and 3 was also observed in the lower layers. Based on the mean concentration within the bottom 20 m of the water column near the dam, warm-season dissolved oxygen increased from approximately 7.40 mg/L under Scenario 1 to 7.72 mg/L under Scenario 2 and 7.73 mg/L under Scenario 3. Figure 4-11 also indicates that the differences among the scenarios in the lower layer became more pronounced from the middle of the warm season through winter, during which the decline in deep-water oxygen was more substantial under Scenario 1.

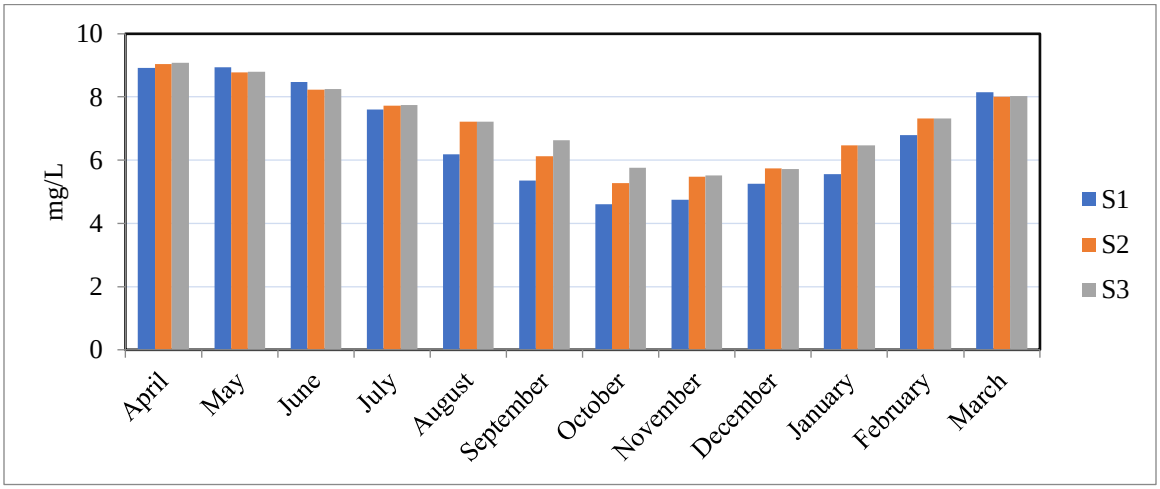

Figure 4-11. Deep-water dissolved oxygen concentrations in Seymareh Reservoir under the three selective-withdrawal scenarios, based on the ten-year mean EFDC+ results.

The same general pattern continued during the cold season. The mean dissolved oxygen concentration within the bottom 20 m increased from approximately 5.38 mg/L under Scenario 1 to 6.05 and 6.15 mg/L under Scenarios 2 and 3, respectively. This finding indicates that the beneficial effect of lower-elevation withdrawal on deep-water oxygen was not limited to the warm season.

During the cold season, although thermal stratification was weaker, the greater involvement of the lower layers in the withdrawal process and the reduction in thermal separation may have contributed to improved oxygen conditions at depth.

Overall, the results indicate that Scenarios 2 and 3 produced more favorable dissolved oxygen conditions than Scenario 1. This improvement was observed both at the surface and within the bottom 20 m of the water column near the dam. However, the difference between Scenarios 2 and 3 was limited. Therefore, increasing the proportion withdrawn from the 640-m outlet from 30% to 50% did not produce a substantial additional improvement relative to Scenario 2.

From a management perspective, this finding indicates that a considerable proportion of the dissolved oxygen benefits associated with lower-elevation withdrawal can already be achieved under Scenario 2.

4.4.3 Effects of the Scenarios on Nutrients in the Water Column

Nutrients, particularly phosphorus and nitrogen compounds, play a central role in determining the potential for algal growth and the trophic status of the reservoir. Changes in withdrawal elevation can alter nutrient distribution throughout the water column by modifying internal circulation, vertical mixing, and the connection between the surface and deep layers. To maintain a focused analysis, this section concentrates on two key indicators: total phosphorus in the lower layer near the dam and nitrate in the surface layer near the dam.

According to Figure 4-12, total phosphorus concentrations in the lower layer near the dam were higher under Scenarios 2 and 3 than under Scenario 1. During the warm months, the mean total phosphorus concentration in the lower layer increased from approximately 0.45 mg/L under Scenario 1 to 0.52 mg/L under Scenario 2 and 0.51 mg/L under Scenario 3. The same pattern was observed during the cold months, when total phosphorus increased from approximately 0.36 mg/L under Scenario 1 to approximately 0.44 mg/L under Scenarios 2 and 3.

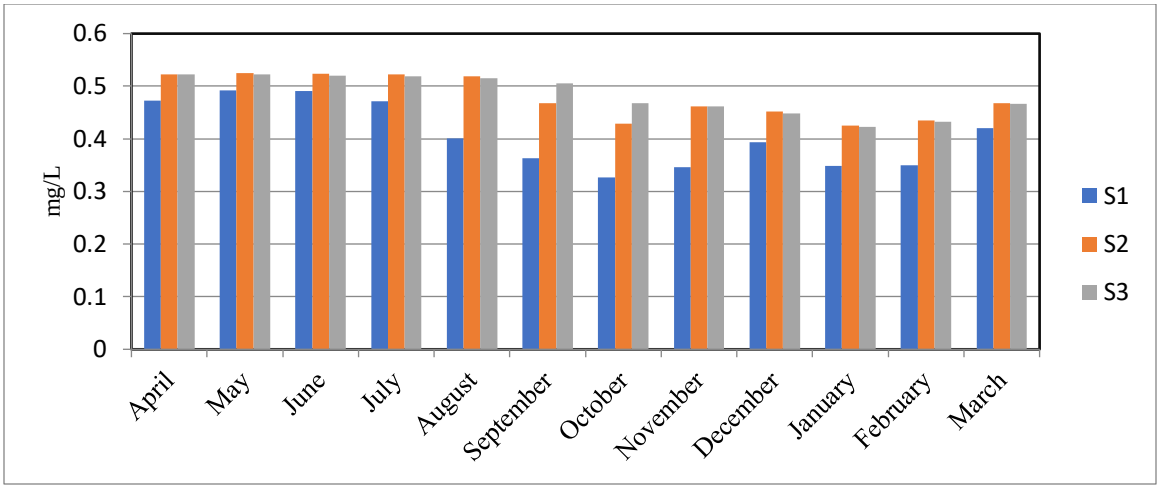

Figure 4-12. Deep-water total phosphorus concentrations in Seymareh Reservoir under the three selective-withdrawal scenarios, based on the ten-year mean EFDC+ results.

This increase indicates that although withdrawal from the lower elevation produced a relative improvement in dissolved oxygen conditions in the deeper layers, it simultaneously increased total phosphorus concentrations in the deep-water region near the dam. From a process-based perspective, this behavior may be attributed to the greater involvement of deeper layers in reservoir circulation and release. In other words, Scenarios 2 and 3 reduced thermal separation and improved oxygen conditions to some extent, while also increasing the transport and redistribution of nutrients stored in the lower part of the water column.

Surface nitrate also increased considerably under Scenarios 2 and 3. As shown in Figure 4-13, the mean surface nitrate concentration near the dam during the warm months increased from approximately 10.85 mg/L under Scenario 1 to 14.92 and 14.90 mg/L under Scenarios 2 and 3, respectively. During the cold months, surface nitrate increased from approximately 12.69 mg/L under Scenario 1 to 14.98 and 14.97 mg/L under Scenarios 2 and 3, respectively.

The increase in surface nitrate under Scenarios 2 and 3 is particularly important for biological interpretation because it indicates that the reduction in chlorophyll-a under these scenarios was not caused by nitrate limitation. On the contrary, nitrate availability in the surface layer increased. However, changes in the physical and biological conditions of the reservoir, particularly lower surface-water temperature, altered stratification intensity, and possible changes in residence time and light conditions, reduced algal growth or accumulation near the surface.

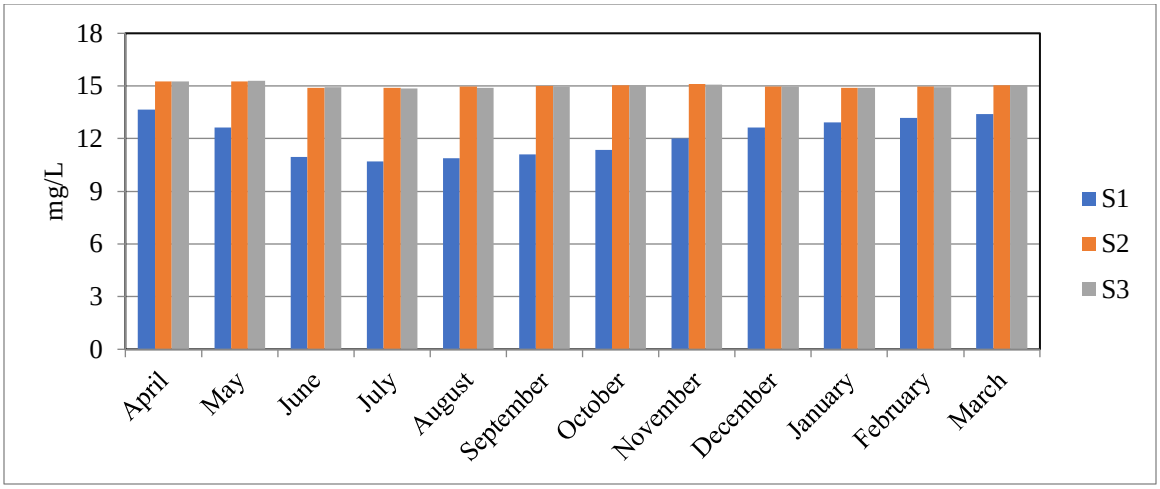

Figure 4-13. Surface nitrate concentrations in Seymareh Reservoir under the three selective-withdrawal scenarios, based on the ten-year mean EFDC+ results.

Overall, the nutrient results indicate that Scenarios 2 and 3 produced higher concentrations of both deep-water total phosphorus and surface nitrate than Scenario 1. The differences between Scenarios 2 and 3 were small, and both exhibited nearly identical behavior. Therefore, lower-elevation withdrawal may improve dissolved oxygen conditions and reduce surface chlorophyll-a concentrations, while simultaneously increasing nutrient concentrations within the water column. This represents one of the most important management trade-offs involved in selecting an appropriate reservoir operating scenario.

4.4.4 Effects of the Scenarios on Chlorophyll-a and Organic-Load Components

Chlorophyll-a, as an indicator of algal biomass, showed a clear response to the operational scenarios. As shown in Figure 4-14, under Scenario 1, surface chlorophyll-a concentrations near the dam were noticeably higher during the early months of the year, particularly May and June, than under Scenarios 2 and 3. This pattern indicates that complete withdrawal from the higher elevation created more favorable conditions for algal accumulation within the surface layer.

During the warm months, the mean surface chlorophyll-a concentration was approximately 3 µg/L under Scenario 1, whereas it decreased to approximately 1.78 and 1.80 µg/L under Scenarios 2 and 3, respectively. Therefore, Scenarios 2 and 3 substantially reduced surface algal biomass. Despite the higher surface nitrate and deep-water phosphorus concentrations under these scenarios, the reduction in chlorophyll-a indicates that nutrient availability was not the only factor controlling algal growth and that the physical conditions of the reservoir also played a determining role.

During the cold months, chlorophyll-a concentrations were considerably lower under all scenarios than during the warm season. The mean surface chlorophyll-a concentration was approximately 0.10 µg/L under Scenario 1 and decreased to approximately 0.03 µg/L under Scenarios 2 and 3. Therefore, the reduction in chlorophyll-a under Scenarios 2 and 3 was not limited to the warm

season, although its importance was much greater during the warm period, when the potential for algal growth was higher.

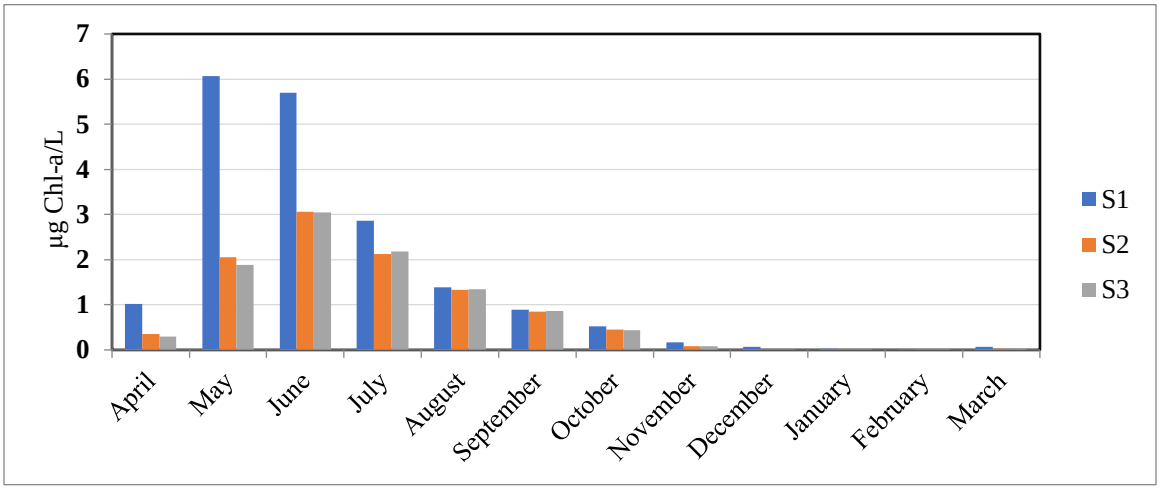

Figure 4-14. Surface chlorophyll-a concentrations in Seymareh Reservoir under the three selective-withdrawal scenarios, based on the ten-year mean EFDC+ results.

The reduction in surface chlorophyll-a under Scenarios 2 and 3 may influence water quality through several mechanisms. First, reduced surface algal biomass may lower the risk of algal blooms and deterioration in the visual quality of the water. Second, a reduction in biological production within the surface layer may decrease part of the autochthonous organic load. This may reduce oxygen consumption associated with organic matter decomposition in the upper layers. Third, reduced chlorophyll-a may alter the balance between oxygen production and consumption. Although photosynthetic production decreased, the combined effects of lower surface-water temperature and reduced organic loading prevented a decline in surface dissolved oxygen under Scenarios 2 and 3; instead, dissolved oxygen increased.

Nevertheless, chlorophyll-a should be interpreted together with nutrient concentrations. The results showed that Scenarios 2 and 3 reduced chlorophyll-a while increasing surface nitrate and deep-water phosphorus. Therefore, although these scenarios were more favorable in terms of controlling surface algal biomass, they should be assessed cautiously with respect to the increased storage or transport of nutrients.

Overall, Scenarios 2 and 3 had a beneficial effect on reducing surface chlorophyll-a compared with Scenario 1 and may therefore represent more favorable options for controlling algal growth within the surface layer. However, the difference between Scenarios 2 and 3 was very small, and increasing the proportion of withdrawal from the lower elevation from 30% to 50% did not produce an additional reduction in chlorophyll-a. Thus, in terms of chlorophyll-a control, Scenario 2 provided nearly the same benefit as Scenario 3.

4.4.5 Effects of the Scenarios on Outflow Water Quality

Outflow water quality is one of the principal criteria for evaluating reservoir operation scenarios because changes in withdrawal elevation directly affect the characteristics of the water released from the reservoir. In this section, dissolved oxygen, total phosphorus, and nitrate were analyzed to assess the operational effects on outflow water quality. The results indicate that combined withdrawal from the 665- and 640-m elevations has a favorable effect on outflow dissolved oxygen, while simultaneously causing a relative increase in the concentrations of nutrients in the released water.

As shown in Figure 4-15, outflow dissolved oxygen was higher under Scenarios 2 and 3 than under Scenario 1 during most months. During the warm months, the mean outflow dissolved oxygen concentration increased from approximately 9.0 mg/L under Scenario 1 to 9.67 mg/L under Scenario 2 and 9.63 mg/L under Scenario 3. During the cold months, outflow dissolved oxygen increased from approximately 7.2 mg/L under Scenario 1 to approximately 7.5 mg/L under Scenarios 2 and 3.

Therefore, withdrawal from the lower elevation produced a relative improvement in the oxygen conditions of the released water. This improvement is particularly important during months in which outflow dissolved oxygen decreases, such as November and December, because it may prevent a more severe deterioration in the oxygen quality of downstream releases.

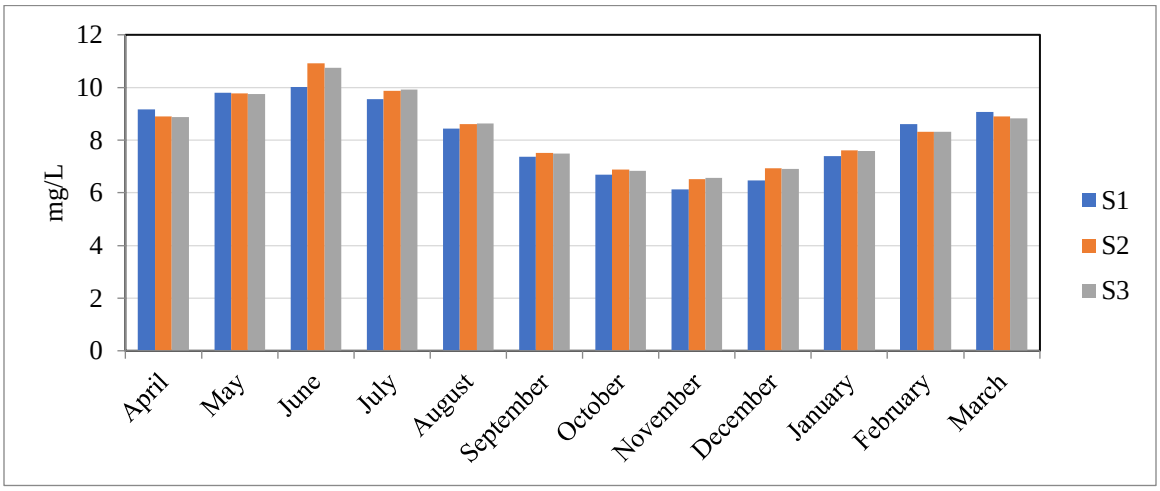

Figure 4-15. Outflow dissolved oxygen concentrations under the three selective-withdrawal scenarios, based on the ten-year mean EFDC+ results.

Despite the improvement in outflow dissolved oxygen, the total phosphorus results presented in Figure 4-16 indicate that Scenarios 2 and 3 produced higher concentrations than Scenario 1 during most months. During the warm months, the mean outflow total phosphorus concentration increased from approximately 0.47 mg/L under Scenario 1 to 0.49 mg/L under Scenario 2 and 0.51 mg/L under Scenario 3. During the cold months, outflow total phosphorus increased from

approximately 0.40 mg/L under Scenario 1 to 0.48 and 0.47 mg/L under Scenarios 2 and 3, respectively.

This pattern indicates that although lower-elevation withdrawal improves the oxygen conditions of the released water, it may also increase phosphorus export from the reservoir. This issue is important for downstream management because phosphorus is one of the principal factors controlling eutrophication in aquatic systems.

The outflow nitrate results presented in Figure 4-17 show a similar pattern. During the warm months, the mean outflow nitrate concentration was approximately 14.96 mg/L under Scenario 1 and increased to approximately 15.24 mg/L under both Scenarios 2 and 3. During the cold months, the differences among the scenarios became more pronounced: outflow nitrate increased from approximately 13.12 mg/L under Scenario 1 to 15.03 mg/L under Scenario 2 and 15.01 mg/L under Scenario 3.

Therefore, withdrawal from the lower elevation increased nitrate transport to the downstream reach, particularly during the cold season, when the differences among the scenarios were greater.

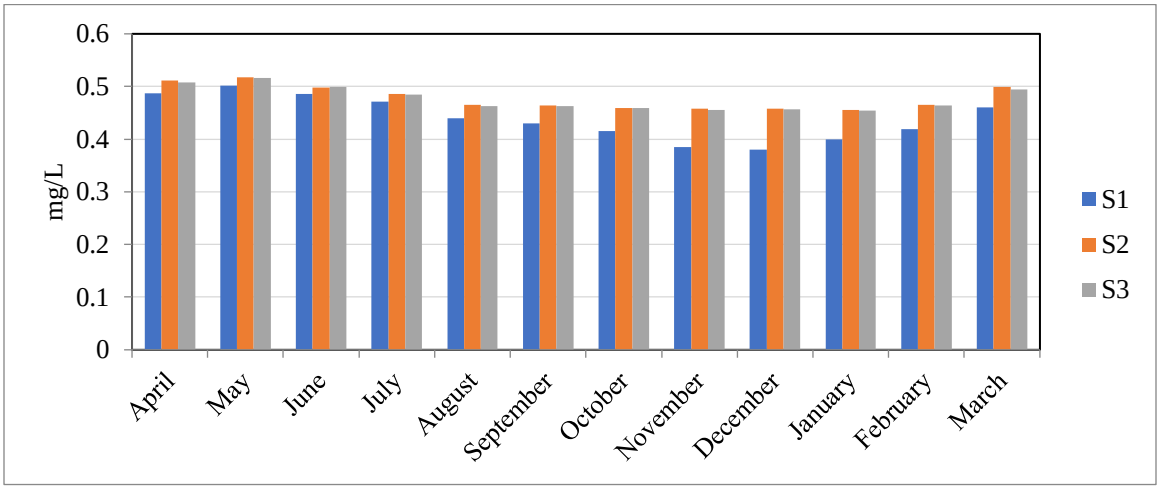

Figure 4-16. Outflow total phosphorus concentrations under the three selective-withdrawal scenarios, based on the ten-year mean EFDC+ results.

Comparison of the three outflow parameters indicates that Scenarios 2 and 3 had contrasting effects on outflow water quality. On the one hand, these scenarios increased dissolved oxygen concentrations and were therefore more favorable than Scenario 1 in terms of the oxygen condition of the released water. On the other hand, they also increased outflow phosphorus and nitrate concentrations. Thus, the improvement in dissolved oxygen was accompanied by an increase in nutrient loading, and Scenarios 2 and 3 cannot be considered unconditionally superior without accounting for this trade-off.

The differences between Scenarios 2 and 3 in terms of outflow water quality were very limited. During the warm months, dissolved oxygen was slightly higher under Scenario 2 than under Scenario 3. Outflow phosphorus was slightly higher under Scenario 3 during the warm months, whereas the difference between the two scenarios was negligible during the cold months. Outflow nitrate also exhibited nearly identical behavior under both scenarios. Therefore, increasing the share of withdrawal from the 640-m outlet from 30% under Scenario 2 to 50% under Scenario 3 did not produce a clear additional improvement in outflow water quality.

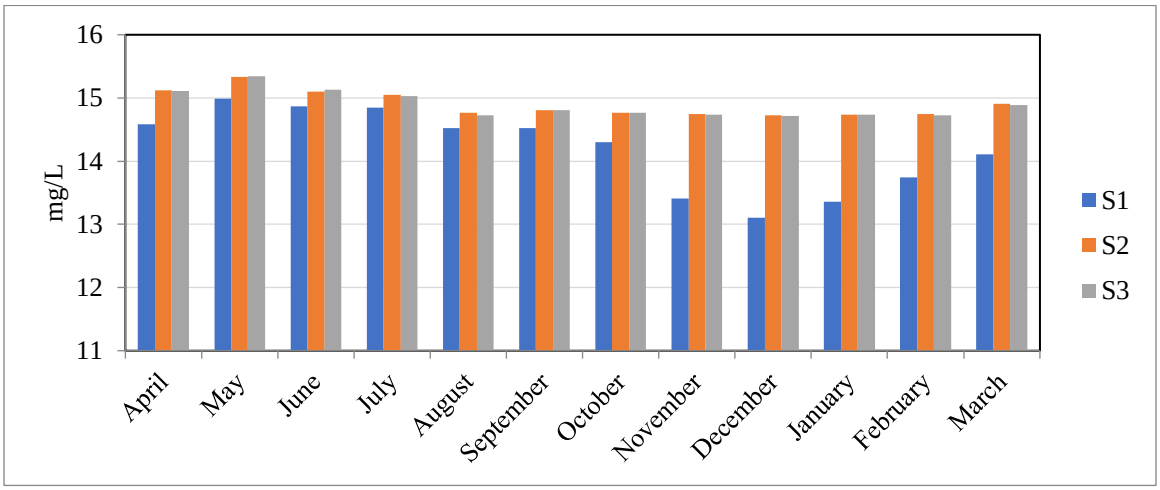

Figure 4-17. Outflow nitrate concentrations under the three selective-withdrawal scenarios, based on the ten-year mean EFDC+ results.

Overall, the outflow water quality results indicate that Scenario 2 may represent a more balanced operational option. This scenario provides a substantial portion of the dissolved oxygen benefit associated with lower-elevation withdrawal, while Scenario 3 does not produce a corresponding additional improvement and, in some cases, results in a slightly greater nutrient load.

Therefore, when the principal operational objective is to improve outflow dissolved oxygen while limiting the increase in nutrient concentrations, Scenario 2 is more defensible than Scenario 3. However, if reducing phosphorus and nitrate transport to downstream waters is the primary objective, Scenario 1 retains a relative advantage.

4.4.6 Longitudinal Variations in Surface Water Quality under the Baseline Scenario

Following the evaluation of the operational scenarios, it is important to examine longitudinal variations in surface water quality under the baseline scenario. The purpose of this section is to demonstrate that surface water quality is not spatially uniform throughout the reservoir and that conditions near the dam, in the middle reach, and in the upstream region may differ. For this purpose, surface chlorophyll-a was evaluated at three locations under Scenario S1.

As shown in Figure 4-18, surface chlorophyll-a under Scenario S1 exhibited a distinct spatial and temporal pattern. At all three locations, the highest concentrations occurred in May and June; however, the magnitude of this increase differed among the locations. The near-dam region showed the highest chlorophyll-a concentration in May, reaching approximately 7.3 µg/L. During the same month, chlorophyll-a concentrations were approximately 5.6 µg/L in the middle of the reservoir and 5.2 µg/L in the upstream region. Therefore, during the period of peak algal growth, the near-dam surface waters represented the most biologically active part of the reservoir in terms of algal biomass.

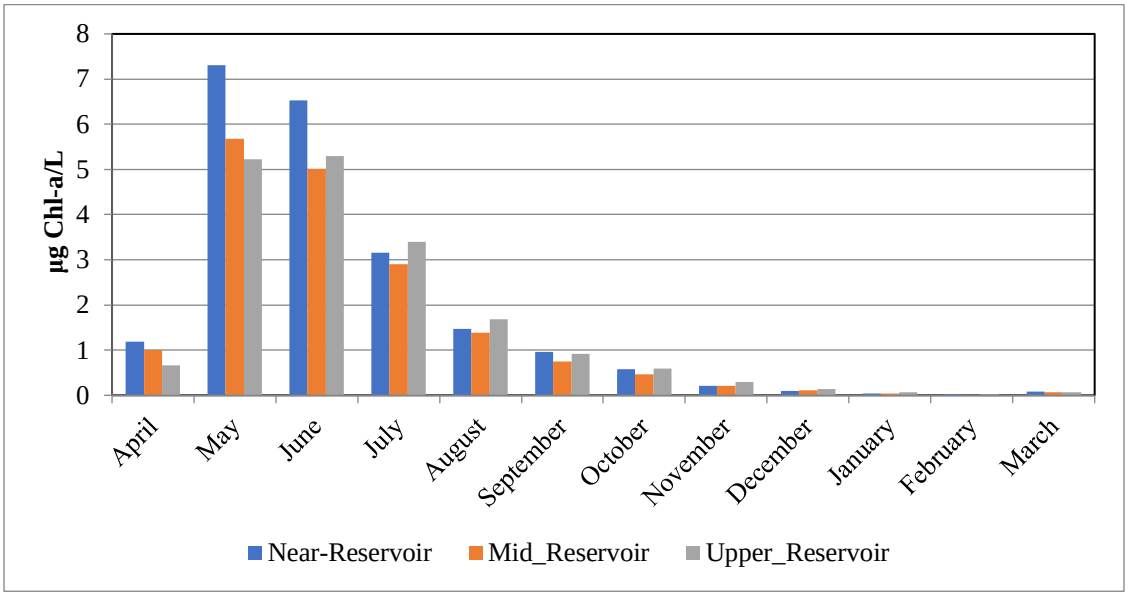

Figure 4-18. Comparison of chlorophyll-a concentrations at three locations in Seymareh Reservoir based on the EFDC+ results.

In June, chlorophyll-a remained relatively high at all three locations, although the spatial differences were smaller than those observed in May. Chlorophyll-a concentrations were approximately 6.5 µg/L near the dam, 5.0 µg/L in the middle of the reservoir, and 5.3 µg/L in the upstream region. This pattern indicates that the peak in algal biomass was not restricted to a single location, although its intensity varied longitudinally throughout the reservoir.

From July onward, chlorophyll-a concentrations decreased at all three locations and reached very low values during autumn and winter. This reduction indicates that favorable conditions for algal growth occurred mainly during spring and early summer. During the remainder of the year, algal biomass likely declined because of changes in temperature, light availability, mixing conditions, nutrient availability, and biological consumption.

The importance of this analysis lies in demonstrating that the surface water quality of Seymareh Reservoir is not longitudinally uniform. During the period of peak algal growth, chlorophyll-a

concentrations were higher near the dam, whereas lower values were observed in the middle and upstream parts of the reservoir. Therefore, when the objective is to monitor algal blooms, select a water-withdrawal location, or define management measures, results from a single station cannot be considered representative of the entire reservoir.

From a management perspective, this longitudinal heterogeneity indicates that withdrawal-location changes and control measures should be designed according to spatial conditions. For example, during periods of increased chlorophyll-a near the dam, withdrawing water from a layer or location less affected by algal accumulation may improve the quality of the released water. Similarly, the water quality monitoring network should be designed to identify longitudinal differences throughout the reservoir rather than concentrating exclusively on a single location.

4.4.7 Comparative Summary of the Operational Scenarios

Comparison of the operational scenarios demonstrated that changing the withdrawal proportions between the outlets at elevations of 665 and 640 m produced multiple effects on reservoir water quality. Scenario 1, under which the entire outflow was withdrawn from the higher elevation, was associated with higher surface chlorophyll-a, lower outflow dissolved oxygen, and lower nutrient concentrations for some indicators. In contrast, Scenarios 2 and 3, which involved partial withdrawal from the lower elevation, improved dissolved oxygen conditions in the surface layer, the lower water column, and the outflow, while simultaneously reducing surface chlorophyll-a.

However, the nutrient results showed that Scenarios 2 and 3 increased phosphorus concentrations in the lower layer and nitrate concentrations at the surface. This increase was also reflected in the released water, with outflow phosphorus and nitrate concentrations being higher under Scenarios 2 and 3 than under Scenario 1. Lower-elevation withdrawal therefore had a dual effect: on the one hand, it improved dissolved oxygen and reduced surface algal biomass; on the other hand, it increased nutrient concentrations within the water column and in the outflow.

With respect to chlorophyll-a, Scenarios 2 and 3 performed more favorably than Scenario 1. During the warm months, mean surface chlorophyll-a decreased from approximately 3 μg/L under Scenario 1 to approximately 1.8 μg/L under Scenarios 2 and 3. This reduction indicates that combined withdrawal can be beneficial for controlling surface algal growth. However, the simultaneous increases in surface nitrate and deep-water phosphorus indicate that the reduction in chlorophyll-a did not result from lower nutrient availability but was primarily associated with changes in the physical and biological conditions of the reservoir.

In terms of dissolved oxygen, Scenarios 2 and 3 produced more favorable conditions both within the reservoir and in the released water. Surface dissolved oxygen and dissolved oxygen within the bottom 20 m near the dam increased under both scenarios, while outflow dissolved oxygen was also higher during the warm and cold months than under Scenario 1. These results indicate that

withdrawal from the lower elevation can alleviate some of the reservoir's oxygen-related limitations.

Comparison of Scenarios 2 and 3 showed that their differences were small for most indicators. In several cases, Scenario 3 produced slight improvements in certain deep-water indicators, but these improvements were not substantial relative to Scenario 2. Conversely, Scenario 3 was associated with somewhat greater nutrient concentrations in some cases. Scenario 2 may therefore represent a more balanced management option because it provides most of the benefits associated with lower-elevation withdrawal, including increased dissolved oxygen and reduced chlorophyll-a, without producing markedly greater positive effects under Scenario 3.

Overall, none of the scenarios can be considered the best option under all conditions. When the primary objectives are to reduce surface chlorophyll-a and improve dissolved oxygen, Scenarios 2 and 3 are more favorable than Scenario 1. However, when minimizing nutrient transport to downstream waters is the principal objective, Scenario 1 retains a relative advantage. Selection of the operational scenario should therefore be based on a balance among improving dissolved oxygen conditions, controlling algal growth, and managing the nutrient load of reservoir releases.

5 Conclusions and Recommendations

5.1 Conclusions

The main objective of this study was to simulate the hydrodynamics and water quality of Seymareh Reservoir using the three-dimensional EFDC+ model and to evaluate the effects of changing the water-withdrawal pattern among different outlet elevations on the water quality of both the reservoir and its outflow. For this purpose, the model was first developed and calibrated to reproduce the reservoir water-surface elevation, thermal structure, and principal water quality parameters. The calibrated model was then used to evaluate three operational scenarios: complete withdrawal from an elevation of 665 m above sea level; withdrawal of 70% of the outflow from an elevation of 665 m and 30% from an elevation of 640 m; and equal withdrawal from the two elevations, with 50% released from 665 m and 50% from 640 m. The total outflow discharge was kept constant under all scenarios, and only the distribution of withdrawal between the two elevations was changed. Therefore, the differences among the results represent the effects of withdrawal elevation on reservoir structure, internal mass and energy circulation, and water quality.

The hydrodynamic calibration results demonstrated that the model reproduced variations in reservoir water-surface elevation with acceptable accuracy. This finding is important because accurate simulation of the reservoir volume balance provides the foundation for subsequent analyses of residence time, flow patterns, withdrawal depth, and the spatial and temporal distribution of water quality parameters. After confirming the model's performance in simulating water-surface elevation, analysis of the thermal structure showed that Seymareh Reservoir develops distinct thermal stratification during the warm months. During this period, a considerable temperature difference develops between the surface and deep layers, and the resulting temperature gradients restrict vertical exchange within the water column. During the cold months, surface-water cooling and weakening density differences reduce the intensity of stratification and enhance vertical mixing within the reservoir.

The satisfactory reproduction of the thermal structure demonstrated that the model had the numerical capability required for water quality analysis. In deep reservoirs, the distributions of dissolved oxygen, nutrients, and chlorophyll-a are strongly influenced by thermal stratification and vertical mixing. The results showed that restricted vertical mixing during the warm period caused dissolved oxygen depletion in the deeper layers. In the surface layer, atmospheric exchange and photosynthetic activity maintained higher dissolved oxygen concentrations. In the lower layers, however, oxygen consumption associated with organic matter decomposition and sediment-related processes, combined with limited vertical exchange, created lower-oxygen conditions.

The water quality results showed that conditions in Seymareh Reservoir result from interactions among several factors and cannot be adequately explained using a single parameter. Dissolved oxygen is directly related to temperature, organic loading, nutrient concentrations, and chlorophyll-a. An increase in biodegradable organic matter, whether originating from upstream inflows or from biological production within the reservoir, may intensify oxygen consumption. In turn, oxygen depletion in the deeper layers may promote phosphorus release or increase its availability, thereby affecting eutrophication processes. Water quality in the reservoir must therefore be analyzed using an integrated approach.

The nitrogen-cycle results showed that ammonium and nitrate exhibited different vertical patterns. Ammonium had a greater tendency to accumulate under low-oxygen conditions and within deeper layers, whereas nitrate concentrations were generally higher in more oxygenated parts of the water column where nitrification was more active. Phosphorus was also identified as an important management concern because it may influence algal growth through both external watershed loading and internal sediment-related processes. Therefore, nitrogen and phosphorus management should be addressed at both the watershed and internal reservoir scales.

The chlorophyll-a results showed that algal growth occurred predominantly in the surface layers and increased during the warm season. This behavior was consistent with greater light availability, more favorable temperatures, and the presence of nutrients within the surface layer. Chlorophyll-a concentrations decreased with increasing depth, demonstrating the limiting role of light within the water column. Overall, the water quality calibration results showed that EFDC+ successfully reproduced the principal behavior of Seymareh Reservoir in relation to thermal stratification, dissolved oxygen, nutrients, organic loading, and chlorophyll-a. The model was therefore considered suitable for evaluating the operational scenarios.

The scenario-analysis results showed that changing the withdrawal elevation had a considerable effect on the reservoir's thermal structure. During the warm season near the dam, the surface-to-depth temperature difference was approximately 14.3 °C under Scenario 1, whereas it decreased to approximately 10.8 and 10.5 °C under Scenarios 2 and 3, respectively. This result indicates that withdrawing part of the flow from the lower elevation can reduce stratification intensity and increase the involvement of deeper layers in reservoir circulation and outflow. However, deeper

withdrawal alone did not eliminate thermal stratification, and the reservoir retained its stratified behavior during the warm season.

In terms of dissolved oxygen, the combined-withdrawal scenarios performed better in the deeper layers than complete withdrawal from the 665-m elevation. During the warm season near the dam, the mean dissolved oxygen concentration at a depth of 80 m increased from approximately 5.36 mg/L under Scenario 1 to approximately 5.92 and 6.07 mg/L under Scenarios 2 and 3, respectively. This increase indicates that withdrawal from the lower elevation can improve deep-water oxygen conditions to some extent.

The effects of the combined-withdrawal scenarios were more pronounced for chlorophyll-a. During the warm season near the dam, mean surface chlorophyll-a decreased from approximately 2.96 µg/L under Scenario 1 to approximately 1.61 and 1.58 µg/L under Scenarios 2 and 3, respectively. This reduction indicates that combined withdrawal can substantially limit surface algal growth. The reduction in chlorophyll-a was not restricted to the near-dam region and was also observed in other parts of the reservoir. Nevertheless, the difference between Scenarios 2 and 3 was very small, and increasing the withdrawal contribution from the 640-m elevation from 30% to 50% did not produce a substantial additional reduction in chlorophyll-a.

Alongside these beneficial effects, the nutrient results showed that withdrawal from the lower elevation had contrasting consequences. During the warm season, surface nitrate concentrations increased under Scenarios 2 and 3 relative to Scenario 1. Phosphorus concentrations also increased in the deeper layers, particularly at a depth of 80 m, under the combined-withdrawal scenarios. Therefore, although lower-elevation withdrawal may reduce chlorophyll-a and improve deep-water oxygen conditions, it may also increase nutrient transport or availability. This finding demonstrates that an operational strategy should not be selected on the basis of a single indicator.

The outflow water quality results confirmed the same trade-off. Combined withdrawal was more favorable than Scenario 1 in terms of increasing outflow dissolved oxygen and reducing surface chlorophyll-a. However, it also resulted in relative increases in outflow phosphorus and nitrate. Therefore, none of the scenarios can be considered unconditionally superior. When the principal objectives are to improve outflow dissolved oxygen and control algal growth within the reservoir, Scenarios 2 and 3 are more favorable. In contrast, when reducing nutrient transport to downstream waters is the primary objective, Scenario 1 has a relative advantage.

Based on the overall comparison, Scenario 2 may be considered the more balanced option. This scenario provides a substantial proportion of the benefits associated with withdrawal from the lower elevation, including reduced stratification intensity, improved deep-water oxygen conditions, and lower surface chlorophyll-a, while requiring a smaller proportion of deep withdrawal than Scenario 3. Because the differences between Scenarios 2 and 3 in reducing chlorophyll-a and improving dissolved oxygen were limited, increasing the deep-withdrawal

proportion from 30% to 50% did not necessarily provide a substantial additional management benefit. Scenario 2 may therefore be considered a reasonable and relatively balanced option for water quality–oriented operation of Seymareh Reservoir.

Overall, the findings demonstrate that Seymareh Reservoir is a deep and stratified system that is sensitive to withdrawal elevation. Changing the withdrawal location can be used as a management tool to influence water quality, but it should be applied cautiously and evaluated using multiple criteria. The simultaneous improvement in dissolved oxygen and reduction in chlorophyll-a under the combined-withdrawal scenarios, together with the relative increase in nutrient concentrations, indicates that reservoir management must balance three principal environmental objectives: improving oxygen conditions, controlling algal growth, and reducing nutrient transport to downstream waters. Within a more comprehensive management framework, quantitative objectives related to water supply, energy production, and downstream water demands should also be considered in future studies.

5.2 Recommendations

Based on the findings of this study and the successful application of EFDC+ in simulating the hydrodynamics, water quality, and eutrophication processes of Seymareh Reservoir, the following recommendations are proposed for future research:

- An operational policy should be developed for Seymareh Reservoir using EFDC+-based numerical simulations and incorporating quantitative objectives related to hydropower generation, agricultural water supply, environmental requirements, and water quality within a selective-withdrawal framework.
- Reservoir operation policies should be formulated to meet the principal reservoir objectives while also considering the environmental characteristics and requirements of the downstream river.
- A reservoir water quality monitoring network and an effective spatial and temporal monitoring program should be designed by accounting for the physical, hydrological, and meteorological characteristics of the reservoir, as well as the configuration and operation of its hydraulic structures.
- The effects of in situ management measures, including artificial aeration, biological interventions, and other restoration techniques, on the water quality of the eutrophic reservoir should be evaluated using the three-dimensional EFDC+ hydrodynamic and water quality model.
- Reservoir water quality management strategies should be developed by controlling pollutants originating from the upstream watershed and applying integrated modeling frameworks such as EFDC+–SWAT, EFDC+–BASIN, or other coupled watershed–reservoir modeling systems.

- Sensitivity and uncertainty analyses should be conducted for the most important and influential EFDC+ parameters to improve understanding of system responses and evaluate the robustness of model performance.
- EFDC+ performance should be further refined by updating model calibration using data assimilation techniques

References

[1] E. Mohammadjani and

N. Yazdanian, "Analysis of the water crisis in Iran and its management requirements," *Ravand*, vol. 21, nos. 65–66, pp. 117–144, 2014 [1393]. (in Persian)

[2] Q. Wang, S. Li, P. Jia, C. Qi, and F. Ding, "A review of surface water quality models," *The Scientific World Journal*, vol. 2013, Art. no. 231768, 2013.

[3] Tetra Tech, Inc., *The Environmental Fluid Dynamics Code Theory and Computation, Volume 1: Hydrodynamics and Mass Transport*. Fairfax, VA, USA: Tetra Tech, 2007.

[4] M. W. Beutel and A. J. Horne, "A review of the effects of hypolimnetic oxygenation on lake and reservoir water quality," *Lake and Reservoir Management*, vol. 15, no. 4, pp. 285–297, 1999.

[5] V. H. Smith, "Eutrophication of freshwater and coastal marine ecosystems: A global problem," *Environmental Science and Pollution Research*, vol. 10, no. 2, pp. 126–139, 2003.

[6] L. Gao and D. Li, "A review of hydrological/water-quality models," *Frontiers of Agricultural Science and Engineering*, vol. 1, no. 4, pp. 267–276, 2014.

[7] E. Jeppesen et al., "Climate change effects on runoff, catchment phosphorus loading and lake ecological state, and potential adaptations," *Journal of Environmental Quality*, vol. 38, no. 5, pp. 1930–1941, 2009.

[8] M. S. Moradi Mousavi, "Simulation of the effects of artificial aeration on algal blooms in eutrophic reservoirs: A case study of Seymareh Reservoir," M.Sc. thesis, Department of Civil Engineering, Water Resources Management, Iran University of Science and Technology, Tehran, Iran, 2021 [1400]. (in Persian)

[9] R. S. Winton, E. Calamita, and B. Wehrli, “Reviews and syntheses: Dams, water quality and tropical reservoir stratification,” *Biogeosciences*, vol. 16, no. 8, pp. 1657–1671, 2019.

[10] V. Istvánovics, “Eutrophication of lakes and reservoirs,” in *Encyclopedia of Inland Waters*, G. E. Likens, Ed., vol. 1. Oxford, UK: Elsevier, 2009, pp. 157–165.

[11] M. J. Paterson et al., “Long-term changes in nutrient dynamics and plankton communities following the creation of a new reservoir,” *Canadian Journal of Fisheries and Aquatic Sciences*, vol. 76, no. 8, pp. 1459–1469, 2019.

[12] C. Liu et al., “Characteristics of water quality response to hypolimnetic anoxia in Daheiting Reservoir,” *Water Science and Technology*, vol. 85, no. 7, pp. 2065–2075, 2022.

[13] H. Zargarpoor, M. Gharavi, and J. Dehghan, “Thermal stratification in cascade reservoirs: A case study of the Karun 1, 2, and 3 reservoirs,” *Iranian Journal of Water Resources Research*, vol. 3, no. 2, pp. 71–77, 2007 [1386]. (in Persian)

[14] F. Firoozi, A. Rouzbahani, and A. Massah Bavani, “Assessment of climate change impacts on the thermal stratification of Latian Reservoir,” *Iranian Journal of Water Resources Research*, vol. 14, no. 3, pp. 268–277, 2018 [1397]. (in Persian)

[15] M. A. Peña, V. Katsev, T. Oguz, and D. Gilbert, “Modeling dissolved oxygen dynamics and hypoxia,” *Biogeosciences*, vol. 7, no. 3, pp. 933–957, 2010.

[16] R. Gu, S. C. McCutcheon, and P. F. Wang, “Modeling reservoir density underflow and interflow from a chemical spill,” *Water Resources Research*, vol. 32, no. 3, pp. 695–705, 1996.

[17] D. E. Ford and M. C. Johnson, *An Assessment of Reservoir Density Currents and Inflow Processes*, Technical Report E-83-7. Vicksburg, MS, USA: U.S. Army Engineer Waterways Experiment Station, 1983.

[18] S. Chen et al., “Three-dimensional effects of artificial mixing in a shallow drinking-water reservoir,” *Water Resources Research*, vol. 54, no. 1, pp. 425–441, 2018.

[19] A. F. Khasanov and A. M. Eremeeva, “Creation of artificial aeration system to improve water quality in reservoirs,” *Hydrology*, vol. 12, no. 3, Art. no. 48, 2025.

[20] G. K. Nürnberg, “Lake responses to long-term hypolimnetic withdrawal treatments,” *Lake and Reservoir Management*, vol. 23, no. 4, pp. 388–409, 2007.

[21] J. P. Zehr and B. B. Ward, “Nitrogen cycling in the ocean: New perspectives on processes and paradigms,” *Applied and Environmental Microbiology*, vol. 68, no. 3, pp. 1015–1024, 2002.

[22] J. W. Labadie, D. G. Fontane, J. H. Lee, and I. H. Ko, “Decision support system for adaptive river basin management: Application to the Geum River basin, Korea,” *Water International*, vol. 32, no. 3, pp. 397–415, 2007.

[23] A. Erturk et al., “Application of water quality modelling as a decision support system tool for planned Buyuk Melen Reservoir and its watershed,” in *Sustainable Use and Development of Watersheds*. Dordrecht, The Netherlands: Springer, 2008, pp. 227–242.

[24] S. Shin, Y. Her, J. H. Song, and M. S. Kang, “Integrated sediment transport process modeling by coupling Soil and Water Assessment Tool and Environmental Fluid Dynamics Code,” *Environmental Modelling & Software*, vol. 116, pp. 26–39, 2019.

[25] J. Wu, R. Zou, and S. L. Yu, “Uncertainty analysis for coupled watershed and water quality modeling systems,” *Journal of Water Resources Planning and Management*, vol. 132, no. 5, pp. 351–361, 2006.

[26] K. M. Pilgrim and P. L. Brezonik, “Treatment of lake inflows with alum for phosphorus removal,” *Lake and Reservoir Management*, vol. 21, no. 1, pp. 1–9, 2005.

[27] F. Torres-Bejarano, J. Padilla, C. Rodríguez-Cuevas, and R. Cantero, “Hydrodynamics modelling utilizing the EFDC Explorer model for the sustainable management of Canal del Dique–Guájaro hydrosystem, Colombia,” *WIT Transactions on the Built Environment*, vol. 168, pp. 423–434, 2015.

[28] F. Torres-Bejarano et al., “Hydrodynamics and water quality assessment of a coastal lagoon using Environmental Fluid Dynamics Code Explorer Modeling System,” *Global Journal of Environmental Science and Management*, vol. 6, no. 3, pp. 289–308, 2020.

[29] G. Pak et al., “Modelling of suspended sediment in a weir reach using EFDC model,” *Water Science and Technology*, vol. 73, no. 7, pp. 1583–1590, 2016.

[30] J. Pyo et al., “Cyanobacteria cell prediction using interpretable deep learning model with observed, numerical, and sensing data assemblage,” *Water Research*, vol. 203, Art. no. 117483, 2021.

[31] S. M. Hong et al., “Autonomous calibration of EFDC for predicting chlorophyll-a using reinforcement learning and a real-time monitoring system,” *Environmental Modelling & Software*, vol. 168, Art. no. 105805, 2023.

[32] S. Sinha, X. Liu, and M. H. Garcia, “A three-dimensional water quality model of Chicago Area Waterway System (CAWS),” *Environmental Modeling & Assessment*, vol. 18, pp. 567–592, 2013.

[33] W. Song et al., “EFDC simulation of fishway in the Diversion Dahaerteng River to Danghe Reservoir, China,” *Ecological Indicators*, vol. 102, pp. 704–715, 2019.

[34] L. Yang, J. Wei, J. Qi, and L. Zhang, “Effect of sewage treatment plant effluent on water quality of Zhangze Reservoir based on EFDC model,” *Frontiers in Environmental Science*, vol. 10, Art. no. 874502, 2022.

[35] R. Xie et al., “Fine silt particle pathline of dredging sediment in the Yangtze River deepwater navigation channel based on EFDC model,” *Journal of Hydrodynamics*, vol. 22, no. 6, pp. 760–772, 2010.

[36] C. Villota-López et al., “Applying EFDC Explorer model in the Gallinas River, Mexico, to estimate its assimilation capacity for water quality protection,” *Scientific Reports*, vol. 11, Art. no. 13023, 2021.

[37] T. Tang, S. Yang, X. Peng, W. Yin, and R. Zou, “Eutrophication control decision making using EFDC model for Shenzhen Reservoir, China,” *Water Resources*, vol. 44, no. 2, pp. 308–314, 2017.

[38] S. Peng, G. Y. Z. Fu, X. H. Zhao, and B. C. Moore, “Integration of Environmental Fluid Dynamics Code (EFDC) model with Geographical Information System (GIS) platform and its applications,” *Journal of Environmental Informatics*, vol. 17, no. 2, pp. 75–82, 2011.

[39] J. M. Ahn, K. Lee, and S. Lyu, “Effect of changes in watershed runoff characteristics on salinity intrusion in estuary using EFDC,” *KSCE Journal of Civil Engineering*, vol. 24, no. 1, pp. 87–98, 2020.

[40] V. Alarcon et al., “Nested hydrodynamic modeling of a coastal river applying dynamic coupling,” *Water Resources Management*, vol. 28, pp. 3227–3240, 2014.

[41] P. Wang, G. Lai, and L. Li, “Predicting the hydrological impacts of the Poyang Lake Project using an EFDC model,” *Journal of Hydrologic Engineering*, vol. 20, no. 12, Art. no. 05015009, 2015.

[42] J. Huang et al., “Risk assessment of hazardous materials loading into four large lakes in China: A new hydrodynamic indicator based on EFDC,” *Ecological Indicators*, vol. 80, pp. 23–30, 2017.

[43] Z.-G. Ji, M. R. Morton, and J. M. Hamrick, “Wetting and drying simulation of estuarine processes,” *Estuarine, Coastal and Shelf Science*, vol. 53, no. 5, pp. 683–700, 2001.

[44] C.-X. Zhang and X.-Y. You, “Application of EFDC model to grading the eutrophic state of reservoir: Case study in Tianjin Erwangzhuang Reservoir, China,” *Engineering Applications of Computational Fluid Mechanics*, vol. 11, no. 1, pp. 111–126, 2017.

[45] Z. Qin, Z. He, G. Wu, G. Tang, and Q. Wang, “Developing water-quality model for Jingpo Lake based on EFDC,” *Water*, vol. 14, no. 17, Art. no. 2596, 2022.

[46] W. Langley, B. Adeyeye, and J. D. Bowen, *Development and Use of a New Three-Dimensional Mechanistic Water Quality Model of Jordan Lake to Predict Responses of Reduced Nutrient Loading*. Charlotte, NC, USA: University of North Carolina at Charlotte, 2020.

[47] H. Naderi, A.-H. Javid, S.-M. Borghei, and M. Eslamizadeh, "Three-dimensional simulation of temperature and water quality parameters using EFDC hydrodynamic model: A case study of Mamloo Dam," *Water Resources Engineering*, vol. 16, no. 57, pp. 47–60, 2023.

[48] L. Chen, Z. Yang, and H. Liu, "Assessing the eutrophication risk of the Danjiangkou Reservoir based on the EFDC model," *Ecological Engineering*, vol. 96, pp. 117–127, 2016.

[49] B. Tasnim, X. Fang, and J. S. Hayworth, "One- and three-dimensional hydrodynamic, water temperature, and dissolved oxygen modeling comparison," *Water*, vol. 16, no. 2, Art. no. 317, 2024.

[50] H. Y. Oh, Y. K. Jeon, H. W. Lee, E. J. Kim, and J. H. Choi, "Simulating water pollution accidents in Asan Lake: Toward proactive water pollution management," *Journal of Hazardous Materials Advances*, vol. 22, Art. no. 101174, 2026.

[51] Mahab Ghodss Consulting Engineers, "Water quality studies of the Seymareh Dam watershed and reservoir: Water quality modeling of Seymareh Reservoir and proposed measures for improving reservoir water quality," Technical Report prepared for Iran Water and Power Resources Development Company, Tehran, Iran, Dec. 2014 [Azar 1393], Project Code 3381070, Section Code 2040. (in Persian)

[52] M. Khalafeh Nilsaz, "Determination of primary production and fish production potential in Seymareh Dam Lake," Final Research Project Report, Iranian Fisheries Science Research Institute, Tehran, Iran, 2020 [1399]. (in Persian)

[53] Ganjayi, T., and M. Saadatpour, "Assessment of point-source pollution control effects on watershed water quality based on the SWAT hydrological and water quality model: A case study of the Seymareh watershed," Iranian Journal of Water Resources Research, vol. 19, no. 5, 2023. (in Persian)

[54] B. Galperin, L. H. Kantha, S. Hassid, and A. Rosati, "A quasi-equilibrium turbulent energy model for geophysical flows," *Journal of the Atmospheric Sciences*, vol. 45, no. 1, pp. 55–62, 1988.

[55] DSI LLC, *EFDC+ Theory*, Version 11. Edmonds, WA, USA: DSI LLC, 2023.

[56] S. Dehghan Madiseh, "Assessment of water and sediment quality in Seymareh Dam Lake using biological and chemical quality indices," Final Research Project Report, Iranian Fisheries Science Research Institute, South Iran Aquaculture Research Center, Iran, 2020 [1399], Registration No. 54565. (in Persian)

[57] J. M. Ahn, J. Kim, L. J. Park, J. Jeon, J. Jong, J.-H. Min, and T. Kang, "Predicting cyanobacterial harmful algal blooms (CyanoHABs) in a regulated river using a revised EFDC model," *Water*, vol. 13, no. 4, Art. no. 439, 2021.

[58] J. C. Young and P. A. Vanrolleghem, "Carbonaceous vs. total biochemical oxygen demand as a basis for WRRF design and performance monitoring," *Water Environment Research*, vol. 93, no. 9, pp. 1510–1515, 2021.

[59] A. B. Sullivan, D. M. Snyder, and S. A. Rounds, "Controls on biochemical oxygen demand in the upper Klamath River, Oregon," *Chemical Geology*, vol. 269, nos. 1–2, pp. 12–21, 2010.

[60] P. K. Zigah, E. C. Minor, H. A. N. Abdulla, J. P. Werne, and P. G. Hatcher, "An investigation of size-fractionated organic matter from Lake Superior and a tributary stream using radiocarbon, stable isotopes and NMR," *Geochimica et Cosmochimica Acta*, vol. 127, pp. 264–284, 2014.

[61] P. Servais, P. Laurent, and G. Randon, "Comparison of the bacterial dynamics in various French distribution systems," *Journal of Water Supply: Research and Technology—AQUA*, vol. 44, no. 1, pp. 10–17, 1995.